Aus dem

Comprehensive Pneumology Center (CPC)

Helmholtz Zentrum München

Direktor: Prof. Dr. Ali Önder Yildirim,
vormals: Prof. Dr. Oliver Eickelberg

Discovery of new cinnamic acid amides as novel antifibrotic drugs

Dissertation
zum Erwerb des Doktorgrades der Medizin
an der Medizinischen Fakultät der
Ludwig-Maximilians-Universität zu München

vorgelegt von

Michael Wolfgang Gerckens

aus

Troisdorf

2023

Mit Genehmigung der Medizinischen Fakultät
der Universität München

Berichterstatter:	Prof. Dr. Oliver Eickelberg
Mitberichterstatter:	Prof. Dr. Claus Neurohr
	Prof. Dr. Jürgen Behr
	PD Dr. Susanne Jonat
Mitbetreuung durch den promovierten Mitarbeiter:	Dr. Gerald Burgstaller
Dekan:	Prof. Dr. med. Thomas Gudermann
Tag der mündlichen Prüfung:	19.10.2023

Meinen Eltern.

Parts of this work have been published in the following research articles and patent applications:

Burgstaller G, Oehrle B, **Gerckens M**, White ES, Schiller HB, Eickelberg O. The instructive extracellular matrix of the lung: basic composition and alterations in chronic lung disease. Eur Respir J. 2017 Jul 5;50(1):1601805. doi: 10.1183/13993003.01805-2016. PMID: 28679607.

Gerckens M, Alsafadi HN, Wagner DE, Lindner M, Burgstaller G, Königshoff M. Generation of Human 3D Lung Tissue Cultures (3D-LTCs) for Disease Modeling. J Vis Exp. 2019 Feb 12;(144). doi: 10.3791/58437. PMID: 30829341.

Gerckens M, Schorpp K, Pelizza F, Wögrath M, Reichau K, Ma H, Dworsky AM, Sengupta A, Stoleriu MG, Heinzelmann K, Merl-Pham J, Irmler M, Alsafadi HN, Trenkenschuh E, Sarnova L, Jirouskova M, Frieß W, Hauck SM, Beckers J, Kneidinger N, Behr J, Hilgendorff A, Hadian K, Lindner M, Königshoff M, Eickelberg O, Gregor M, Plettenburg O, Yildirim AÖ, Burgstaller G. Phenotypic drug screening in a human fibrosis model identified a novel class of antifibrotic therapeutics. Sci Adv. 2021 Dec 24;7(52):eabb3673. doi: 10.1126/sciadv.abb3673. Epub 2021 Dec 22. PMID: 34936468.

Helmholtz Zentrum München Deutsches Forschungszentrum für Gesundheit und Umwelt (GmbH); Inventors: Burgstaller G, **Gerckens M**, Plettenburg O, Yildirim AÖ, Ma H. Novel anti-fibrotic drugs. European Patent Application No. 21178481.4-1112. Filed 2021 Jun 9.

TABLE OF CONTENT

1. ABBREVIATIONS

3D	three-dimensional
4D	four-dimensional
°C	degree Celsius
ΔCt	delta cycle of threshold
µ	micro
A	
A	adenosine
AF	AlexaFluor
ANOVA	analysis of variance
αSMA	alpha smooth muscle actin
APS	ammonium peroxydisulfate
B	
BSA	bovine serum albumin
C	
C	cytosine
cDNA	complementary DNA
CNN	convolutional neural network
COPD	chronic obstructive pulmonary disease
CT	computed tomography
CTGF	connective tissue growth factor
CC	control cocktail
Cat.-No.	catalogue number / product number
D	
DNA	desoxyribonucleic acid
dNTP	desoxynucleotide triphosphate
DPLD	diffuse parenchymal lung disease
E	
ECM	extracellular matrix
EDHB	ethyl 3,4-dihydroxybenzoate
ELISA	enzyme-linked Immunosorbent Assay
EMT	epithelial-mesenchymal-transition
EtOH	ethanol

F

FANTAIL	fibrotic pattern detection by artificial intelligence
FBS	fetal bovine serum
FC	profibrotic / fibrotic cocktail
FVC	forced vital capacity
fw	forward

G

g	gram
G	guanosine
GPCR	g-protein coupled receptors
GSEA	gene-set enrichment analysis

H

HC	high-content
hPCLS	human precision cut lung slices
HRCT	high-resolution CT
HT	high-throughput

I

IgG	immunoglobulin G
IL-11	interleukin-11
ILD	interstitial lung disease
IPF	Idiopathic Pulmonary Fibrosis
IU	international units

J

JNK	c-Jun N-terminal kinase

L

L	liter
LC-MS^2	Liquid chromatography-tandem mass spectrometry
LPA	lysophosphatidic acid
mRNA	messenger RNA

M

M	molar
m	meter
m	milli
MAPK	mitogen-activated protein kinase
mc	monoclonal
min	minute
MRI	magnet resonance imaging
mRNA	messenger RNA
MTT	3-(4,5-dimethylthiazol-2-yl)-2,5-diphenyltetrazolium bromide

N

n	nano
N23Ps	N-(2-butoxyphenyl)-3-(phenyl)acrylamides and N-(2-benzoxyphenyl)-3-(phenyl)acrylamide
NAC	n-acetylcysteine
NaCl	
NK cells	natural killer cells

P

PBS	phosphate buffered saline
PAH	pulmonary arterial hypertension
PAI-1	plasminogen activator inhibitor type 1
pc	polyclonal
PCR	polymerase chain reaction
PDGF	platelet-derived growth factor
PFA	paraformaldehyde
PI3K	phosphoinositid-3-kinase
PVDF	polyvinylidene fluoride

Q

qPCR	quantitative PCR

R

RNA	ribonucleic acid
rv	reverse

S

SAR	structure-activity-relationship
SD	standard deviation
SDS-PAGE	sodium dodecylsulfate polyacrylamide gel electrophoresis
SEM	standard error of mean
siRNA	small interfering RNA

T

TAK1	transforming growth factor beta activated kinase 1
TGFβ	transforming growth factor beta
TGFβ1	transforming growth factor beta 1
TNFα	tumor necrosis factor alpha

U

UIP	usual interstitial pneumonia
UMAP	uniform manifold approximation and projection
UMAP-RPC	uniform manifold approximation and projection for regulation pattern clustering

Gene names are written in italic uppercase letters (e. g. “*ACTA2*”), while protein names are written in capital non-italic letters with the except of Greek letters written in lowercase for readability reasons (e. g. “αSMA”).

2. ZUSAMMENFASSUNG

Fibrotische Gewebeveränderungen stellen ein gemeinsames Merkmal der häufigsten letalen Erkrankungen in der industrialisierten Welt dar. Unter den Lungenerkrankungen ist hier allen voran die Idiopathische Lungenfibrose (IPF) durch einen fortschreitende fibrotischen Umbau des Lungenparenchyms charakterisiert. Zugelassene antifibrotische Pharmakotherapien verlangsamen das Progress der Erkrankung, können diesen jedoch nicht aufhalten. IPF-Patienten überleben im Median 3-5 Jahre nach Diagnosestellung. Hieraus ergibt sich ein dringender Bedarf an neuen antifibrotischen Wirkstoffen und Therapien. Wie in anderen fibrotischen Erkrankungen, ist die Pathogenese der IPF durch die pulmonale Deposition erhöhter Mengen von extrazellulärer Matrix (EZM), größtenteils durch aktivierte Myofibroblasten charakterisiert.

Es wurde ein phänotypisches immunocytochemisches, sogenanntes *high-content*, Hochdurchsatz-Assay zur Messung von fibrotischer EZM-Deposition durch mit transforming growth factor β 1 (TGFβ1) und Wirkstoffen behandelten primäre humane Lungenfibroblasten (phLFs) entwickelt, welche aus Lungengewebe von IPF-Patienten isoliert wurden. 1509 niedermolekulare Wirkstoffe wurden auf eine Inhibition TGFβ1-stimulierter Extrazellulärmatrix-Deposition durch phLFs gescreent. Mithilfe einer Deeplearning-basierten Immunofluoreszenzanalyse des Assays konnten 31 antifibrotische Wirkstoffkandidaten identifiziert werden. Der Wirkstoff Tranilast wies eine niederpotente Inhibition von TGFβ1-induzierter Fibroblasten-Myofibroblasten-Transdifferenzierung sowie TGFβ1-induzierter Extrazellulärmatrix-Deposition auf. Durch die Untersuchung der Struktur-Wirkungsbeziehung von Tranilast-Derivaten, konnte eine neue Gruppe hochpotenter Inhibitoren von TGFβ1-induzierter Fibroblasten-Myofibroblasten-Transdifferenzierung sowie TGFβ1-induzierter Extrazellulärmatrix-Deposition, bestehend aus den Zimtsäureamiden der N-(2-butoxyphenyl)-3-(phenyl)acrylamid- and N-(2-benzoxyphenyl)-3-(phenyl)acrylamid-Gruppe (N23Ps), entdeckt werden. Im Folgenden konnte gezeigt werden, dass N23Ps eine starke Morphologie-Änderung in den pHLFs induzieren, wahrscheinlich aufgrund einer Regulation zytoskeletaler

Proteine. Anschließende Transkriptom- und Proteomanalysen zeigten, dass N23Ps spezifische fibrotische Signaturen in TGFβ1-behandelten pHLFs sowie in einem humanen *ex-vivo* Model für frühe lungenfibrotischen Veränderungen, basierend auf Gewebekulturen von humanen precision cut lung slices (hPCLS), inhibieren. RNA-Interferenz-Experimente zeigten, dass die Inhibition von TGFβ1-Signalwegen durch N23Ps von der Ubiquitin-Protein-Ligase SMURF2 abhängig ist.

Zusammenfassend wurde eine neue Gruppe an Zimtsäureamiden entdeckt, welche TGFβ1-induzierte profibrotische Myofibroblastenaktivität SMURF2-abhängig hemmt.

3. SUMMARY

Fibrosis is a common hallmark of most fatal chronic diseases in the industrialized world. Among pulmonary disease, progressive fibrosis is the pivotal pathomechanism of the Idiopathic Pulmonary Fibrosis (IPF), a devastating progressive interstitial lung disease with a median patient survival time of 3-5 years. Approved pharmacotherapies only slow down, but do not stop disease progression. Thus, new antifibrotic therapeutic strategies are urgently needed. Like most fibrotic diseases, IPF pathogenesis is characterized by the deposition of excessive amounts of fibrotic extracellular matrix of activated myofibroblasts resulting in increasing loss of lung function.

A phenotypic high-content ECM deposition assay was developed measuring fibrotic ECM deposition by primary human lung fibroblasts (phLFs) derived from IPF patients upon transforming growth factor beta 1 (TGFβ1) and drug treatment. To identify antifibrotic compounds, 1509 small molecule compounds were screened for inhibition of TGFβ1-induced ECM deposition. Using a deep learning model 31 hit compounds were identified. Here, for the compound Tranilast a low-potent inhibitory activity on TGFβ1-induced fibroblast-myofibroblast-transdifferentiation and ECM deposition was found. By structure-activity-relationship studies of Tranilast derivatives, a group of novel cinnamic acid amides, in particular N-(2-butoxyphenyl)-3-(phenyl)acrylamides and N-(2-benzoxyphenyl)-3-(phenyl)acrylamides (N23Ps), with high potency for the inhibition of TGFβ1-dependent αSMA induction and ECM deposition was discovered. N23Ps induced strong morphological changes in phLFs, possibly due to a regulation of cytoskeletal proteins as seen in transcriptome-wide microarray analysis. Furthermore, proteomics and transcriptomics analysis showed N23Ps to inhibit specific fibrotic signatures in TGFβ1-treated phLFs as well as in a human *ex-vivo* injury and early 3D fibrosis model based on human precision cut lung slice tissue cultures. RNA interference rescue experiments showed an inhibition of TGFβ1 signaling by N23Ps to be SMURF2-dependent.

In conclusion, a novel group of cinnamic acid amides was discovered that inhibit TGFβ1-induced profibrotic behavior of myofibroblasts in a SMURF2-dependent way.

4. INTRODUCTION

4.1. Fibrosis

Tissue fibrosis is a pathophysiological mechanism involved in the majority of pathologies in human medicine affecting heart, lung, kidney and skin amongst others (Zeisberg und Kalluri 2012). Thereby, fibrotic diseases account for 45% of mortality in the industrialized world (Cox und Erler 2011). Fibrosis, also tissue scarring, describes a cascade of cellular and molecular responses to acute or chronic tissue injury that results through the deposition of excessive amounts of extracellular matrix and tissue remodeling in an aberrant wound healing response without full reconstitution of the injured tissue's former architecture and function (Wynn 2007).

The common mechanism of fibrosis across organs is characterized by epithelial injury which triggers the influx and stimulation of inflammatory cells, such as macrophages, T cells and NK cells, and the subsequent activation and proliferation of fibrogenic effector cells. Fibrogenic effector cells include myofibroblasts derived from fibroblasts, fibrocytes and possibly cells from epithelial origin by epithelial-mesenchymal transition (EMT) (Rockey et al. 2015). Perpetuated myofibroblast activation results in excessive extracellular matrix deposition (Gabbiani et al. 1971; Gabbiani et al. 1976; Pakshir und Hinz 2018). Here, TGFβ1-induced fibroblast-myofibroblast-transdifferentiation and concomitant extracellular matrix deposition is described as the final common pathway of fibrosis (D'Urso und Kurniawan 2020). Besides TGFβ1, a plethora of other growth factors and the consecutive activation of developmental pathways in myofibroblasts orchestrates fibrotic tissue remodelling across organs (Ng et al. 2019):

Cardiac fibrosis is observed in a multitude of heart pathologies. E. g. following myocardial infarction, cardiac tissue remodelling is characterized by replacement of the myocardium with reactive interstitial fibrosis of infarction borders and uninjured myocardium with concomitant stiffening of the ventricular wall compromising organ function (Talman und Ruskoaho 2016). Moreover, myocardial fibrosis plays a role in heart insufficiency and atrial fibrillation (Mishra et al. 2013; Nattel 2017).

Lung fibrosis is the dominating pathogenetic mechanism underlying diffuse parenchymal lung diseases (DPLDs), but also interstitial lung diseases (ILDs). Moreover, peribronchial fibrosis is also present in asthma (Royce et al. 2012) and COPD (Barnes 2019), while. Endothelial fibrosis is described in Pulmonary Arterial Hypertension (PAH) (Samokhin et al. 2018; Thenappan et al. 2018).

Renal fibrotic processes of tubulointerstitial fibrosis and glomerular sclerosis, involved in chronic kidney disease (Humphreys 2018; Ruiz-Ortega et al. 2020), are characterized by fibrotic replacement of kidney parenchyma, affecting up to 10% of adults (Nogueira et al. 2017). Furthermore, the rare retroperitoneal fibrosis, as known as Morbus Ormond, is a progressive fibrosing condition characterized by a fibrotic retroperitoneal mass frequently associated with an ureteral obstruction of multiple etiologies (Vaglio und Maritati 2016).

Skin fibrosis is present in many skin pathologies of different origin including post-traumatic skin scarring and keloids as well as skin manifestation of autoimmune diseases, such as scleroderma (Do und Eming 2016; Andrews et al. 2016; Schulz et al. 2018). Furthermore, fibrotic tissue remodelling is underlying also a multitude of myopathic condition, such as Duchenne muscular dystrophy and age-related sarcopenia (MacDonald und Cohn 2012). Upon transplant organ rejection, minor human leukocyte antigen mismatches in allograft transplants can induce fibrosis associated with chronic organ dysfunction as pivotal obstacle to long term allograft survival (Wynn und Ramalingam 2012). E. g. in cardiac allografts, tissue remodelling involving fibrotic extracellular matrix deposition plays a role (Booth et al. 2012). Also in chronic kidney allograft rejection an inflammatory cascade involving macrophage activation immune cell influx triggers renal fibrogenesis (Vanhove et al. 2017). In lung grafts, the restrictive allograft syndrome presents with fibrotic remodelling of the alveolar lung parenchyma (Glanville et al. 2019).

Organ fibrosis is also reported as adverse effect of irradiation, therapeutic drugs, and diagnostic (contrast) agents. Compounds include chemotherapeutics such as bleomycin, cyclophosphamide, busulfan, immune checkpoint inhibitors, such as pembrolizumab

(Delaunay et al. 2017), as well as amiodarone and gadolinium (Farver und Zander 2018). Gadolinium-associated systemic fibrosis occurs in a minority of patients undergoing gadolinium-based contrast agent enhanced magnetic resonance imaging (MRI) and can manifest with fibrosis of skin, skeletal muscle and numerous visceral organs (Todd und Kay 2016; Wagner et al. 2016). The antiarrhythmic drug therapy with amiodarone results in a substantial number of patients in pulmonary fibrosis where amiodarone and its metabolites accumulate phospholipid-bound in membrane-rich intracellular structures leading to type II pneumocyte toxicity (Mason 1987; Papiris et al. 2010). Bleomycin is a chemotherapeutic agent that induces skin and pulmonary fibrosis is up to 10% of treated patients, due to low expression of the drug metabolizing bleomycin hydrolase in lung and skin (Nuver et al. 2005; Haas et al. 2008; Reinert et al. 2013). Furthermore, ionizing radiation-related tissue injury can result in organ fibrosis. Fibrotic tissue remodelling, for example, plays a role in long-term cutaneous changes of chronic radiation dermatitis (Hegedus et al. 2017). Thoracic irradiation imposes the risk of radiation-induced lung fibrosis (Bledsoe et al. 2017; Lierova et al. 2018) as irreversible end stage of radiation pneumonitis triggered by reactive oxygen species generation, type I pneumocyte apoptosis and the resulting wound healing response (Bledsoe et al. 2017; Lierova et al. 2018). Similarly, a severe complication of radiation therapy of hepatocellular carcinoma is the radiation-induced liver disease where hepatic fibrosis develops upon response of liver sinoid injury (Kim und Jung 2017). Despite a wide range of triggers known for fibrotic diseases, for a number of pulmonary fibrosis entities, including the Idiopathic Pulmonary Fibrosis, the etiology is unknown.

4.2. Idiopathic Pulmonary Fibrosis

Perpetuated organ fibrosis is best exemplified by the Idiopathic Pulmonary Fibrosis (IPF) (Hamman und Rich 1935). IPF is the most common diffuse parenchymal lung disease (DPLD) (American Thoracic Society, European Respiratory Society 2002) where fibrosis of the alveolar lung parenchyma progresses perpetually until the patient's death, on median 3-5 years post diagnosis (Kim et al. 2015a; Khor et al. 2020; Fujimoto et al. 2015). IPF is the most

lethal amongst the diffuse lung diseases (Antoniou et al. 2014). It is defined as “specific form of chronic, progressive fibrosing interstitial pneumonia of unknown cause, occurring primarily in older adults, limited to the lungs, and associated with the histopathologic and/or radiologic pattern of UIP” (Raghu et al. 2011).

IPF presents in patients with unexplained chronic exertional dyspnea and commonly presents with cough, bi-basilar inspiratory crackles and finger clubbing, typically occurring in their sixth or seventh decade of life (Raghu et al. 2011). IPF is more common in men than in woman. Smoking history as well as gastroesophageal reflux is highly prevalent in IPF patients, other risk factors associated with IPF are chronic viral infections, hepatitis, but also pulmonary comorbid conditions including emphysema, lung cancer or pulmonary hypertension (Baumgartner et al. 1997; Raghu et al. 2006; Fernandez Perez et al. 2010; Raghu et al. 2018).

4.2.1. Epidemiology

IPF prevalence in the United States of America estimates range from 14 to 27.9 cases per 100.000 using narrow case definitions, whereas prevalence estimates in Europe ranges from 1.25 to 23.4 cases per 100.000 in general population (Nalysnyk et al. 2012; Meyer und Nathan 2014). Annual incidence of IPF was estimated between 6.8 and 8.8 per 100.000 in the USA and between 0.22 and 7.4 per 100,000 in Europe. Incidence of IPF rises to more than 40 per 100,000, when only the population between 65 and 84 years is considered, however estimations incidence and prevalence are still difficult due to changed diagnostic criteria within the last decades. The estimated prevalence of IPF defines it as orphan disease under the US-American Orphan Drug Act and under the European Medicines Agency criteria for Orphan designation (Nalysnyk et al. 2012).

4.2.2. Usual Interstitial Pneumonia

The term "Usual Interstitial Pneumonia" (UIP) is defined as the pathologic finding of IPF (Hashisako und Fukuoka 2015). UIP is historadiologically defined by a specific combination of fibrosis with patchy involvement of parenchyma in fibrosis and architectural distortion of the

lung tissue. Radiologically, basal and predominantly subpleural honey combing, reticular pattern with peripheral traction bronchiectasis and bronchiolectasis are seen in HRCT in absence of imaging features suggesting alternative diagnosis (Lynch et al. 2018). Histopathologically, lung architecture remodelling by patchy, subpleural or paraseptal located dense fibrosis with frequent honeycombing and fibroblast foci observed at the interface of advanced fibrosis and normal lung tissue is seen (Farver und Zander 2018).

4.2.3. Diagnosis

IPF is considered in adult patients with chronic dyspnea on exertion, dry cough, bibasilar inspiratory 'Velcro'-like crackles without symptoms suggesting an underlying multisystem disease (Raghu et al. 2018). For diagnosis, the high-resolution CT (HRCT) plays a central role for the detection of UIP pattern (Lynch et al. 2018). If certain radiological diagnosis of UIP pattern cannot be made, lung tissue sampling and pathohistological assessment is performed. IPF diagnosis requires, besides the exclusion of ILDs of known etiologies, the presence of UIP patterns of HRCT or a specific combination of probably UIP or indeterminate HRCT pattern and histopathological patterns (Raghu et al. 2011; Meyer und Nathan 2014).

4.2.4. Therapy

While until the first decade of the 21st century anti-inflammatory therapies played a pivotal role in the treatment of idiopathic pulmonary fibrosis, treatment of IPF patients today is dominated by antifibrotic pharmacotherapies (Raghu et al. 2011). With the PANTHER-IPF study reporting increased mortality of a combination therapy of prednisone, azathioprine and N-Acetylcysteine (NAC) compared to placebo (Raghu et al. 2012), immunosuppressive and glucocorticoid therapies (American Thoracic Society (ATS), and the European Respiratory Society (ERS) 2000) were replaced as conventional IPF therapy by new antifibrotic medications (Raghu und Selman 2015). The tyrosine kinase inhibitor Nintedanib and pyridinone derivative Pirfenidone showed efficacy in slowing down patient's decline in forced vital capacity (FVC) (Richeldi et al. 2011; Richeldi et al. 2014; King et al. 2014). In 2021, the observation that nintedanib and

pirfenidone can slow down disease progression in progressive non-IPF-ILDs extended the application of the class of antifibrotic drugs beyond the disease entity IPF/UIP (Flaherty et al. 2019; Behr et al. 2021).

Lung transplantation remains the final therapeutic option for IPF patients (Lederer und Martinez 2018) and patients with other progressive lung diseases (Kapnadak und Raghu 2021). In conclusion, with no curative pharmacotherapy available (Raghu et al. 2011) and a mean survival time of 5 years post transplantation (Kapnadak und Raghu 2021), there is a high medical need for novel pharmacotherapies for IPF patients (Mora et al. 2017).

4.2.5. Pathophysiology

Significant efforts have been undertaken to unravel the pathophysiology of IPF disease progression to facilitate the development of novel antifibrotic therapies. The current concept of the IPF pathophysiology involves repeated alveolar epithelial cell injury that results in a perpetuated alveolar tissue wound healing response (Fernandez und Eickelberg 2012). Type 2 pneumocyte and macrophage secreted cytokines trigger a common final signaling pathway of fibrosis with fibroblast-myofibroblast-transdifferentiation and myofibroblast-mediated fibrotic extracellular matrix deposition (Eickelberg et al. 1999; Bonnans et al. 2014). The thickening and stiffening of the interstitial extracellular matrix results in an increased thickness of the air-blood-barrier and decreased compliance of the lung tissue leading to a limited diffusion capacity and a restrictive lung disease (King, JR et al. 2011)

4.3. Myofibroblast biology and TGFβ1 signalling

Despite the description of a multitude of cytokines such as connective tissue growth factor (CTGF), platelet-derived growth factor (PDGF), interleukin-11 (IL-11) and tumor necrosis factor alpha (TNFα), transforming growth factor β (TGFβ1) is widely accepted as the central regulator of fibroblast-myofibroblast-differentiation (Sheppard 2006). TGFβ1 is a cytokine of the TGF protein superfamily is predominantly secreted by bronchial epithelial cells, type 2 pneumocytes and macrophages (Yue et al. 2010). It binds to the TGFβ1 receptor activating the canonical

Smad2/3 signaling pathway through the TGFβ1 receptor 1 (Nakao et al. 1997; Aschner und Downey 2016) as well as multiple non-canonical signaling pathways. Those non-canonical signaling pathways include the mitogen-activated protein kinase (MAPK), Phosphoinositide 3-kinase (PI3K) / Akt, c-Jun N-terminal kinase (JNK), TGFβ activated kinase 1 (TAK1), tumor necrosis factor receptor-associated factor and Rho-like GTPase signaling (Zhang 2009; Zhao et al. 2020). Canonical and non-canonical TGFβ signaling triggers fibroblast-myofibroblast-transdifferentiation and upregulation of the extracellular matrix synthesis apparatus (Eickelberg und Laurent 2010). As central signaling pathway in the fibrosis pathophysiology the canonical Smad2/3-dependent TGFβ1 signaling has been extensively characterized: Briefly, the TGFβ1 signaling cascade can be activated by the binding of the activated TGFβ1 isoform to the TGFβ receptor heterotetrametric receptor complex comprising two TGFβ type I receptors and one TGFβ type II receptor. The receptor-ligand interaction effects the phosphorylation of Smad proteins by the cytoplasmic kinase domain of type I, in particular, the phosphorylation of the Smad proteins Smad2 and Smad3 (Hata und Chen 2016). Phosphorylated Smad2 and Smad3 couple with their coregulator Smad4. This Smad2/3-Smad4 complex translocates into the cell nucleus and serves there as a transcription factor regulating the expression of a multitude of genes involved in fibroblast-myofibroblast-transdifferentiation and extracellular matrix synthesis (Itoh et al. 2000). As a major cellular signaling pathway involved in embryonic development, cell differentiation and in the regulation of a plethora of other cell type-dependent cellular functions, Smad2/3 signaling is tightly regulated. Amongst a multitude of other regulating mechanisms, the ubiquitin E3 ligase SMURF2 has been shown to inhibit canonical TGFβ signaling by the ubiquitination of Smad3 subsequently impeding with the Smad3-Smad4 complex formation (Zhang et al. 2001; Bai und Ying 2020).

Additionally, the fibrotic extracellular matrix influences the behavior of cells in general and (myo-)fibroblasts in particular. Recently accumulated evidence supports the concept of the instructive extracellular matrix that influences tissue homeostasis in disease (Burgstaller et al. 2017). Fibrotic extracellular matrix deposited by myofibroblasts provides biochemical and biomechanical cues for cells to activate (myo)fibroblasts, perpetuating the fibrosis progression

in a profibrotic positive feedback loop (Parker et al. 2014), resulting in a dense interstitial accumulation of extracellular matrix of the alveolar lung tissue (Kulkarni et al. 2016). The aberrant myofibroblast behaviour and subsequent disruption of extracellular matrix homeostasis (Kulkarni et al. 2016; Parker et al. 2014b) mark the final common path of lung fibrosis leading to an excessively dense and stiff interstitial extracellular matrix in the alveolar pulmonary region.

4.4. Extracellular matrix of the lung (ECM)

The extracellular matrix is a complex network of cross-linked extracellular proteins that provide biophysical and biochemical cues regulating cell activity. (Naba et al. 2012). Extracellular matrix and ECM-associated proteins are summarized under the term *matrisome (Mecham 2011)*. The *matrisome* comprises fibrillar proteins, glycoproteins, and proteoglycans. Naba et. al (2012) defined a *core matrisome* excluding the *matrisome-associated proteins*. The human *core matrisome* has 278 genes (200 ECM glycoproteins, 43 collagens, 35 proteoglycans) and 778 *matrisome-associated* genes (176 ECM-affiliated proteins, 250 ECM regulators, 352 secreted factors) (Naba et al. 2012).

The extracellular matrix serves a multitude of functions in tissue homeostasis: It provides morphological tissue structure organizing cell groups and cell layers. It ensures the integrity of the tissue (Dunsmore und Rannels 1996; White 2015). Additionally, the ECM provides a chemical buffering capability and ensures water retention in the tissue to maintain the extracellular homeostasis (Frantz et al. 2010). Altogether the ECM plays a defining role in the cell's microenvironment (Lu et al. 2011). It influences various cellular responses including cell adhesion, cell spreading, cell proliferation, cell migration as well as cellular changes in cytoskeleton, the induction of cell polarity, and other cell differentiation-associated processes. In summary, the ECM plays a crucial role in regulating cellular behaviour, tissue homeostasis and organ function. Thus, a tight regulation of extracellular matrix synthesis and degradation is critical to maintain cells and tissue healthy (Stetler-Stevenson 1996). Deposition of extracellular matrix is regulated on various levels: a) ECM synthesis, involving the mRNA

transcription of matrisome genes, protein translation, and posttranslational modifications, b) ECM secretion, the vesicular transport of ECM components into the extracellular space, and c) ECM deposition itself involving the conversion of soluble into insoluble ECM components and their assembly into a three-dimensional network extracellularly, and d) ECM degradation (Laurent et al. 2007).

In the lung, the ECM serves as an important mechanical scaffold ensuring lung integrity during ventilation. Furthermore, the ECM compartmentalizes tissues by separating epithelium or endothelium from the interstitium and serves as physical barrier (Dunsmore und Rannels 1996). Here the extracellular matrix can be subdivided into the basement membranes and the interstitium.

The basement membrane is found abluminal of the layer of both airway and alveolar epithelial cells and surrounds the vascular endothelium (Dunsmore und Rannels 1996). As part of the pulmonary interstitium, the alveolar wall is composed of extracellular matrix and interjacent interstitial cells. Proteoglycans, elastin and mostly collagens (in particular collagen I, II, III, V, XI) determine the lung tissues rigidity and elasticity (Suki et al. 2011). Fibrillar proteins such as collagens and fibronectins contribute to the tensile strength of the lung tissue. Elastic fibers composed of elastin and fibrillin, fibulin and microfibril-associated glycoproteins amongst others provide the elastic recoil of the tissue, important for lung inflation and deflation. Furthermore, the ECM serves as reservoir for growth factors and other secreted signalling molecules forming gradients within the tissue driving pattern forming in tissue development and tissue homeostasis (Hynes und Naba 2012).

The importance of the pulmonary extracellular matrix of lung function is reflected by the heavy pathophysiological involvement of the ECM in chronic pulmonary diseases. Critical changes of extracellular matrix play a significant role in chronic obstructive pulmonary disease, pulmonary hypertension, asthma, and lung cancer, as well as in Idiopathic Pulmonary Fibrosis and other ILDs, where the changes in composition and quantity of ECM are very evident (**Figure 1**).

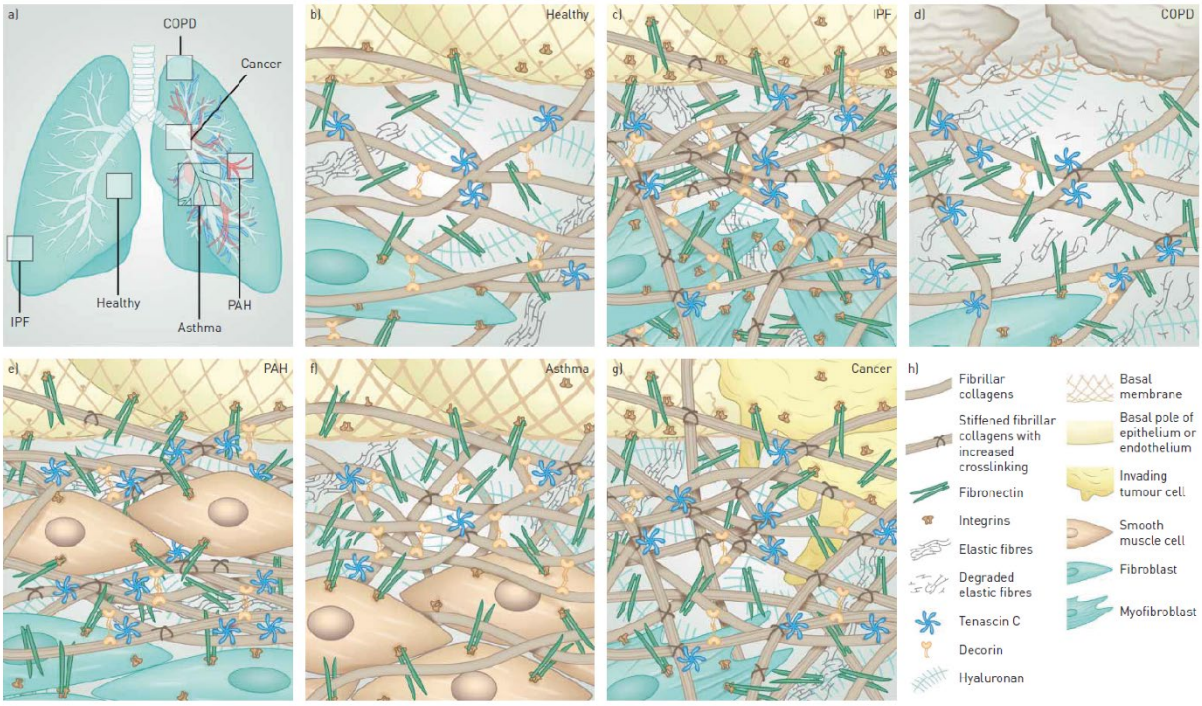

Figure 1: Pathological changes within the interstitial extracellular matrix (ECM) in the diseased lung.

(A) Overview of the lung and sites of disease formation. **(B)** Healthy interstitial ECM is maintained by the activity of resident fibroblasts and represents a loose meshwork of collagens, elastin and fibronectin anchored to the basal membrane of the epithelial cell layer. **(C)** In Idiopathic Pulmonary Fibrosis (IPF), fibroblasts transdifferentiate to highly contractile myofibroblasts, which deposit high levels of ECM molecules into the interstitium and dramatically increase ECM rigidity by enzymatic covalent crosslinking of collagen and elastin. **(D)** The hallmarks of pathological changes within the ECM in chronic obstructive pulmonary disease (COPD) are the extensive destruction of elastic fibers by ECM-degrading enzymes released by inflammatory cells, along with elevated levels of hyaluronan and tenascin C, and decreased deposition of decorin. The destruction of the epithelial cell layer leads to air space enlargements (emphysema). **(E)** In pulmonary arterial hypertension (PAH), remodelling of the ECM within the arterial wall is characterized by an increase in elastin and collagen fibers, fibronectin, and tenascin C, and hyperplasia of smooth muscle cells. **(F**) In asthma, the characteristic ECM changes take place beneath the bronchial epithelium and thickened basal membrane. In addition, smooth muscle cells undergo hyperplasia, and deposition of collagens, fibronectin, hyaluronan and decorin are increased. **(G)** In cancer, tumors at primary and metastatic sides are surrounded by an extensive stiff stroma that contains highly crosslinked collagens, and high levels of fibronectin, tenascin C and hyaluronan. **(H)** Legend depicting molecules and cell types. Reprinted from Burgstaller et al. 2017 including the figure legend.

4.5. Drug discovery in lung fibrosis

The overwhelming majority of antifibrotic drug discovery approaches for IPF are guided by target-based drug discovery (TDD), where the single genes/proteins, causally involved in lung fibrosis disease mechanisms, are identified (Patel 2013; Liu et al. 2016). This is often determined in target gene deficient rodents and cell cultures using *in-vivo* and *in-cellulo* lung fibrosis models. Based on this information, therapeutics targeting the respective proteins are developed or selected and evaluated in clinical trials. While TDD was responsible for important drug discovery breakthroughs (Capdeville et al. 2002), recently phenotypic drug discovery has been over-proportionally successfully in the discovery of small-molecule, first-in-class medicines (Swinney 2013).

The phenotypic drug discovery approach identifies small molecule therapeutics, unbiased of a molecular mechanism of action or target protein information (Zheng et al. 2013). Here, often cell culture-based disease models are used to identify molecules that can alter disease-specific cell behaviour *in-cellulo*. (Horman 2016). Phenotypic drug discovery requires drug screening assays recapitulating the complexity of the replicated disease biology (Vincent et al. 2015) but also high-throughput (HT) suitability (Sittampalam et al. 2004) in order to confidently identify novel therapeutics interfering with key mechanisms of disease.

4.6. Drug screening in drug discovery

Drug screening describes processes to identify drugs with a particular biological activity from (large) libraries of chemicals to select candidate drugs, so-called hit compounds, for further preclinical and clinical testing. Drug screenings play a critical role in systematic drug discovery efforts. Typically, drug screening libraries comprising thousands to hundreds of thousands of chemicals are used. Examples for drug screening libraries are the Prestwick Chemical Library (to date 1520 compounds) (Poroikov und Filimonov 2002) or the European Chemical Biology Library Diversity Library (96,096 compounds) (Brennecke et al. 2019; European Research Infrastructure Consortium (ERIC) for chemical biology and early drug discovery 2021). These

drug screening libraries are tested routinely against a high-throughput screening assay to identify library compounds with a specific pharmacological activity.

In comparison to conventional biomolecular or pharmacological assays, drug screening assays must be high-throughput suitable and apt for conducting tests on thousands of compounds per day. This is typically achieved by automated robotic plate and liquid handling systems as well as automated data acquisition and data processing (Hughes et al. 2011). As an increasing amount of drug screening assays are utilizing conventional or immunofluorescence microscopy as readouts, a detailed image analysis of the micrographs acquired in the screening process evolved under the term high-content (HC) screening. As microscopic images provide more information than oligo-dimensional measurements from conventional e. g. colorimetric assay readouts, high-content screening using microscopy and imaging can facilitate the selection of hit compounds for further follow-up tests (Fraietta und Gasparri 2016).

4.7. Preclinical drug development

Prior to investigations of drug candidates in clinical trials, hit compounds found in drug discovery studies, undergo a lengthy development process (Bleicher et al. 2003). Typically, compounds undergo extensive structure-activity-relationship studies to improve the pharmacological activity of the compound. Certain chemical modifications of a hit compound's pharmacophores often improve binding geometries between the compound and the pharmacological target, and thus lead to a higher compound potency (Keserü und Makara 2009). Optimizations of compound activity considering the compound's physiochemical properties can yield improved drug candidates. These can be used for further tests of the compound's pharmacological activity and pharmacokinetic and pharmacodynamic properties (Keseru und Makara 2006). Only after completion of an array of preclinical tests (Hughes et al. 2011), compounds can be considered for clinical trials.

4.8. Lung fibrosis models

In biomedicine, experimental lung fibrosis models are essential for interrogation of disease mechanisms. Here, both, experimental *in-vivo* animal models and *in-vitro* models of disease, play an important role (Jenkins et al. 2017). Examples for *in-vitro* models are cell culture and organoid disease models, while more complex disease models are *in-vivo* animal models as well as *ex-vivo* tissue culture models (Degryse und Lawson 2011; Skronska-Wasek et al. 2017).

4.8.1. *In-vitro* models for lung fibrosis

In-vitro models can recapitulate cellular aspects of lung fibrogenesis such as activation of lung fibroblast activation, fibroblast-myofibroblast-transdifferentiation and myofibroblast behavior, such as migration, invasion, contractility, and extracellular matrix synthesis (White 2015). Most often transcriptomic or proteomic changes of cells are assessed by cDNA-PCR, western blotting techniques or immunofluorescence staining of cells (Woodcock et al. 2019). More complex functional assays which assess cell functions and cell behaviour by microscopic means are also used (Oehrle et al. 2015).

While extracellular matrix expression plays a major role in *in-vitro / in-cellulo* lung fibrosis models, few assays have been developed as or converted into a drug screening suitable assay format (Chen et al. 2009; Rønnow et al. 2020). Therefore, no *in-cellulo* lung fibrosis model recapitulating extracellular matrix deposition is reported in a drug screening suitable assay format, to date.

4.8.2. Animal models for lung fibrosis

The most commonly used animal disease model for lung fibrosis remains the murine bleomycin-induced lung fibrosis model (Adamson und Bowden 1974). Here, a temporary pulmonary fibrosis is typically induced in (often male) mice by the intratracheal installation of bleomycin sulfate (Liu et al. 2017). Bleomycin, a chemotherapeutic antibiotic, induces DNA damage by the production of superoxide and hydroxide free radicals (Boger und Cai 1999). This trigger an inflammatory lung tissue response and fibrosis development (Chaudhary et al.

2006). Here, low levels of the bleomycin inactivating enzyme bleomycin hydrolase in the lung tissue exacerbate this organ specific effect – analogue to the bleomycin-induced lung fibrosis in humans as adverse event in different chemotherapy regimens (Froudarakis et al. 2013). Notably, human bleomycin-induced fibrosis is irreversible, while murine bleomycin-induced fibrosis resolves after approximately 28 days post instillationem (Izbicki et al. 2002). Complementary animal models for lung fibrosis such as the radiation-, silica-, asbestosis-, fluorescent isothiocyanate, or adenoviral gene transfer of TGFβ1-induced lung fibrosis models as well as animal species other than mice (e. g. dogs, cats, donkeys and horses) are less commonly used (B Moore et al. 2013; Tashiro et al. 2017).

While *in-vivo* lung fibrosis models, foremost the murine bleomycin-induced lung fibrosis model, have been extensively used in antifibrotic drug discovery (Jenkins et al. 2017), a variety of differences to human lung fibrosis impairs translation of knowledge of the murine bleomycin induced lung fibrosis biology into human IPF disease (Moeller et al. 2008). This is confirmed by the frequent discordance of between observations in murine fibrosis models and human disease (Wang et al. 2015) .

4.8.3. Tissue culture models for lung fibrosis

Cultures of resected lung tissue were established as early as the 1987 (Placke und Fisher 1987). Here, resected lung tissue from model animals or humans were prepared for *ex-vivo* cultures. *Ex-vivo* culture of tissue enables experimentation and analysis of the tissue that are not feasible or harder to perform *in-vivo* (Robyn L. Fisher et al. 1994).

With *ex-vivo* lung tissue models being multicellular and containing most cell types and extracellular tissue scaffold of *in-vivo* lung tissue, they closely resemble native physiological lung architecture (Alsafadi et al. 2020). Furthermore, *ex-vivo* disease tissue cultures can reduce the number of animals needed for experimentation according to the 3R-paradigm (Lehmann et al. 2018). Therefore, *ex-vivo* murine lung tissue models are used to model lung fibrosis (Lehmann et al. 2017) but also other pulmonary diseases (Ebsen et al. 2002; Cooper et al. 2011; Koch et al. 2014; Donovan et al. 2015; Skronska-Wasek et al. 2017).

Unlike in *in-vivo* experiments, *ex-vivo* lung tissue cultures enable the use of human lung tissue. Thus, human *ex-vivo* tissue cultures are specifically used to overcome inter-species-differences and the associated challenges translating biomedical findings in mice to humans (Alsafadi et al. 2020). As 90% of drugs reported to be efficient in the murine bleomycin model, fail in clinical trials (Moeller et al. 2008; van der Worp et al. 2010), the development of novel alternative models for human lung fibrosis are urgently needed (Spagnolo und Maher 2017). Therefore, human lung tissue cultures were used to perform pneumotoxicological studies but recently also became an important tool for investigations in lung fibrosis (Alsafadi et al. 2017) as well as in other pulmonary diseases (Switalla et al. 2010; Banerjee et al. 2012; Uhl et al. 2015).

Here, human tissue culture systems, such as three-dimensional lung tissue cultures prepared from precision cut lung slices (PCLS) and accompanying novel disease models could potentially bridge between murine *in-vivo* disease models and human ILD biology (Alsafadi et al. 2020) .

5. AIMS OF THE STUDY

There is an urgent medical need for novel antifibrotic drug candidates. Phenotypic drug discovery approaches have proven useful in the past for the development of novel drugs.

Aims of this study were

1. the development of a high-content suitable cellular fibrosis model of fibrotic ECM deposition
2. the identification of potential small molecule therapeutics inhibiting fibrotic ECM deposition by phenotypic drug screening
3. structure-activity-relationship study of an antifibrotic drug candidate
4. validation of antifibrotic activity of an antifibrotic drug candidate in a human tissue culture model of lung fibrosis.

6. MATERIALS

6.1. Laboratory equipment and software

Table 1: Laboratory equipment

Product	Manufacturer
Benchtop devices	
Corning LSE Mini Microcentrifuge, 120V	Corning, Wiesbaden, Germany
Analytical scale XS20S Dual Range	Mettler Toledo, Gießen, Germany
Plate centrifuge 5430	Eppendorf, Hamburg, Germany
Centrifuge MiniSpin plus	Hettich, Tuttlingen, Germany
Centrifuge Rotina 420R	Hettich, Tuttlingen, Germany
Fisher Science Education 4-Way Microtube Racks	ThermoFisher Scientific, Darmstadt, Germany
Eppendorf Thermomixer compact	Eppendorf, Hamburg, Germany
Shaker Duomax 1030	Heidolph Instruments, Schwabach, Germany
Roll mixer	VWR International, Darmstadt, Germany
Vortex Mixer	IKA, Staufen, Germany
VWR Tube Rotater and Rotisseries	VWR International, Darmstadt, Germany
pH meter InoLab pH 720	WTW, Weilheim, Germany
Centrifuge with cooling, Micro200R	Hettich, Tuttlingen, Germany
Magnetic stirrer KMO 2 basic	IKA, Staufen, Germany
Cooling/freezing devices	
-80°C freezer U570 HEF	New Brunswick/ Eppendorf, Hamburg, Germany
-20°C freezer MediLine LGex 410	Liebherr, Biberach, Germany
Liquid nitrogen cell tank BioSafe 420SC	Cryotherm, Kirchen/Sieg, Germany
Dry ice container Forma 8600 Series, 8701	ThermoFisher Scientific, Darmstadt, Germany

Ice machine ZBE 110-35	Ziegra, Hannover, Germany
Fridge MediLine LKv 3912	Liebherr, Biberach, Germany
Liquid handling	
INTEGRA Assist Plus	INTEGRA Biosciences, Biebertal, Germany
INTEGRA Viaflo II Pipette	INTEGRA Biosciences, Biebertal, Germany
Multipipette Stream	Eppendorf, Hamburg, Germany
Pipettes Research Plus	Eppendorf, Hamburg, Germany
Ultra-pure water supply MilliQ Avantage A10	Merck Millipore, Darmstadt, Germany
Cell and tissue culture	
CO2 cell Incubator BBD6620	ThermoFisher Scientific, Darmstadt, Germany
Water bath Aqua Line AL 12	Lauda, Lauda-Königshofen, Germany
Nalgene Freezing Container (Mr. Frosty)	Omnilab, Munich, Germany
Cell culture work bench Herasafe KS180	ThermoFisher Scientific, Darmstadt, Germany
Vibratome Hyrax V55	Zeiss, Jena, Germany
Autoclave DX-45	DX-45 Systec, Wettenberg, Germany
Autoclave VX-120	Systec, Wettenberg, Germany
RNA analysis	
NanoDrop 1000	PeqLab, Erlangen, Germany
Mastercycler Nexus	Eppendorf, Hamburg, Germany
Light Cycler LC480II	Roche Diagnostic, Mannheim Germany
Protein Analysis	
Film developer Curix 60	AGFA, Morsel, Belgium
Gel imagine system ChemiDoc XRS+	Biorad, Hercules, USA
Plate reader Sunrise	Tecan, Crailsheim Germany
Power Supply Power Pac HC	Biorad, Hercules, USA

Microscopy	
Axiovert 40C microscope	Zeiss, Jena, Germany
Confocal microscope LSM710	Zeiss, Jena, Germany
AxioObserver.Z1	Zeiss, Jena, Germany
EC Plan-Neofluar 20x/0.8 NA	Zeiss, Jena, Germany
LD C-Apochromat 40x/1.1 NA	Zeiss, Jena, Germany
LCI PLN-NEOF DICIII 63x/1.30 NA	Zeiss, Jena, Germany
Zeiss Incubator Chamber	Zeiss, Jena, Germany
Vibratome Hydrax V50	Zeiss, Jena, Germany
Hyrax CU 65	Zeiss, Jena, Germany
Synthetic Single Crystal Sapphire	Delaware Diamond Knives, Wilmington, USA

Confocal laser scanning microscope setup

The confocal laser scanning microscope LSM710 system (Zeiss) with inverted AxioObserver.Z1 stand equipped with phase-contrast and epi-illumination optics and operated by ZEN2009 software (Carl Zeiss) was used. Microscope objectives are the EC Plan-Neofluar 20x/0.8 NA (Carl Zeiss), the LD C-Apochromat 40x/1.1 NA water objective lens (Zeiss) and the LCI PLN-NEOF DICIII 63x/1.30 NA water objective lens (Zeiss). For live cell imaging the microscope was equipped with an incubation chamber to maintain cell culture conditions with an incubation temperature 37 °C and 5 % (v/v) CO_2 concentration.

Table 2: Software

Product	Manufacturer
Adobe InDesign	Adobe, Mountain View, USA
AxioVision	Carl Zeiss Microscopy, Jena, Germany
CellProfiler version v3.1.8	Broad Institute of MIT and Harvard, Cambridge, USA

GraphPad Prism v5-8	GraphPad Software, San Diego, USA
Imaris 9.0 software	Bitplane, Zurich, Switzerland
LightCycler 480 SW 1.5	Roche Molecular Systems, Pleasanton, USA
Magelan Software	Tecan, Männedorf, Switzerland
Microsoft Office	Microsoft, Redmond, USA
Image Lab Software	Biorad, Hercules, USA
ZEN Digital Imaging for Light microscopy Software	Carl Zeiss Microscopy, Jena, Germany
ACD/ChemSketch	Advanced Chemistry Development, Inc., Toronto, Canada

6.2. Consumables

Table 3: Consumables

Product	Manufacturer	Cat. No.
125 µL GripTips	INTEGRA	6464
15ml / 50ml Falcon Tube	BD Bioscience, Heidelberg, Germany	352070
384-well CellCarrier plates	Perkin Elmer	6007550
50 mL reagent reservoirs	Corning, New York, USA	4870
96-well imaging plates, Falcon		353219
Amicon Ultra 3K-0.5 mL centrifugal filters	Merck Millipore, Darmstadt, Germany	UFC500396
Peripheral venous catheter	B. Braun Melsungen AG	4268113 S-01
PVDF membrane	Merck Millipore, Darmstadt, Germany	IPVH00010
Sterile reagent reservoirs	INTEGRA	4311
Vasofix Braunüle 18 G	B. Braun Melsungen AG	4268130B
30 mL NORM-INJECT	Henke Sass Wolf	4830001000

Guarded disposable scalpels, sterile	Swann-Morton	No E/11
Loctite 406 glue	Henkel	406
Disposable Biopsy Punch	pfm medical	48401
0.5 mL, 1.5 mL, 2.0 mL reaction tubes	Eppendorf, Hamburg, Germany	
5 mL, 10 mL, 25 mL, 50 mL measuring pipettes, sterile for single use	VWR International, Darmstadt, Germany	
5 mL, 25mL syringes	Neolab, Heidelberg, Germany	
Cell culture dishes	Corning, Thermo Fisher Scientific, Schwerte, Germany	
Cell culture multi-well plates	TPP Techno Plastic Producers, Trasadingen, Switzerland	
Glass Pasteur pipettes	VWR International, Darmstadt, Germany	
Micropipette tips	Eppendorf, Hamburg, Germany	
Filter Tips	Biozym Scientific, Hessisch Oldendorf, Germany	
Combitips advanced	Eppendorf, Hamburg, Germany	
Nalgene cryogenic tubes	Thermo Fischer Scientific, Waltham, MA	
Hyperfilm ECL Film	Amersham, GE Healthcare, Freiburg, Germany	
PCR plates, 96-well plate	Kisker Biotech, Steinfurt, Germany	
Sealing foils for PCR plates	Kisker Biotech, Steinfurt, Germany	

Table 4: Reagents and chemicals

Product	Manufacturer	Cat.-No.
0.25% Trypsin - EDTA solution	Sigma-Aldrich, Taufkirchen, Germany	5001213
2-phospho ascorbate	Sigma-Aldrich, Taufkirchen, Germany	49752

Agarose, low gelling temperature	Sigma-Aldrich, Taufkirchen, Germany	A9414-100G
Ammonium peroxydisulfate (APS)	AppliChem, Darmstadt, Germany	A0834,0250
Amphotericin B	Sigma-Aldrich, Taufkirchen, Germany	A2942-100ML
Bovine serum albumin (BSA)	Sigma-Aldrich, Taufkirchen, Germany	A3059-50G
Desoxyribonucleotides mix (dNTPs)	Applied Biosystems, LifeTechnologies, Carlsbad, USA	N8080007
Dimethyl sulfoxide (DMSO)	Sigma-Aldrich, Taufkirchen, Germany	D4540-500ML
Dithiothreitol (DTT)	AppliChem, Darmstadt, Germany	A2948,0010
DMEM F-12	Gibco Life Technologies	1132033
DNase I AppliChem	AppliChem, Darmstadt, Germany	A3778,0100
ECL Plus Western Blotting Substrates	Pierce, Thermo Fisher Scientific, Schwerte, Germany	34087, 34095 34076,
Ethanol	AppliChem, Darmstadt, Germany	1.00983.1000
Fetal Bovine Serum (FBS)	PAN Biotech	P30-3702
Isopropanol	AppliChem, Darmstadt, Germany	A0900,1000
Lipofectamine RNAi Max	Invitrogen, Life Technologies, Carlsbad, USA	13778-075
Methanol	AppliChem, Darmstadt, Germany	1.06009.2500
Non-fat dried milk powder	AppliChem, Darmstadt, Germany	A0830,1000
Nonidet P-40	AppliChem, Darmstadt, Germany	A1694,0250
Paraformaldehyde	Sigma-Aldrich, Taufkirchen, Germany	15,812-7

Penicillin/Streptomycin	Gibco, Life Technologies	15140122
Random hexamers	Invitrogen, Life Technologies, Carlsbad, USA	N8080127
Recombinant TGFβ1	R&D Systems, Minneapolis, USA	240-B-002
RNase inhibitor 20U/µL	Invitrogen, Life Technologies, Carlsbad, USA	N8080119
Roche complete mini protease inhibitor cocktail	Roche Diagnostics, Mannheim, Germany	11697498001
Thiazolyl Blue Tetrazolium	Sigma-Aldrich, Taufkirchen, Germany	M5655-1G
Triton X-100	AppliChem, Darmstadt, Germany	A1388,1000
Low-melting agarose	Sigma-Aldrich, Taufkirchen, Germany	A9414
Restore Plus Western Blot Stripping	Thermo Fisher Scientific, Schwerte, Germany	46430

6.3. Chemicals

Table 5: Compounds for pharmacological testing

Product	Manufacturer	Cat. No.
EDHB / ethyl 3,4-dihydroxybenzoate	Sigma-Aldrich, Taufkirchen, Germany	E24859-5G
Tranilast / N-(3',4'-dimethoxycinnamoyl)-anthranilic-acid	SelleckChem, Houston TX, USA	S1439
Compound 1: 2-[(3,4-dimethoxy-benzoyl) amino]benzoic acid	Hit2lead.com / ChemBridge	5131540
Compound 2: N,3-bis(3,4-dimethoxy-phenyl) acrylamide	Hit2lead.com / ChemBridge	6067289
Compound 3: Methyl 2-{[3-(3,4,5-trimethoxyphenyl)acryloyl]amino} benzoate	Hit2lead.com / ChemBridge	6864264

Compound 4: N-(2-butoxyphenyl)-3-(3,4-dimethoxyphenyl)acrylamide	Hit2lead.com / ChemBridge	7184876
Compound 9: ethyl 2-{[3-(3,4,5-trimethoxyphenyl)acryloyl]amino}benzoate	Hit2lead.com / ChemBridge	6800388
Compound 10: ethyl 3-{[3-(3,4,5-trimethoxyphenyl)acryloyl]amino}benzoate	Hit2lead.com / ChemBridge	6809494
Compound 11: methyl 4-{[3-(3,4,5-trimethoxyphenyl)acryloyl]amino}benzoate	Hit2lead.com / ChemBridge	6830366
Compound 12: N-(2-butoxyphenyl)-3-(4-ethoxy-3-methoxyphenyl) acrylamide	Hit2lead.com / ChemBridge	7122430
Compound 13: 3-(4-butoxyphenyl)-N-(2,4-dimethoxyphenyl)acrylamide	Hit2lead.com / ChemBridge	7382109
Compound 14: N-(4-butoxyphenyl)-3-(3,4-dimethoxyphenyl)acrylamide	Hit2lead.com / ChemBridge	5771568
Compound 15: 3-(4-butoxyphenyl)-N-(3,4-dimethoxyphenyl)acrylamide	Hit2lead.com / ChemBridge	7412534
Compound 16: N-(2-Butoxyphenyl)-3-phenylprop-2-enamide	Mcule, Inc., Palo Alto, USA	MCULE-9166507278
Compound 17: N-(2-Butoxyphenyl)-3-phenylprop-2-enamide	Mcule, Inc., Palo Alto, USA	MCULE-9550766187
Compound 18: N-(2-Butoxyphenyl)-3-(4-methoxyphenyl)prop-2-enamide	Mcule, Inc., Palo Alto, USA	MCULE-9282677202
Compound 19: N-(2-propoxyphenyl)-3-(3,4-dimethoxyphenyl)acrylamide	Mcule, Inc., Palo Alto, USA	MCULE-8837428659
Compound 20: N-(2-ethoxybutoxyphenyl)-3-(3,4-dimethoxyphenyl)acrylamide	Mcule, Inc., Palo Alto, USA	MCULE-5507319887
Compound 24-35	synthesized at the Laboratory of Prof. Dr. Oliver Plettenburg, Institute für Medicinalchemie, Hannover, Helmholtz Center Munich, as described in Gerckens et al. 2021.	

The drug screening library “FDA-Approved Drug Library (1509 compounds)” (Cat.-No. HY-L022) was purchased from MedChemTronica, Sollentuna, Sweden. For the drug screening, the drug screening library was prepared by dissolving all compound to reach a 10 mM stock solution in 100 % DMSO.

6.4. Buffers and solutions

Tris-Glycine (‘Lämmli’) loading buffer (6x)

Substance	Concentration/amount
Glycerol	60% (v/v)
SDS	12% (w/v)
Bromophenol blue	0.06% (w/v)
Tris/HCl, pH 6.8	375 mM
DTT	600 mM

Phosphate buffered saline (PBS) pH 7.4 (10x)

Substance	Concentration/amount
NaCl	1.37 M
KCl	27 mM
Na_2HPO_4	100mM
KH_2PO_4	20mM

Radio-immunoprecipitation assay (RIPA) buffer

Substance	Concentration/amount
Tris-Cl pH 7.4	50mM
NaCl	150mM
NP40	1% (v/v)
Na-deoxycholate	0.25% (v/v)

Sodium dodecyl sulphate (SDS) solution (20%, w/v)

Substance	Concentration/amount
SDS	200g
Millipore-H_2O	1 L

SDS polyacrylamide gel electrophoresis (SDS-PAGE) Running buffer

Substance	Concentration/amount
Tris/HCl, pH 7.4	250 mM
Glycine	1.92 M
SDS	1% (w/v)

SDS-PAGE Stacking Gel (4%)

Substance	Concentration/amount
Millipore-H_2O	1.8 mL
0.5 M Tris/HCl pH 6.8	750 µL
20 % SDS	15 µL
Acrylamide	400 µL
10 % APS	15 µL
TEMED	3 µL

SDS-PAGE Separation Gels (10%, 12%)

Substance	Concentration/amount	
	10%	**12%**
Millipore-H_2O	3.7 mL	3.1 mL
1.5 M Tris/HCl pH 8.8	2.25 mL	2.25mL
20 % SDS	45 µL	45 µL
Acrylamide	3 mL	3.6 mL
10 % APS	30 µL	30 µL
TEMED	6 µL	6 µL

Transfer buffer (1x)

Substance	Concentration/amount
Tris/HCl	25 mM
Glycine	192 µM
Methanol	10% (v/v)

Tris-buffered saline (TBS) buffer (10x)

Substance	Concentration/amount
Tris/HCl pH 7.4	10 mM
NaCl	150 mM

TBS-TWEEN 20 (TBS-T) buffer (1x)

Substance	Concentration/amount
10x TBS	10%
TWEEN 20	0.1%
Milliporse-H_2O	89,9%

5 % Milk Blocking Solution

Substance	Concentration/amount
Skim milk powder	10% (w/v)
1x TBS-T	90% (w/v)

4 % Paraformaldehyde Solution

4 % (w/v) paraformaldehyde was prepared in 1x PBS.

6.5. Antibodies and dyes

Table 6: Primary antibodies for Western blot

Antigen name	Host/Clonality	Dilution	Manufacturer	Cat.-No.
αSMA	Mouse/mc	1:5000	Sigma-Aldrich, Taufkirchen, Germany	A5228
Collagen I	Rabbit/pc	1:2000	Rockland Immunochemicals Inc., Pottstown, USA	600-401-103-0.5
Collagen III	Rabbit/pc	1:1000	Rockland Immunochemicals Inc., Pottstown, USA	600-401-105-0.1
Collagen V	Mouse/mc	1:500	Santa Cruz Biotechnology Inc., Dallas, USA	sc-166155
Fibronectin	Rabbit/pc	1:1000	Santa Cruz Biotechnology Inc., Dallas, USA	sc-9068
Fibulin-1	Mouse/mc	1:500	Santa Cruz Biotechnology Inc., Dallas, USA	sc-25281

Table 7: Horse radish peroxidase-coupled secondary antibodies for Western blots

Antigen name	Host	Dilution	Manufacturer	Cat.-No.
Mouse IgG	Sheep	1:15,000	GE Healthcare	NA931V
Rabbit IgG	Donkey	1:15,000	GE Healthcare	NA934V
βActin	Mouse	1:15,000	Sigma-Aldrich, Taufkirchen, Germany	A3854

Table 8: Fluorophore-labeled secondary antibodies for immunofluorescence staining

Antigen name	Fluorophore	Host/Clonality	Dilution	Manufacturer	Cat.-No.
Mouse IgG	AF488	donkey	1:250	Invitrogen, LifeTechnologies, Carlsbad, USA	A21202
Mouse IgG	AF568	donkey	1:250		A11004
Rabbit IgG	AF	goat	1:250		A11011

Table 9: Labeled antibodies for direct immunofluorescence staining and dyes

Antigen name	Fluorophore	Host/Clonality	Manufacturer	Cat.-No.
αSMA	Cy3	Mouse/mc	Sigma-Aldrich, Taufkirchen, Germany	C6198-2ML
Collagen V	AF488	Mouse/mc	Sigma-Aldrich, Taufkirchen, Germany	sc-166155AF488
Fibulin-1	AF647	Mouse/mc	Santa Cruz Biotechnology Inc., Dallas, USA	sc-25281AF647
Phalloidin	AF568	-	Invitrogen, LifeTechnologies, Carlsbad, USA	A12380
4',6-diamidino-2-phenylindole			Sigma-Aldrich, Taufkirchen, Germany	D9564
Hoechst-33342	-	-	Sigma-Aldrich, Taufkirchen, Germany	B2261
Calcein	-	-	Biotium Inc., Fremont, USA	#30002

AlexaFluor-555 conjugation of the Collagen I antibody was achieved using the AlexaFluor-555 Protein Labeling Kit (Invitrogen, Cat.-No. A20174). Labelling efficacy was controlled by photometry.

6.6. Primary cells

Primary human lung fibroblasts (phLFs), derived from peritumor tissue of patients undergoing lobectomy or derived from explanted IPF patient lungs, were obtained from the Munich Lung Tissue cohort of the BioArchive CPC-M at the University Hospital Großhadern of the Ludwig

Maximilian University (Munich, Germany) and by the Asklepios Biobank of Lung Diseases (Gauting, Germany). Participants provided written informed consent to participate in this study, in accordance with approval by the local ethics committee of the LMU, Germany (Project 333-10, 454-12). Commercially available primary dermal fibroblasts were obtained from Zen Bio, Durham NC, USA (Cat. No. DF-F).

Table 10: Patient characteristics of tissue donors for phLF isolations

Pseudonym	Age at explantation	Sex	Diagnosis
IPF#1	46 years	male	Idiopathic Pulmonary Fibrosis
IPF#2	63 years	male	Idiopathic Pulmonary Fibrosis
IPF#3	63 years	female	Idiopathic Pulmonary Fibrosis
IPF#4	55 years	male	Idiopathic Pulmonary Fibrosis
IPF#5	48 years	female	Idiopathic Pulmonary Fibrosis

6.7. Primers

Table 11: qPCR primers for human genes

Gene	Sequence	
FBLN1	fw	5´-AGA GCT GCG AGT ACA GCC T-3´
	rev	5´-CGA CAT CCA AAT CTC CGG TCT-3´
COL1A1	fw	5´-CAA GAG GAA GGC CAA GTC GAG-3´
	rev	5´-TTG TCG CAG ACG CAG ATC C-3´
COL5A1	fw	5´-CTT CAA GGT TTA CTG CAA C-3´
	rev	5´-CCC TTC GGA CTT CTT G-3´
ACTA2	fw	5´-CGA GAT CTC ACT GAC TAC CTC ATG A-3´
	rev	5´-AGA GCT ACA TAA CAC AGT TTC TCC TTG A-3´
GAPDH	fw	5´-TGA CCT CAA CTA CAT GGT TTA CAT G-3´
	rev	5´-TTG ATT TTG GAG GGA TCT CG-3´

HPRT	fw	5´-AAG GAC CCC ACG AAG TGT TG-3´
	rev	5´-GGC TTT GTA TTT TGC TTT TCC A-3´

fw: forward primer; **rev:** reverse primer

6.8. Short interfering RNA (siRNA)

siRNA	Manufacturer	Cat.-No.
Silencer Pre-designed Smurf2	Ambion, Life Technologies; USA	4390843
Silencer Negative control No. 1	Ambion, Life Technologies; USA	AM4611

6.9. Standards and Kits

Product	Manufacturer	Cat.-No.
Protein marker V	Peqlab, Erlangen, Germany	27-2211
BCA Protein Assay Kit	Pierce, Thermo Fisher Scientific, Schwerte, Germany	10741395
Viability/Cytotoxicity Assay Kit for Animal Live and Dead Cells	Biotium, Fremont, USA	3002
PeqGold RNA kit	Peqlab, Erlangen, Germany	12-6834-02
GeneAMP PCR kit	Applied Biosystems, LifeTechnologies, Carlsbad, USA	N8080192
LightCycler 480 SYBR Green I Master	Roche Diagnostics, Mannheim, Germany	4887352001
Human IL-8/CXCL8 DuoSet ELISA	R&D Systems, Minneapolis, USA	DY208-05

7. Methods

7.1. Cell culture

7.1.1. Culture, sub-culturing, and cryopreservation of primary cells

Cells were cultured in 15 cm cell culture dishes with DMEM F-12 medium with 20% (v/v) FBS, 100 IU/mL penicillin and 100 µg/mL streptomycin at 37°C and room air with 5% CO_2. Medium was changed every 2-3 days. Cells were sub-cultured at 80-90% confluency in a ratio 1:5-1:6. Cells were used until passage 8. Cryopreservation medium was prepared from 90% (v/v) FBS and 10% (v/v) DMSO. For cryopreservation, 0.5-1.0 million cells were suspended of 1mL or cryopreservation medium and frozen slowly using methanol filled Mr. Frosty container. For reseeding, phLFs were thawed at 37 °C and cryopreservation medium was removed and cells were plated in culture medium. Dermal fibroblasts were cultured according to the manufacturer's instructions.

7.1.2. ECM deposition assay

6000 cells per well were seeded in a 384-well CellCarrier plates. After 24 h cells were starved in serum-reduced DMEM F-12 medium with 1% (v/v) FBS, 100 IU/mL penicillin, 100 µg/mL streptomycin and 0.1 mM 2-phosphoascorbate. Following a 24 h incubation period, cells were treated with or without 1 ng/mL TGFβ1 and with a small molecule drug or an appropriate vehicle control. Following 72 h of incubation, medium was exchanged for serum-reduced DMEM F-12 medium with 1 µg/mL of labelled Collagen V, Fibulin-1 antibody, and Hoechst and 0.66 µg/mL of Collagen I antibody. After 4 h of incubation at 37 °C cells were washed three times with PBS and fixed with paraformaldehyde (PFA). In each step, solutions were removed from the well, by manual inversion of the plate. All automated pipetting steps with the INTEGRA Assist Plus were performed at a dispense speed of 9.5 µL/s in order to ensure the integrity and attachment of the deposited ECM to the culturing surface within the wells of the 384-well plates. Only for the cell seeding step, automated liquid handling was performed at 89.3 µL/s, where

no cells and ECM were in danger of detachment. Automated immunofluorescence imaging was performed using a confocal laser scanning microscope for three-dimensional image acquisition (1024 px x 1024 px x 9 px covering a space of 1417 µm x 1417 µm x 16 µm). For quantification of deposited ECM, the surface detection and consecutive volume rendering of Bitplane IMARIS software was used. Alternatively, the intensity fluorescence was determined as surrogate for amounts of deposited ECM using mean fluorescence intensity calculation. Cell counts were determined by the spot detection function of the IMARIS software.

7.1.3. Live cell imaging

For live cell imaging, cells were prepared as described for the ECM deposition. After TGFβ1 treatment, 0.1 µg/mL of the respective antibody and 1 µg/mL of Hoechst were added to the medium. The Cell Carrier plate was transferred on the confocal laser scanning microscope for repeated three-dimensional image acquisition for the time span of the study. An incubation chamber ensured standard cultivation conditions (37 °C and 5 % CO2).

7.1.4. Immunocytochemistry

For standard immunofluorescence staining, 5000 cells were seeded 96-well plates. After the respective treatments, cells were fixed with 4 % (w/v) PFA or 100% methanol. Optionally, cells were permeabilized with 0.25 % (v/v) Triton X-100 in PBS for 15 min. Cells were washed with PBS, prior to the addition of the primary antibody in PBS. After incubation overnight, cells were washed three times with PBS and secondary antibody solution in PBS was added and incubated for 1 h at room temperature in light-protected environment.

7.1.5. Liposome-based siRNA forward transfection of phLFs

siRNA was dissolved in DNase/RNase free water. Reverse transfection of phLFs with 10 nM of Silencer Pre-designed Smurf2 or 10 nM scrambled Silencer Negative control No. 1 siRNA in Lipofectamine RNAiMax was performed, followed by optional TGFβ1 and compound treatment. 114 µL OptiMem media were mixed with 15 µL of siRNA and 114 µL OptiMem

media were mixed with 7 µL of Lipofectamine. Both reagent mixes were incubated for 5 minutes at room temperature. Then both solutions were pooled. This transfection mix was incubated for another 20 minutes at room temperature to form siRNA-lipofectamine complexes. 200,000 cells were seeded in 2 mL of DMEM F-12 medium with penicillin and streptomycin mixed with 250 µL of transfection mix and cultured at standard cell culture conditions. Following 48 hours of transfection, media was exchanged for fresh cell culture media before further experiment steps were performed.

7.1.6. MTT cellular metabolic activity assay

Cellular metabolic activity was determined by the rate of NAD(P)H-dependent reduction of 3-(4,5-dimethylthiazol-2-yl)-2,5-diphenyltetrazolium bromide (MTT) into formazan. Cells cultured in 96-well plates were incubated with 1 mg/mL MTT at cell culture conditions for 30 min. Medium was aspirated. Then cells were lysed, and formazan was dissolved in 0.1 % (v/v) Triton X-100 in isopropanol. Following 30 minutes of incubation on a shaker, absorbance was measured at 570 nm.

7.2. Generation and culture of human precision cut lung slices (hPCLS) for modelling for lung fibrosis

Fresh, native tumor-free lung resection derived from lung cancer patients undergoing lobectomies were obtained from the CPC-M BioArchive. hPCLS were generated in the first 48 h after lung tissue resection by the surgeons at the department of thoracic surgery at the Asklepios Lung Clinic Munich-Gauting. In order to generate lung tissue stiff enough for the precise slicing of 500 µM thick tissue sheets, the bronchoalveolar area of the tissue was filled with low melting agarose at the day of resection (Gerckens et al. 2019). Subsequently, the agarose filled tissue was sliced. Slices were subsequently cultures submerged in DMDM F-12 medium. Following overnight incubation in DMEM F-12 medium + antibiotics, medium was exchanged, and treatments were started. After 120 h of culture, samples were harvested (**Figure 2**).

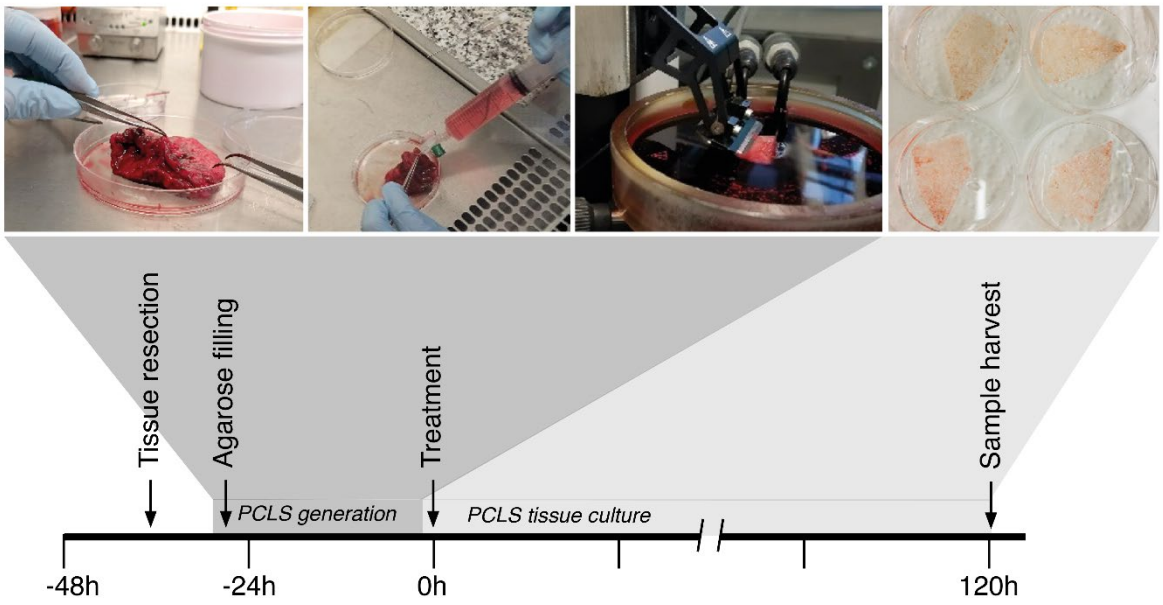

Figure 2: Timeline for the hPCLS generation and tissue cultures.
Tumor-free peri-tumorous lung tissue resections of patients undergoing lobectomy were obtained from the Asklepios Lung Clinic Munich-Gauting. Within 24 h post resection the bronchoalveolar space of a part of the tissue was filled with low-melting agarose. The agarose solidified in the tissue and thus the tissue was stiffened. The tissue was sliced into 500 µm thick precision cut lung slices and cultured submerged in cell culture medium. After 24 h medium was changed and treatments were started.

Following 120 h of incubation hPCLS samples were harvested for protein isolation and subsequent analysis procedures.

For agarose filling, open bronchi of the tissue's cut surface were cannulated using a peripheral venous catheter. Using a 25 mL syringe attached to the catheter, 40 °C fluid 3% (w/v) low melting agarose in DMEM F-12 solution was filled into the bronchoalveolar spaces of the tissue inflating the respective of parts of the tissue (**Figure 3 A-D**). The tissue was incubated in 4 °C cold DMEM F-12 medium for the agarose to solidify. 1-1.5 cm^3 large tissue blocks were excised from the tissue (**Figure 4 A**). Tissue blocks were glued on a tissue holder using cyanoacrylate glue (**Figure 4 B**). The tissue blocks glued to the tissue holder were submerged in 4 °C cool cell culture medium and cut into 500 µm thick tissue slices using a vibrating sapphire knife in the vibratome (**Figure 4 E-F**).

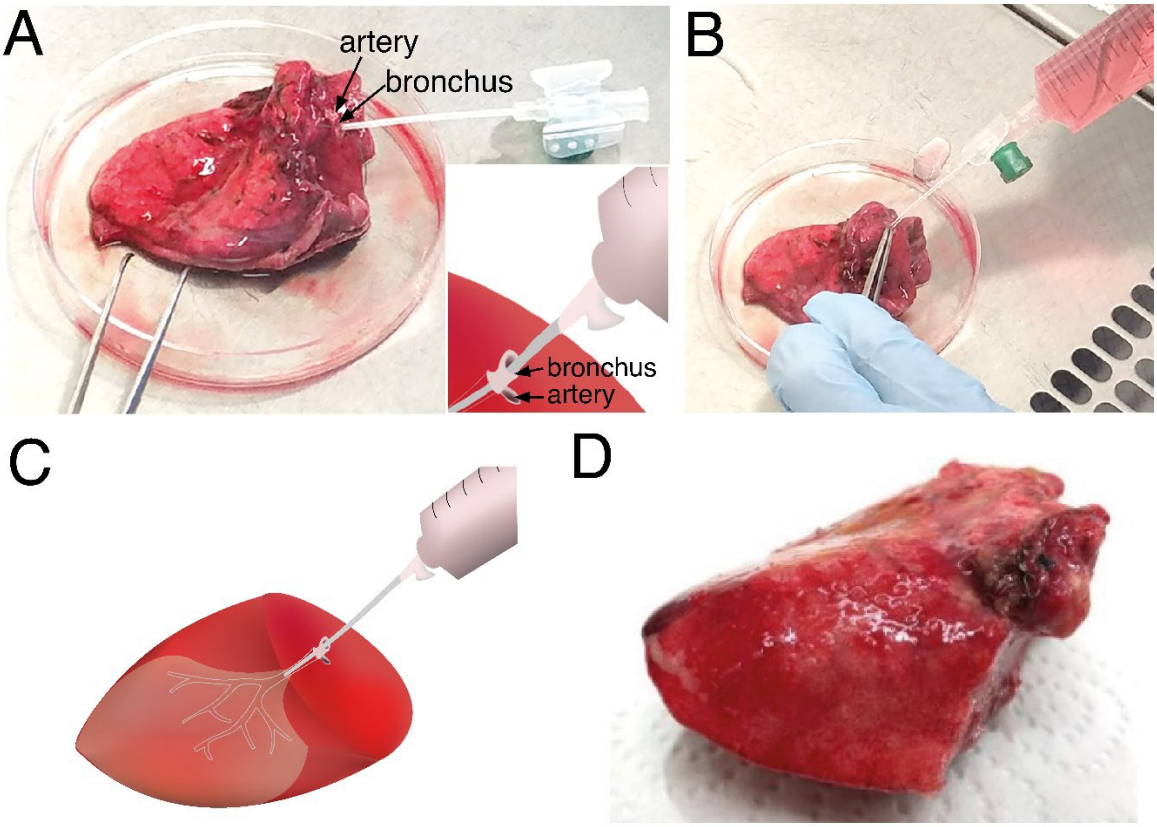

Figure 3: Preparation of lung tissue with low-melting point agarose.
(A) Photograph of a representative lung tissue resectate with localized open bronchus and adjacent pulmonary artery. **(B)** Cannulation of the bronchus and injection of low-melting agarose inflating the lung tissue. **(C)** Schematic graphic of filling the bronchoalveolar space associated the cannulated bronchus. **(D)** Agarose-inflated lung tissue part after the filling procedure.

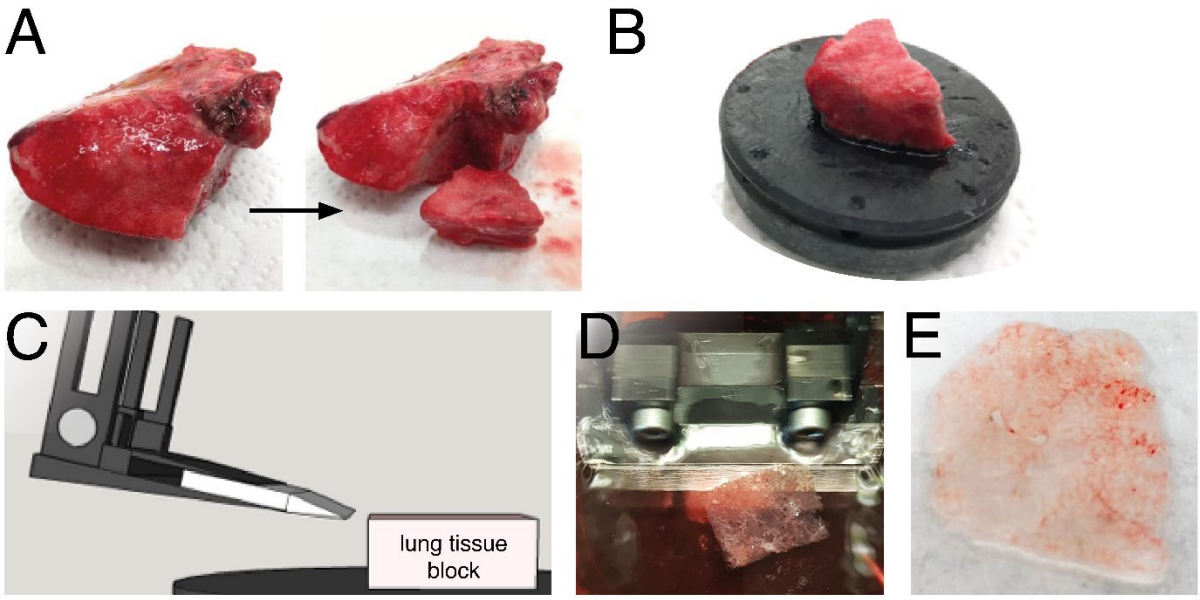

Figure 4: Generation of precision-cut lung slices using a vibratome.
(A) Excision of small, approximately 1.0x1.5x1.0 cm^3 large tissue blocks. **(B)** Fixation of the tissue blocks on the vibratome tissue holder by cyanoacrylate glue. **(C)** Schematic graph of cutting 500 µM thick slides by a vibrating sapphire knife in 10-15° angle to the tissue. **(D)** Photograph of the slicing procedure with the tissue block submerged in cell culture media cooled down to 4 °C. **(E)** Photograph of a 500µM thick hPCLS before culture.

7.3. Molecular biological methods

7.3.1. mRNA isolation, cDNA synthesis and qRT-PCR from phLFs

mRNA was extracted from cultured phLFs using the PeqGold RNA kit according to manufacturer's instructions including the elimination of genomic DNA. RNA concentrations were determined spectrophotometrically. RNA was denaturated in an Eppendorf Mastercycler using the following settings: lid 45 °C, 70 °C for 10 minutes and 4 °C for 5 minutes. For cDNA synthesis, reverse transcription was performed with 1 µg of isolated RNA using the GeneAMP PCR Kit in an Eppendorf Mastercycler using the following settings: lid 105 °C, 20 °C for 10 minutes, 42 °C for 60 minutes and 99 °C for 5 minutes. qRT-PCR was performed using the primers, described in the Materials section, the SYBR Green I Master mix and the LightCycler 480II with the following conditions: 95 °C for 5 min followed by 45 cycles of 95 °C for 5 s

(denaturation), 59 °C for 5 s (annealing) and 72 °C for 20 s (elongation). Relative transcript abundance was approximated by

$$\Delta Ct = Ct^{target\ gene} - Ct^{housekeeping\ gene}.$$

Changes in in transcript abundance were calculated as

$$\Delta\Delta Ct = \Delta Ct^{condition\ A} - \Delta Ct^{condition\ B} \text{ and } fold\ change = 2^{\Delta\Delta Ct}.$$

7.3.2. Microarray

phLF RNA was isolated as described above. The following steps were performed by Dr. Martin Irmler at the Institute of Experimental Genetics, Helmholtz Center Munich. RNA quality was assessed using the Agilent 2100 Bioanalyzer (Agilent, Santa Clara, USA) was used to assess RNA quality. 150 ng of total RNA was amplified using the WT PLUS Reagent Kit (Thermo Fisher Scientific Inc., Waltham, USA). Amplified cDNA was hybridized on Human Clariom S arrays (Thermo Fisher Scientific Inc., Waltham, USA). Staining and scanning were performed using the GeneChip Scanner 3000 7G (Thermo Fisher Scientific Inc., Waltham, USA).

7.3.3. Protein isolation from phLF cell lysate

Cells were seeded in a density of 200,000 phLFs per well into a 6-well cell culture plates, incubated for 24 h. Then cell were starved in serum-reduced DMEM-F12 medium with 1 % (v/v) FBS for another 24 h before treatment± TGFβ1 ± compounds. After a 72 h of culture phLF protein content was harvested, as followed: Upon addition of 200 µl ice-cold RIPA buffer containing 1x Roche complete mini protease inhibitor cocktail, cells were scraped of the 6-well cell culture plates. After 30 minutes of incubation on ice, lysates were centrifuged at 14,000 g for 15 minutes at 4°C and the supernatant was sampled. Protein concentration was determined using the BCA Kit according to the manufacturer's instruction.

7.3.4. Protein isolation from phLF cell supernatant

Supernatant medium was harvested from the cell culture 6-well plates. Insoluble material and cell debris were removed by centrifugation of the sample at 14,000 g for 5 minutes at 4°C and supernatants were sampled.

7.3.5. Protein isolation from hPCLS lysate

After treatment as described above, hPCLS were incubated in 600 µL ice-cold RIPA buffer containing 1x Roche complete mini protease inhibitor cocktail for 6 h at 4 °C in 1 mL microtubes under constant rotation. Supernatant lysates were separated from the remaining tissue and centrifuged at 14,000 g for 15 minutes at 4°C to remove tissue debris and the supernatant was sampled. Protein concentration was determined using the BCA Kit according to the manufacturer's instruction.

7.3.6. Protein isolation from hPCLS supernatant

After tissue culture, supernatant medium from hPCLS was harvested. Insoluble material and cell debris were removed by centrifugation of the sample at 14,000 g for 5 minutes at 4°C and supernatants were sampled.

7.3.7. Western blotting and ELISA

Protein lysates were mixed with the Lämmli loading buffer. Proteins were separated using sodium dodecylsulfate polyacrylamide gel electrophoresis (SDS-PAGE) as described in Gerckens et al. 2021. Proteins were transferred to a polyvinylidene fluoride (PVDF) membrane. The PVDF membrane was blocked with 5% milk in TBS-T for 30 minutes at room temperature and incubated over night with the primary antibody solution overnight at 4°C, followed by the secondary antibody solution for 1 h at room temperature. Western blots were developed using X-Ray films and a film developer machine or chemiluminescent signal was imaged by the

ChemiDoc XRS+ system. Densitometric quantification was performed using ChemiDoc XRS+ system and the BioRad Image Lab software version 3.0.1.

The DuoSet ELISA kits were used according to the manufacturer's protocol.

7.3.8. Liquid chromatography-tandem mass spectrometry (LC-MS^2) analysis of PCLS protein lysates

The following steps were performed by Dr. Juliane Merl-Pham at the Core Facility Proteomics, Helmholtz Center Munich: Proteomic analysis was performed with digested protein extract using a QExactive HF-X mass spectrometer (ThermoFisher Scientific, Waltham, USA) on line coupled to an Ultimate 3000 nano-RSLC (Dionex, Sunnyvale, USA). Label-free protein quantification from raw data was performed using Progenesis QI for proteomics and using a Mascot search engine against Swissprot human protein database. Proteins were quantified as the sum of all unique peptides per protein after normalization to identified Glyceraldehyde-3-phosphate dehydrogenase and βActin peptides. Resulting protein abundancies were used for calculation of fold-changes between conditions and repeated-measures ANOVAs within the Progenesis QI software.

7.4. In silico analyses

7.4.1. Interferential statistics

Interferential statistics was done using the GraphPad Prism v5-v8. Data are presented as mean ± standard deviation (SD) or standard error of mean (SEM). Statistical analysis was performed using unpaired and paired two-tailed t-tests or One-way ANOVA with Bonferroni's or Dunnett's multiple comparison test. For microarray experiments, initial statistical analyses were performed using a statistical programming environment R (R Development Core Team Ref1). For proteomics experiments, initial statistical analysis was performed in the Progenesis QI software.

7.4.2. Microarray and proteomics analysis

For subsequent analysis, python-based analysis packages were used in jupyter notebooks. For primary data handling, numpy and pandas were used. For visualization, matplotlib and seaborn were used. For Uniform Manifold Approximate Projection (UMAP) the umap-learn packages were used. Code sections were published in Gerckens et al. 2021.The STRING database was used for analysis of functional interactions between regulated genes or proteins, (Szklarczyk et al. 2021).

For additional, in-silico analysis proteomic data from experiments previously published by Heinzelmann and colleagues (Heinzelmann et al. 2016) were analyzed.

7.4.3. Cell morphology analysis by the CellProfiler cell image analysis software

Cell morphology of phLFs was evaluated by the phalloidin staining. Automated morphology analysis was performed using the CellProfiler version 3.1.8 (Sanz et al. 2019) (Sanz et al. 2019) software.

7.4.4. Deep learning classification of images

For deep learning experiments, additional python-based software packages were used. Here, Keras-based on TensorFlow was used with opencv-python for image handling, scipy for data normalization, TensorBoard for deep learning surveillance. The FANTAIL convolutional neural network was developed by Francesco Pelizza and myself, as described in Gerckens et al. 2021.

8. Results

8.1. Establishment of an ECM deposition assay

Extracellular matrix deposition is a central pathogenetic mechanism of fibrosis, however assays quantifying the cellular deposition of insoluble extracellular matrix fibers are widely unavailable. Previously, assays to quantify collagen deposition used biomolecular methods such as the hydroxyproline-detection assay (Neuman und Logan 1950) or assays such as Enzyme-linked Immunosorbent Assays (ELISA) for matrix metalloprotease-cleaved collagen fragments (Sand et al. 2013; Rønnow et al. 2020). Other assays, most prominently the 'scar-in-a-jar' assay (Chen et al. 2009), used conventional ECM staining techniques following cell membrane permeabilizing methanol fixation (Hetzel et al. 2005; Jamur und Oliver 2010).

However, matrisome components in intracellular cell compartments, such as the endoplasmic reticulum might be detected together with the actual extracellular matrix consisting of insoluble, extracellular ECM proteins. With *extracellular* ECM fibers playing a fundamental role in fibrosis development, a clear differentiation of ECM fibers from intracellular ECM proteins was considered to be key for an ECM *deposition* assay (**Figure 5**).

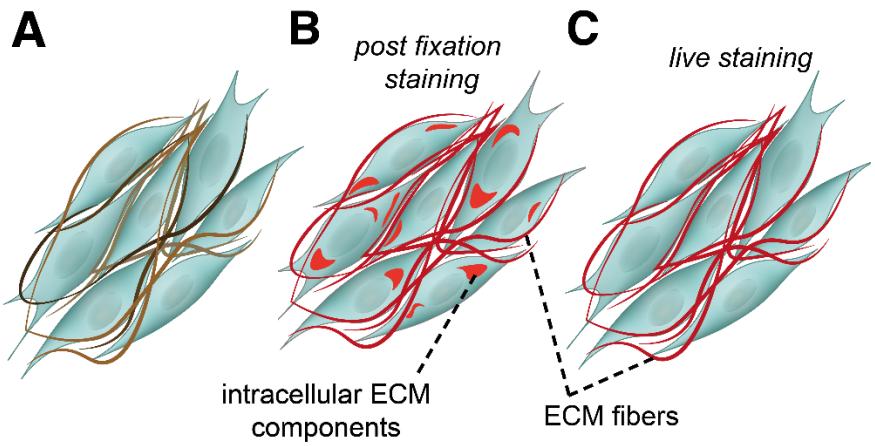

Figure 5: Detection of intracellular and extracellular matrisome components.
(A) Matrisome proteins exist within different intracellular cell compartments as soluble proteins during their synthesis, intracellular transport, and intracellular post-translational modification, on the cell surface and in the extracellular space mostly as insoluble extracellular matrix fibers. **(B)** Routine immunofluorescence staining techniques are likely to detect intra- and extracellular matrisome proteins, **(C)** while assays quantifying ECM deposition should only detect extracellular matrisome proteins.

Exclusive staining of matrisome components in the extracellular space can only be achieved by immunofluorescence staining which prevents antibodies from entering the cells. Antibodies are large hydrophilic protein complexes which cannot enter living cells by diffusion, as the cell's membrane restricts the passage for larger hydrophilic molecules.

While it is known that the ice-cold methanol fixation or the use of permeabilization detergents allow the intracellular IF staining (Jamur und Oliver 2010), it was hypothesized that also the most used fixation method induces enhanced cell membrane permeability for antibody in consecutive staining without additional permeability reagents. I observed an intracellular staining for Collagen I in cells treated with paraformaldehyde (PFA) ± permeabilization agent, in particular a intracellular perinuclear staining besides extracellular staining (**Figure 6 A**). This was also seen in cells that were only PFA-fixed: Here smaller amounts of intracellular staining were seen – possible associated with minor cell membrane damages due to the PFA fixation (Zhao et al. 2014). To verify intracellular staining in PFA fixed cells, I treated cells with the (extracellular matrix) secretion inhibitor Brefeldin A (**Figure 6 B**) to an accumulation of ECM protein within the cells (Ktistakis et al. 1992). In Brefeldin A treated cells, intracellular staining was well observed in cells that were PFA-fixed and permeabilized by Triton-X or only PFA-fixed prior to staining, but no intracellular ECM staining was observed in cells that were stained alive (**Figure 6 A**).

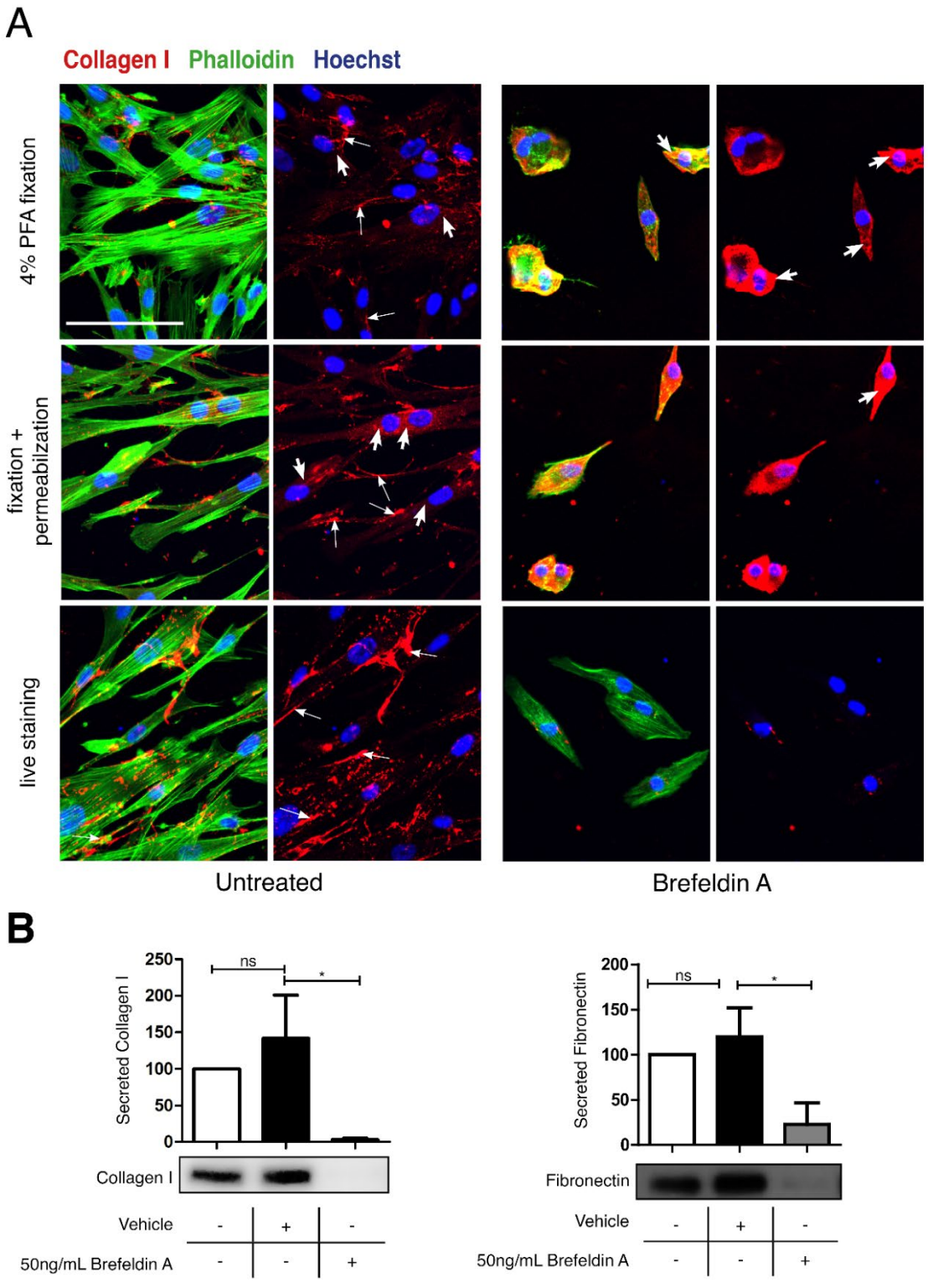

Figure 6: Immunofluorescence staining of intracellular and extracellular matrisome components with different staining protocols.

(A) Collagen I immunofluorescence staining (red), Phalloidin (green) and Hoechst (blue) staining of primary human lung fibroblasts ± with 50 ng/mL Brefeldin A. **(B)** Effect of the Brefeldin A treatment on Collagen I and fibronectin secretion into the cell culture supernatant. Statistics in (B): Paired t-test. * $p<0.05$. n = 3 (phLFs from three different donors). Data are presented as means ± SEM.

Low to high magnification laser confocal microscopy (LSM) imaging of live-cell-stained extracellular matrix revealed stained ECM fiber extracellularly between and on-top of the cell tracker-labeled cell bodies (**Figure 7 A**). Interestingly, co-staining of Collagen I and Collagen V in the ECM showed thin ECM fibers containing only Collagen V (►) and thicker fibers containing Collagen I and V fibers (→) (**Figure 7 B**) appearing as a woven net of thicker but also more delicate fibers.

Live staining is not only apt for exclusive extracellular ECM staining. It also allows for live imaging with a confocal laser microscopy. This can be achieved through directly detecting antibody-labeled collagen I accumulating on assembling ECM fibers. Direct live immunofluorescence staining enables visualization of time-resolved extracellular matrix deposition, as shown in **Figure 7 C**. Here, I observed that collagen fibers are predominantly formed in areas with higher cell density with cells moving in between the forming fibers. Often fibers originated from small collagen ‘coils’ that were unfolded and stretched, potentially by cell movement and contractility. Here fiber folding and stretching appeared to be associated with cell movement and nucleus deformation, a sign of cell contraction (compare **Figure 7 C**).

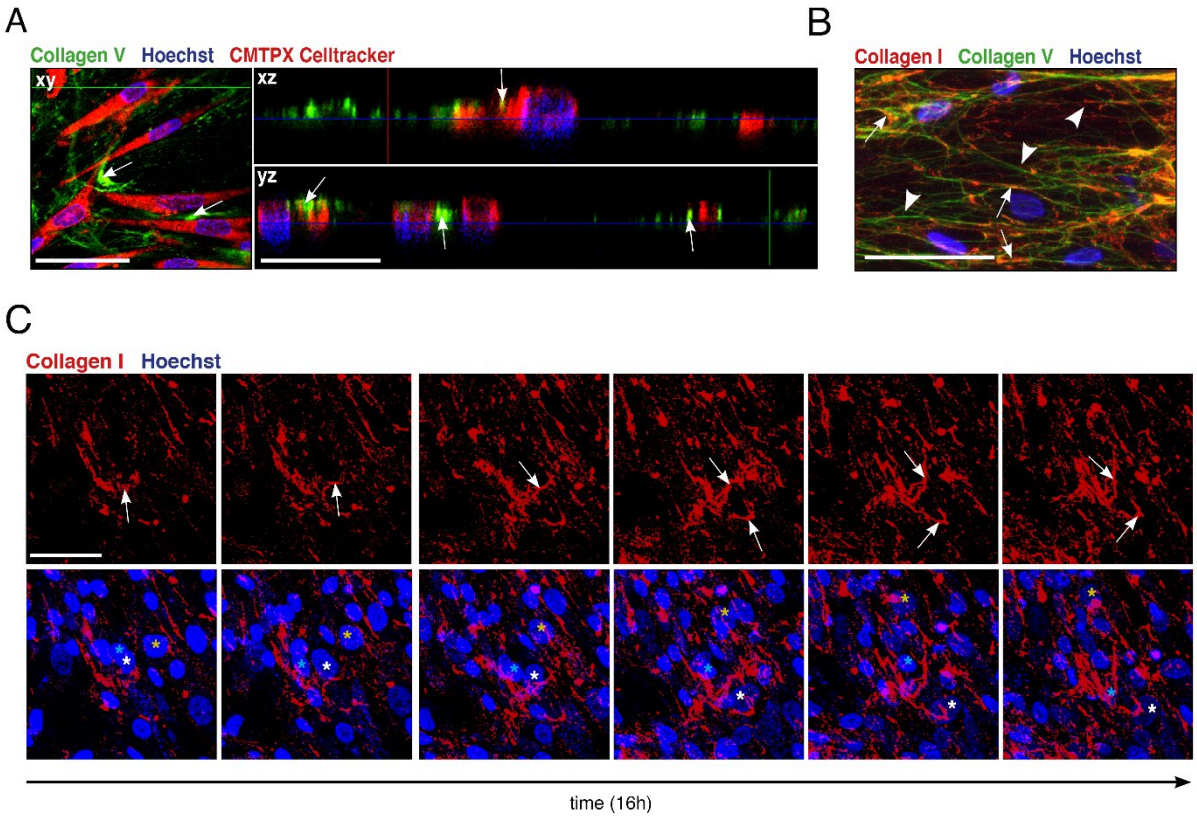

Figure 7: High-resolution immunofluorescence imaging of deposited Collagen I and V fibers. **(A)** Orthogonal plane views of confocal z-stack imaging with tomographic 3D reconstruction with collagen V containing ECM fibers and Hoechst (blue) nuclei and CMTPX Cell tracker (red) cell soma counterstaining. ECM fibers between and on top of cell soma (→). Scale bars, 50 (left) and 25 (right) µm. **(B)** High-magnification confocal imaging of Collagen I (red) and Collagen V (green) containing ECM fibers with Hoechst nuclei counterstaining (blue). ECM fibers containing Collagen I and Collagen V (→) and thin ECM fibers containing Collagen V only (►). Scale bar 50 µm. **(C)** Confocal immunofluorescence images from time lapse imaging cell (nuclei) movement (*) and Collagen I containing ECM fiber movement and assembly (→) over 16 hours. Scale bar 50 µm.

In summary, multiple complementary experiments showed that live immunofluorescence staining of ECM components in primary human fibroblast cultures prior to PFA fixation of cells can specifically detect matrix fibers outside of the cells. Therefore, immunofluorescence staining for deposited ECM components in the ECM deposition assay was routinely performed as live staining performing an indirect immunofluorescence labeling *prior* to cell fixation with PFA, as extensively described in the methods section.

8.2. Development of a HT/HC cellular fibrosis model of fibrotic ECM deposition

This newly developed ECM deposition assay was used to develop an automated high-throughput/high-content drug screening method for compounds inhibiting fibrotic ECM deposition. For this purpose, a cellular fibrosis model was implemented into the ECM deposition assay: IPF-patient derived primary human lung fibroblasts (phLFs) were seeded into 96- or 384-well plates and treated with TGFβ1 to induce fibrosis-characteristic fibroblast-myofibroblast-transdifferentation to trigger subsequent fibrotic extracellular matrix synthesis and deposition. Treatment of phLFs with 1 ng/mL TGFβ1 increased α smooth muscle actin expression (**Figure 8 A**) measured by immunofluorescence staining. Furthermore, TGFβ1 treatment increased intracellular Collagen I expression as well as Collagen I protein secretion into the cell culture medium (**Figure 8 B**). Similarly, TGFβ1 treatment significantly increased intracellular Collagen V protein expression as well as Collagen V protein secretion into the cell culture medium (**Figure 8 C**).

To identify additional matrisome proteins which are more deposited by phLFs upon TGFβ1 treatment, a proteomics dataset published by Heinzelmann et al. (2016) was re-analyzed for its increased abundant matrisome proteins detected on the phLF cell surface following TGFβ1 treatment (**Figure 8 D-E**). As the cell surface plays an important role in extracellular matrix assembly (Hay 1991), I hypothesized that matrisome proteins which show a higher abundancy on the cell's surface after TGFβ1 stimulation might also increasingly be deposited extracellularly by phLFs upon TGFβ1 treatment.

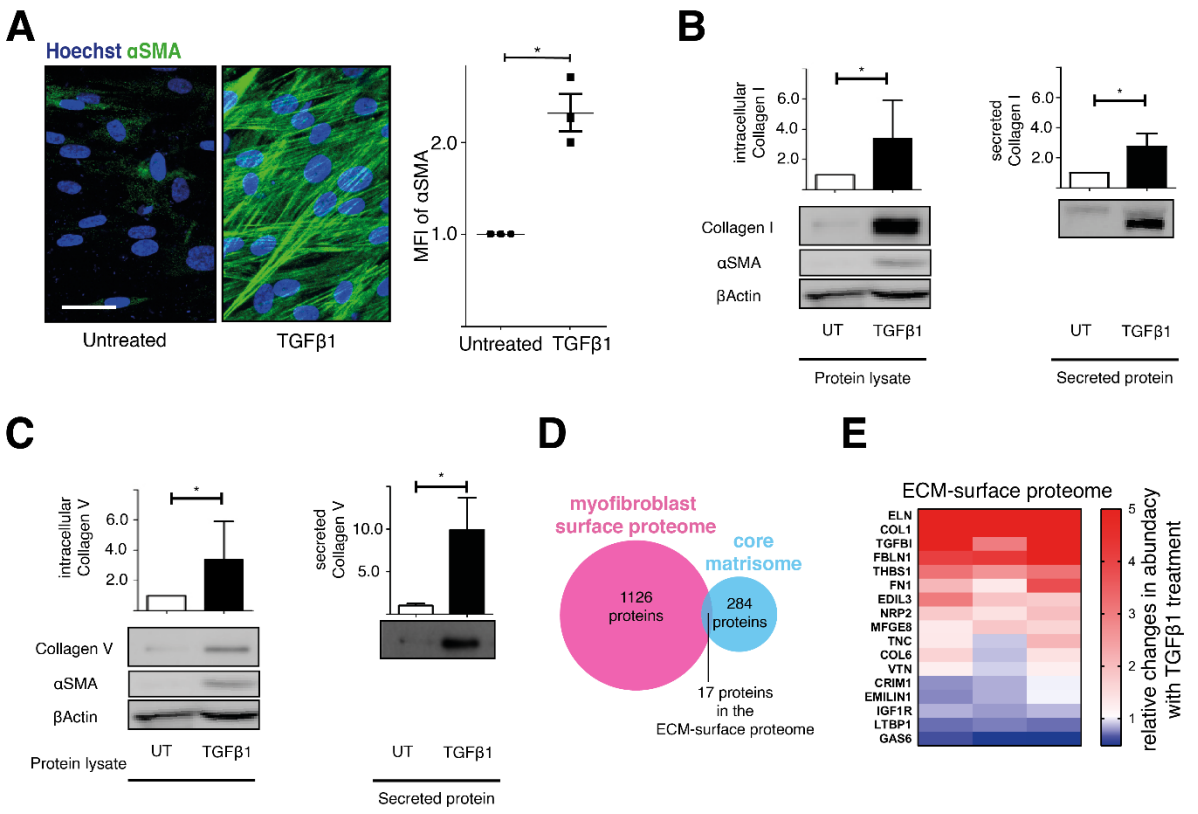

Figure 8: Fibroblast-myofibroblast transdifferentiation and concomitant changes in ECM protein expression and secretion.

(A) Immunofluorescence staining of α smooth muscle actin (αSMA) in untreated and TGFβ1-treated primary human lung fibroblasts and quantification of αSMA expression using the normalized mean fluorescence intensity (MFI). Scale bar 200 µm. **(B)** Western blot of intracellular and secreted Collagen I and quantification using densitometry. **(C)** Western blot of intracellular and secreted Collagen V protein and quantification using densitometry. **(D)** Analysis of changes of extracellular matrix proteins in the fibroblast surface proteome from the publication Heinzelmann et al. 2016. **(E)** A heatmap indicating changes in abundancy of ECM proteins significantly regulated in the fibroblast surface proteome by TGFβ1 treatment. Statistics in (A), (B) and (C): Paired t-test. * p<0.0.5. n = 3-4 (phLFs from three to four different donors). Data are presented as means ± SEM.

Conclusively, I chose Collagen I and the glycoprotein Fibulin-1 as markers for ECM deposition. I added Collagen V as an additional ECM marker, as its expression and secretion were significantly upregulated upon TGFβ1 stimulation in primary human lung fibroblasts (**Figure 8 C**).

For all experiments using the ECM deposition assay, the following workflow was designed: Primary human lung fibroblasts were isolated from explanted lungs from patients with IPF undergoing lung transplantation. Those IPF-derived phLFs were expanded into approximately

5 x 10^8 cells in passage 4 or 5 and subsequently were cryoconserved. For each experiment cells were thawed and cultured in 15 cm cell culture plates for one passage before cells were seeded into 384-well plates. Following 24 hours of cell attachment, the fibroblasts were starved with serum-reduced medium for another 24 h. Then treatment ± TGFβ1 ± compounds was performed, and after 72 h live staining and fixation of the cells were performed. . Finally, the immunofluorescently labeled ECM was imaged using confocal microscopy (**Figure 9 A**). Assessment of ECM deposition was either achieved by quantifying the volume of the respective deposited ECM component using Bitplane's Imaris software (**Figure 9 B**) or by measuring the mean fluorescence intensity of the maximum intensity projection of the immunofluorescence images.

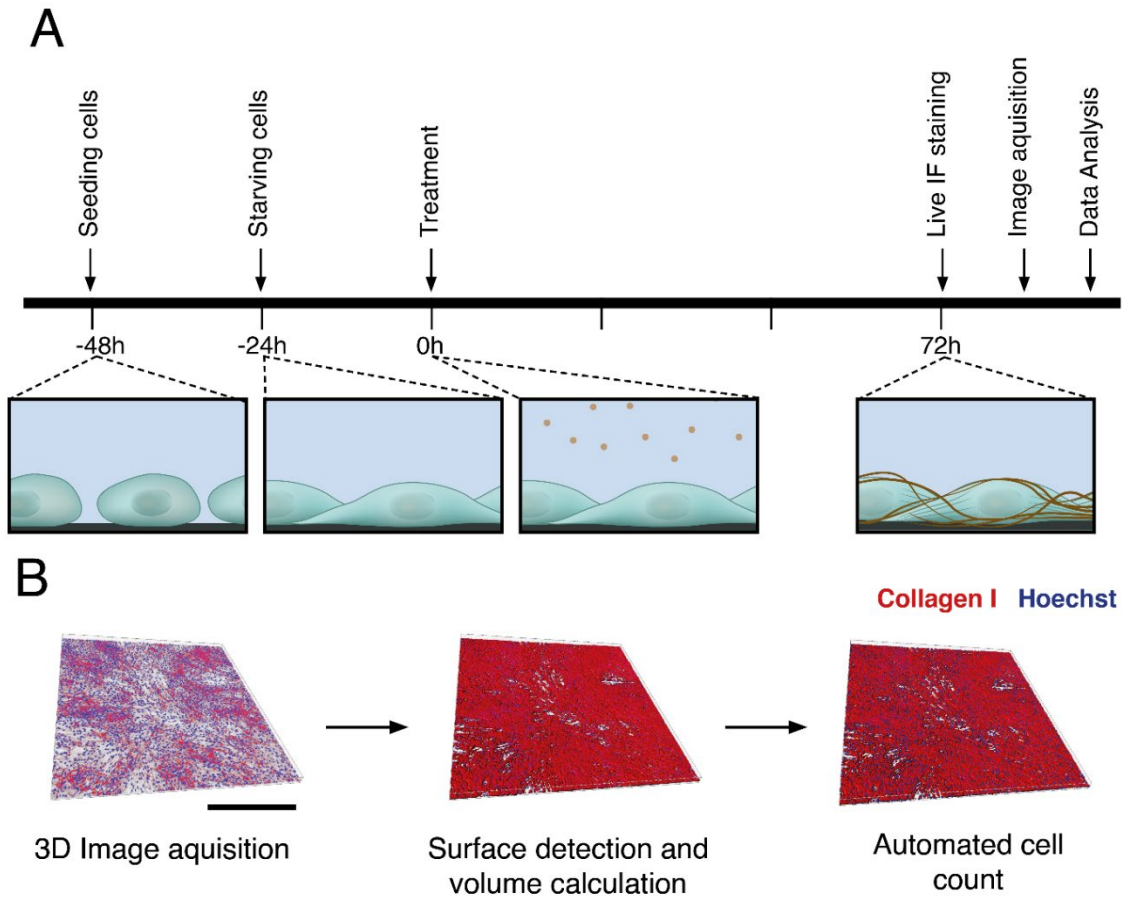

Figure 9: Workflow of the drug discovery campaign using a high-throughput ECM deposition assay.

(A) Graphical representation of the ECM deposition assay protocol timeline. **(B)** Visual illustration of quantification of ECM deposition using Bitplane IMARIS surface rendering, ECM volume calculation and automated cell count using the Hoechst counterstaining.

Next, the assay was validated regarding its ability to detect and quantify pharmacological inhibition in TGFβ1-induced ECM deposition. First, I assessed the effects of a well characterized collagen synthesis inhibitor ethyl-3,4-dihydroxy-benzoate (EDHB) on TGFβ1-induced extracellular matrix protein synthesis in phLFs. EDHB is a collagen prolyl 4-hydroxylase inhibitor (Vasta et al. 2016) and thus impedes with collagen synthesis. Next, I assessed effects of TGFβ1 treatment on intracellular Collagen I, Collagen V and Fibulin-1 content in phLF by Western blot . Intracellular Collagen I, V and Fibulin-1 was increased in phLFs upon TGFβ1 treatment whereas EDHB inhibited this increase. Similarly, secreted Collagen I increased upon showing TGFβ1 treatment which was inhibited by EDHB (**Figure 10 D**). the upregulation.

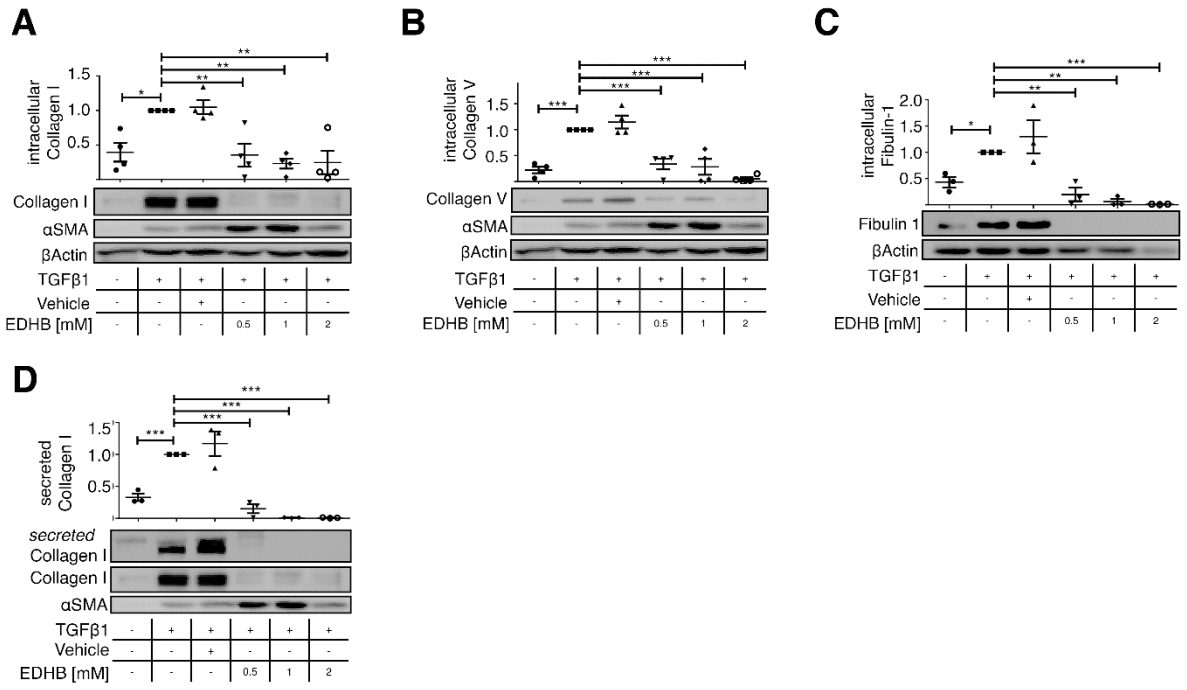

Figure 10: Effects of TGFβ1 and ethyl-2,3-dihydroxy-benzoate (EDHB) on the expression and secretion of ECM proteins in primary human lung fibroblasts.

Assessment of intracellular **(A)** Collagen I, **(B)** Collagen V and **(C)** Fibulin-1 protein expression in phLFs ± TGFβ1 ± EDHB treatment by Western blot and quantification by densitometry. **(D)** Assessment of secreted Collagen I in phLFs ± TGFβ1 ± EDHB treatment by Western blot and quantification by densitometry. Statistics in (A-D): One-way ANOVA with Bonferroni-correction. * p<0.0.5, ** p<0.01, *** p<0.001. n = 3-4 (phLFs from three or four different donors). Data are presented as means ± SEM.

Next, I assessed the effects of TGFβ1 treatment of phLFs on the deposition of extracellular Collagen I, Collagen V and Fibulin-1 . Here, TGFβ1 increased Collagen I, V and Fibulin-1 deposition in pHLFs significantly(**Figure 11 A-B**). Additionally and similar to the protein expression before, EDHB inhibited the TGFβ1-induced increase in Collagen I, Collagen V and Fibulin-1 deposition (**Figure 11 C-D**).

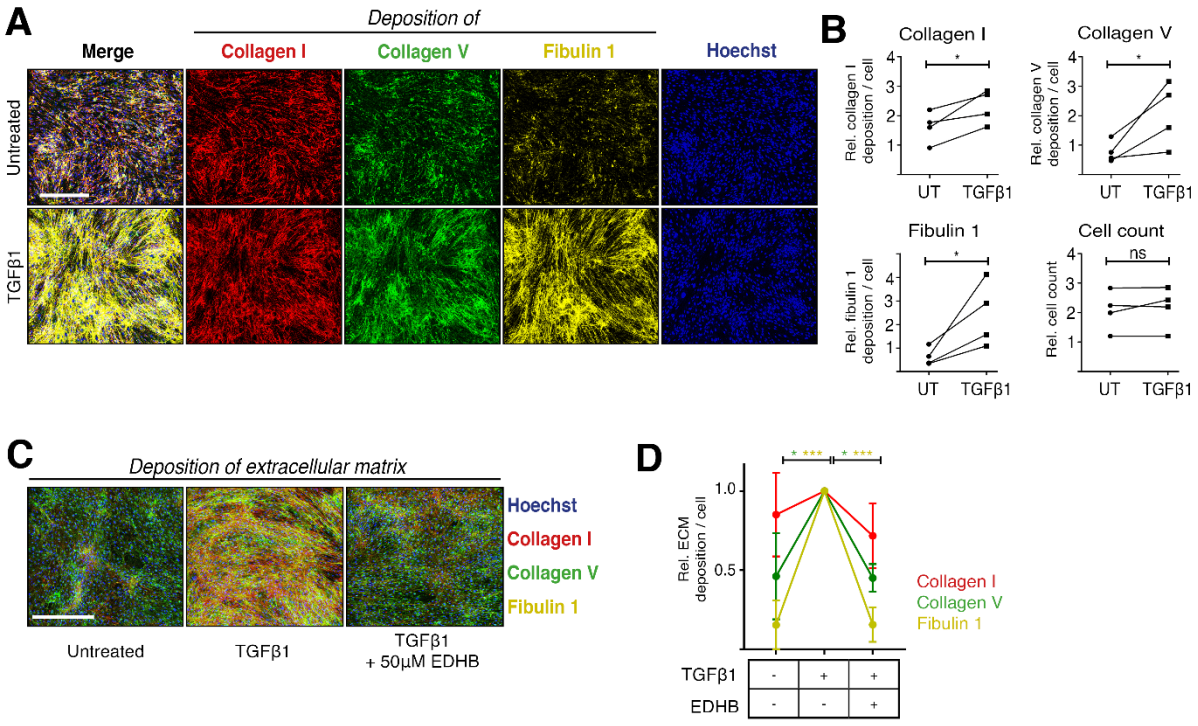

Figure 11: Effects of TGFβ1 and EDHB treatment on ECM deposition in primary human lung fibroblasts in the ECM deposition assay.

(A) Representative images of deposited ECM with Hoechst counterstaining of phLFs ± TGFβ1 treatment for 72 h. **(B)** Quantified changes in Collagen I, Collagen V and Fibulin-1 deposition as well as changes in cell count by TGFβ1 treatment. **(C)** Representative immunofluorescence micrographs of deposited Collagen I, Collagen V and Fibulin-1 in phLFs^{untreated}, phLFs$^{+TGFβ1}$ and phLFs$^{+TGFβ1+EDHB}$ and **(D)** quantification of ECM deposition. Of note, data in subpanel A-B presented in this figure are also presented as part of Figure 16. Statistics in (B): Paired t-test. *p<0.0.5. n = 4 (phLFs from four different donors). Data are presented as means ± SEM. Statistics in (D): One-way ANOVA with Bonferroni-correction. * p<0.0.5, ** p<0.01, *** p<0.001. n = 4 (phLFs from four different donors). Data are presented as means ± SEM.

Following this proof-of-concept experiment for the pharmacological inhibition of TGFβ1-induced fibrotic ECM deposition in phLFs, the ECM deposition assay was miniaturized into a

384-well plate format. This miniaturization enabled testing of larger numbers of compounds using the ECM deposition assay in so-called high-throughput drug screenings. More than 5 x 10^8 of phLFs were derived from an explanted lung of a single IPF patient (**Figure 12 A**). The previous experiments used technical and biological replicates of each tested condition by using three replicates of the ECM deposition assay with three different phLF cell lines. In drug screening however, compounds are tested in a single replicate, as the sheer number of tested compounds neither allows technical nor biological replicates in the primary screen. Thus in primary drug screen, each compound was tested at a single concentration including positive (TGFβ1-stimulation phLFs with increased ECM deposition) and negative controls (unstimulated phLFs with low ECM deposition) within every 384-well plate (**Figure 12 B**).

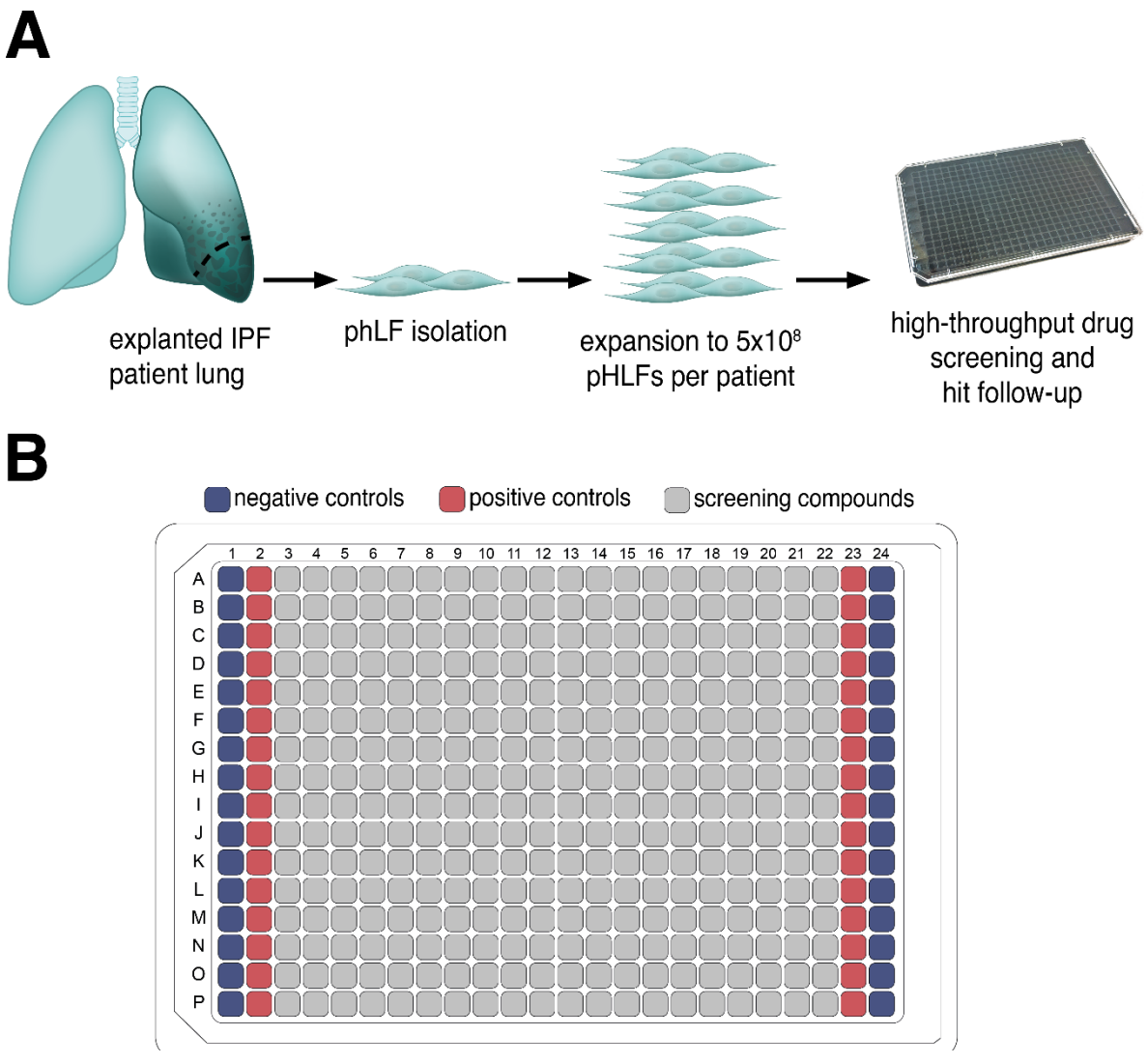

Figure 12: Workflow of the high-content drug screening utilizing the ECM deposition assay.

(A) Primary human lung fibroblasts were derived from diseased lung tissue from lung explants of IPF patients undergoing lung transplantation. Fibroblast were expanded and cryoconserved at -160°C. For each assay run, cells were thawed and cultured for one passage on 15 cm dishes and before seeding in 384-well plates. **(B)** Plate layout for the ECM deposition in 384-well plates. This illustration was adopted from Wikimedia Commons 2020 and used under the Creative Commons CC0 1.0 Universal Public Domain Dedication license.

8.3. Automated image analysis for a high-throughput / high-content drug screen for antifibrotic compounds using machine learning approaches.

ECM deposition was measured by deposited ECM volume using surface rendering of the three-dimensional immunofluorescence images with the IMARIS software in the previous experiments. For the analysis of the high-throughput drug screening, a different approach was used: Here an algorithm was needed that can differentiate simply between normal ECM deposition and excessive fibrotic ECM deposition.

In order to set up an automated image analysis tool that can differentiate between normal and excessive (fibrotic) ECM deposition, a machine learning tool using an established multilayer convolutional neural network (CNN) was created. Multilayer CNNs are frequently used in machine learning for image classification making use of quantitative and qualitative image features. For a deep learning-based image analysis which identifies antifibrotic hits, a custom multilayer convolutional neural network termed FANTAIL (Fibrotic Pattern Detection by Artificial Intelligence) was designed. FANTAIL was set-up to identify via ECM deposition in TGFβ1-stimulated phLFs an inhibitory activity of the tested screening compound or drug candidate. The screening experiments used untreated pHLFs as “negative” or “low” controls with only few ECM deposited. TGFβ1-treated pHLFs were used as “positive” or “high” control with excessive fibrotic ECM deposited (because of the TGFβ1-stimulation). Negative and positive controls performed on all plates on the outer right and left columns of the well plates (**Figure 12B**), as a reference for normal and excessive fibrotic ECM. Thus, an inhibition of TGFβ1-stimulated fibrotic ECM deposition by a screening compound was identified by comparing the ECM deposition in each compound treated condition to the controls, The FANTAIL’s CNN architecture is shown in **Figure 13**.

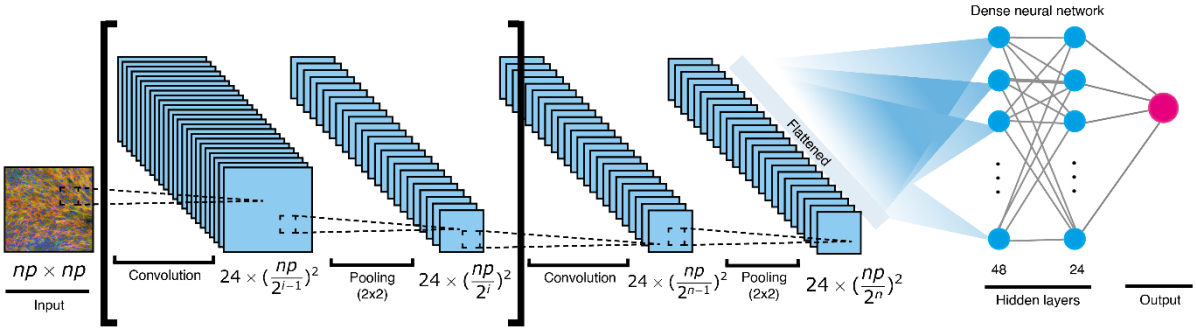

Figure 13: Deep learning convolutional neural network architecture of FANTAIL.
Graphical representation of the architecture of the multilayer convolutional neural network of FANTAIL. The FANTAIL model was designed as a simple multilayer convolutional neural network, as reportedly used for different image classification tasks in the literature, consisting of three convolution and pooling layers, a flattening function and a consecutive one-dimensional dense neural network with a binary output encoding for “normal” and “fibrotic” extracellular matrix deposition (Gerckens et al. 2021) similar to the architecture of other image classification CNN (A. A. M. Al-Saffar et al. 2017).

8.4. Phenotypic drug screening for inhibitors of fibrotic ECM deposition

In order to screen for inhibitors of TGFβ1-induced (fibrotic) ECM deposition in phLFs, a Repurposing Drug Screening Library comprising 1509 compounds used in clinical routine or in clinical trials, was applied.

The FANTAIL model was trained by using negative and positive controls to distinguish between “normal” and “fibrotic”, as well as cytotoxic conditions. In addition to the controls performed on the drug screening plates (compare **Figure 12 B and 14 B**), another control plate of ECM deposition assays with control conditions only was performed: This plate included not only positive (TGFβ1-treated) and negative (untreated) controls, but also cytotoxic controls, where cells were treated 5 % (v/v) ethanol to produce a cytotoxic phenotype.

FANTAIL was trained to identify images of the category “hits” and distinguish them from the category “others”. The category “hits” defined as an immunofluorescence image of reduced ECM deposition, while all IF images showing excessive ECM deposition or cytotoxic cell changes, or cell layer detachment were summarized in the category “others”.

Finally, FANTAIL analysis identified 31 compounds as potential inhibitors of TGFβ1-induced extracellular matrix deposition. Among others, compounds could be classified as anti-infective and antibiotic agents, g-protein coupled receptors (GPCR)-agonists/antagonists, inhibitor autophagy as well as compounds targeting metabolic enzymes, TGFβ/Smad, as well as cell cycle/DNA synthesis. Excluding anti-infectives and chemotherapeutics and compounds containing toxophoric groups, the compound Tranilast was selected for a hit follow-up because of well documented *in-vivo* bioavailability and *in-vivo* human safety data (Tamai et al. 2002; Holmes 2002; Darakhshan und Pour 2015).

In summary, the combination of a complex high-throughput / high-content drug screening with the machine learning tool FANTAIL was able to identify 31 small molecules from a drug repurposing library, which are suggestive of antifibrotic activity.

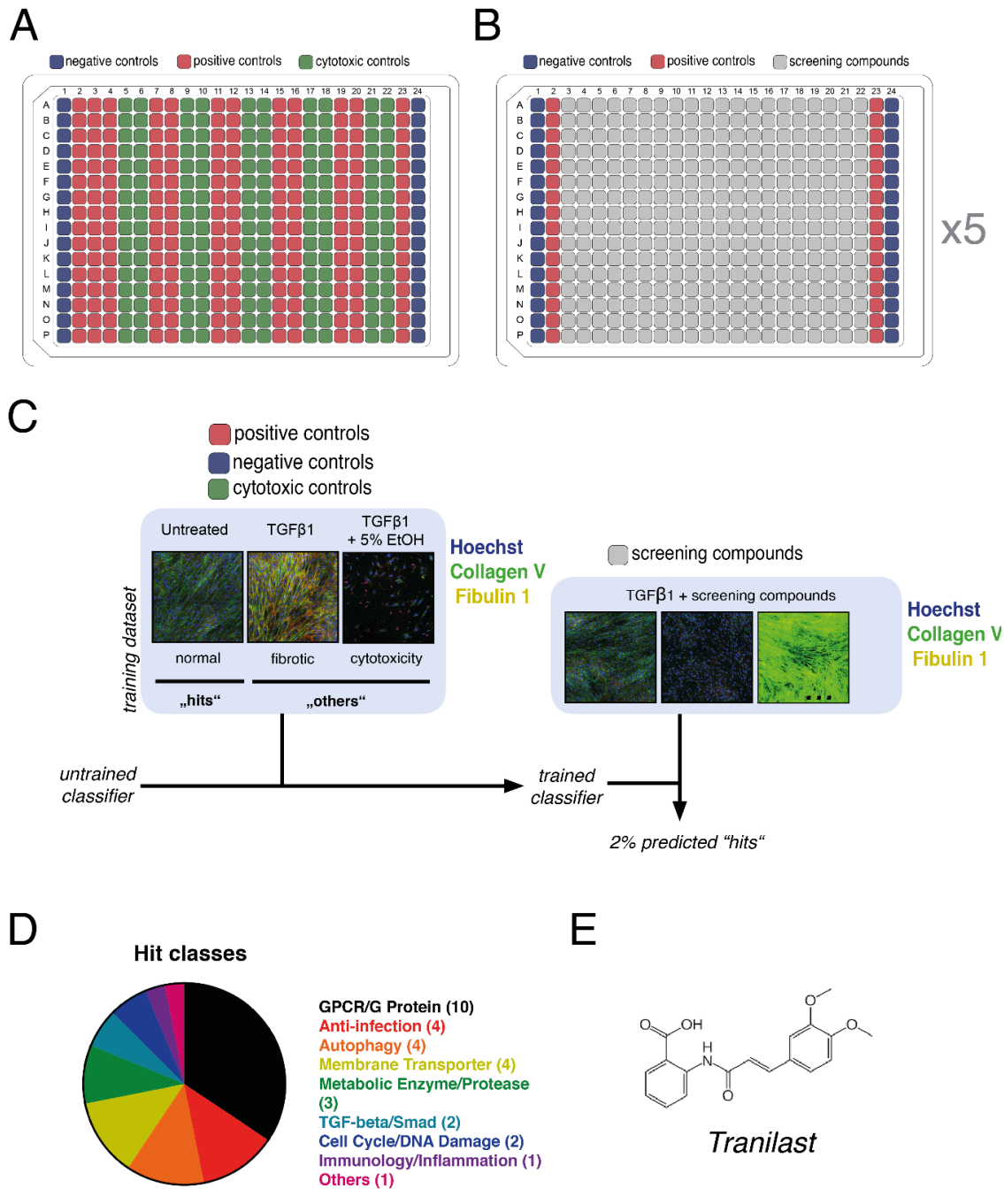

Figure 14: Phenotypic screening for fibrotic ECM deposition inhibitor in a drug repurposing library.

(A) Plate layout for a control plate with negative, positive, and cytotoxic controls. **(B)** Screening plate of up to 320 wells with test compounds as well as negative and positive controls**. (C)** The FANTAIL classifier was trained using ECM deposition by phLFs^{untreated} for the “hits” class and phLFs$^{+TGFβ1}$ and pHLFs$^{+TGFβ1+5\ \%\ ethanol\ (EtOH)}$ as “others” class. Thus, the FANTAIL model was trained to distinguish reduced ECM of phLFs$^{+TGFβ1+screening\ compound}$ from wells with excessive ECM of phLFs$^{+TGFβ1+screening\ compound}$ or ECM changes due to cytotoxic changes ECM of phLFs$^{+TGFβ1+screening\ compound}$. **(D)** Pie chard demonstrating the classification of detected hits into groups of similar drug target or mode of action. © Chemical structure of Tranilast, a hit compound from the screening.

8.5. Validation of Tranilast as inhibitor of TGFβ1-induced ECM deposition

Prior to validation, Tranilast was tested for cytotoxic effects in phLFs. Here no significant decrease in the cells' metabolic activity upon Tranilast treatment was observed (**Figure 15**).

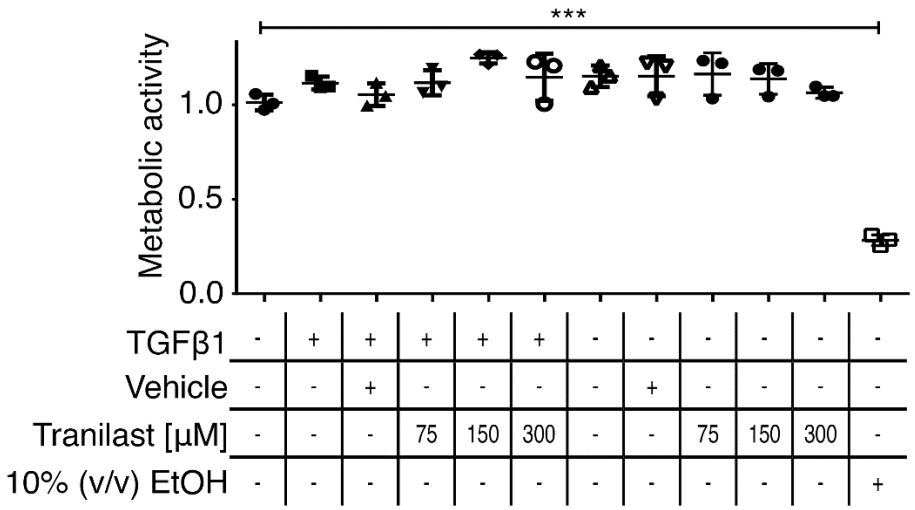

Figure 15: Cytotoxicity tests of Tranilast on primary human lung fibroblasts.
Metabolic activity of primary human lung fibroblasts treated ± TGFβ1 and ± Tranilast or vehicle. Statistics: One-way ANOVA with Bonferroni-correction. *** $p<0.001$. n = 3 (phLFs from three different donors). Data are presented as means ± SEM.

In the next step, the dose-dependency of the inhibitory activity of Tranilast on TGFβ1-induced ECM deposition was assessed. Here, a significant dose-dependent inhibition of TGFβ1-induced Collagen I, Collagen V and Fibulin-1 was observed by treatment with Tranilast (**Figure 16 A-B**). Further cell culture experiments using phLFs were performed to investigate changes in gene and protein expression. Here, a significant increase of ACTA2, COL1A1, COL5A1 and FBLN1 gene expression in phLFs upon TGFβ1 stimulation was observed, as well as a significant decrease in the expression of ACTA2 and COL1A1 by the addition of Tranilast (**Figure 17 A-D**). The significant upregulation of αSMA, Collagen I, Collagen V and Fibulin-1 expression in phLFs by TGFβ1 as well as a significant inhibition of this upregulation by Tranilast were demonstrated also on protein level by Western Blotting (**Figure 18 A-D**).

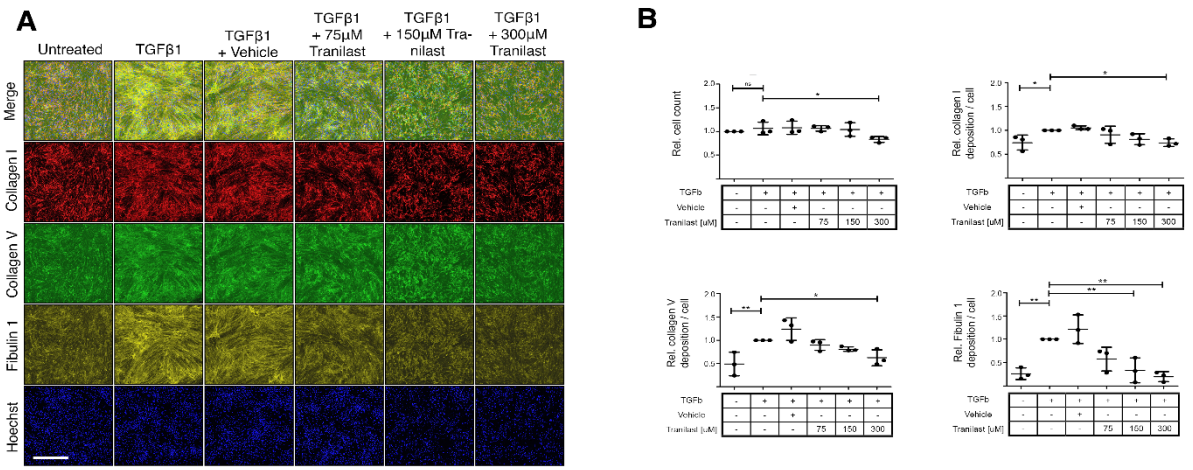

Figure 16: Effects of Tranilast on TGFβ1-induced ECM deposition by phLF (A) Representative images of the Collagen I, Collagen V and Fibulin-1 deposition and Hoechst counter-staining in phLFs treated ± TGFβ1 ± Tranilast. Scale bar 500 µm. **(B)** Quantification of cell counts as well as cell count normalized Collagen I, Collagen V and Fibulin-1 deposition. Statistics in (B): One-way ANOVA with Bonferroni-correction. * p<0.0.5, ** p<0.01, *** p<0.001. n = 3 (phLFs from three different donors). Data are presented as means ± SEM.

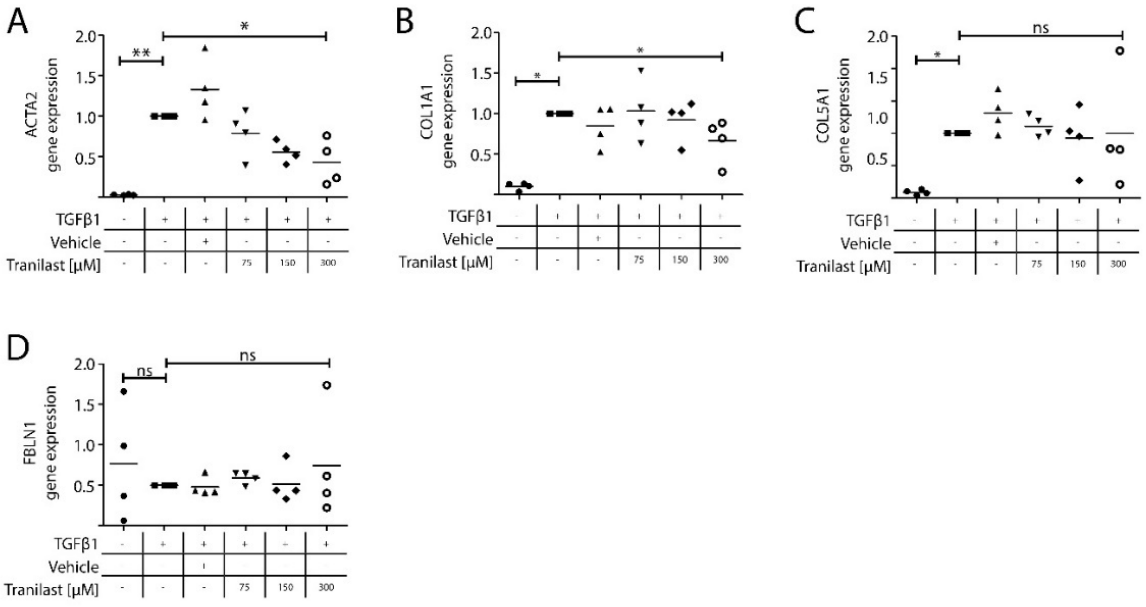

Figure 17: Effects of Tranilast of primary human lung fibroblast gene expression by qPCR. Gene expression of **(A)** ACTA2, **(B)** COL1A1, **(C)** COL5A1, **(D)** FBLN1 of primary human lung fibroblasts treated ± TGFβ1 and ± Tranilast or vehicle. Statistics: One-way ANOVA with Bonferroni-correction. * p<0.0.5, ** p<0.01, *** p<0.001. n = 3-4 (phLFs from three or four different donors). Data are presented as means ± SEM.

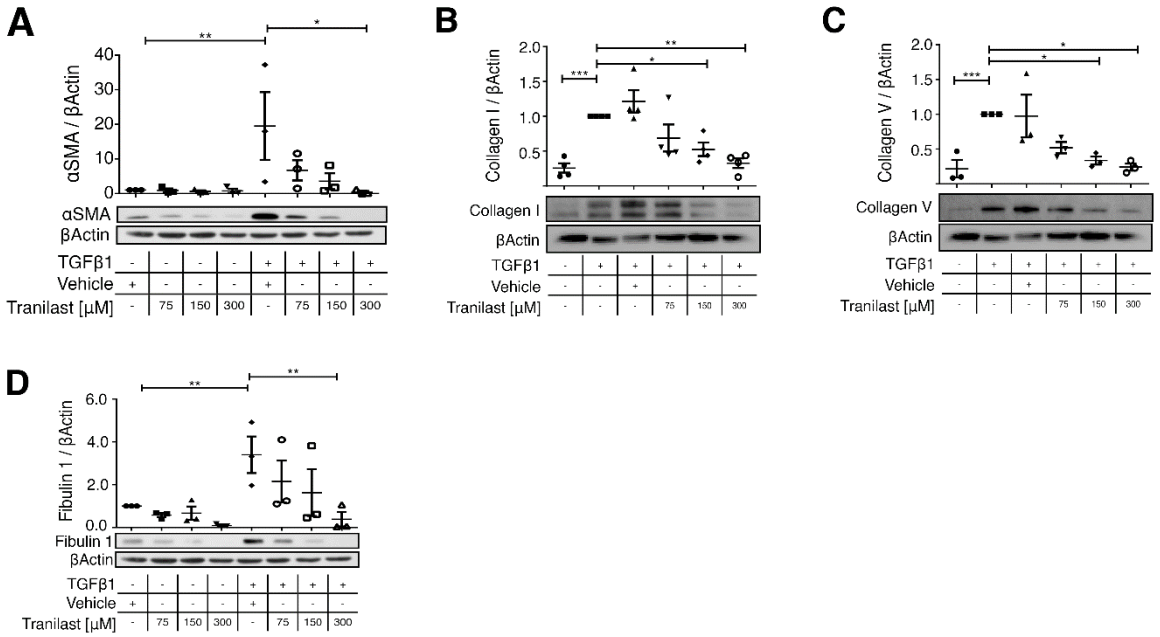

Figure 18: Effects of Tranilast of primary human lung fibroblast protein expression by Western blot.

Protein expression of **(A)** αSMA, **(B)** Collagen I, **(C)** Collagen V, **(D)** Fibulin-1 of primary human lung fibroblasts treated ± TGFβ1 ± Tranilast or vehicle assessed by Western blotting. Statistics: One-way ANOVA with Bonferroni-correction. * p<0.0.5, ** p<0.01, *** p<0.001. n = 3-4 (phLFs from three or four different donors). Data are presented as means ± SEM.

8.6. Discovery of novel cinnamic acid amides for their antifibrotic activity

Inhibition of TGFβ1-induced ECM deposition of phLFs by Tranilast only occurred at high concentrations beyond 100 µM. To identify possible more potent Tranilast derivatives, I performed a structure-activity-relationship (SAR) studies of commercially available compounds ("catalog SAR") making use of a N-2-phenyl-3-phenyl-acrylamide Markush formula, shown in **Figure 19 A-B**.

A

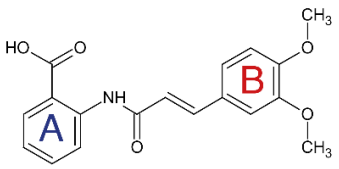

B

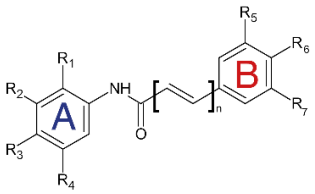

C

Compound	n	R1	R2	R3	R4	R5	R6	R7	active at 10µM
Compound 1	0	-COOH	-H	-H	-H	-H	-O Methyl	-O Methyl	-
Compound 2	1	-COOH	-H	-H	-H	-H	-O Methyl	-O Methyl	-
Compound 3	1	-H	-O Methyl	-O Methyl	-H	-H	-O Methyl	-O Methyl	-
Compound 4	1	-O*n* Butyl	-H	-H	-H	-H	-O Methyl	-O Methyl	yes
Compound 9	1	-COO-Eth	-H	-H	-H	-O Methyl	-O Methyl	-O Methyl	*cytotoxic*
Compound 10	1	-H	-COO-Me	-H	-H	-O Methyl	-O Methyl	-O Methyl	*cytotoxic*
Compound 11	1	-H	-H	-COO-Me	-H	-O Methyl	-O Methyl	-O Methyl	*cytotoxic*
Compound 12	1	-O*n* Butyl	-H	-H	-H	-H	-O Methyl	-O Ethyl	yes
Compound 13	1	-H	-H	-O*n* Butyl	-H	-O Methyl	-H	-O Methyl	-
Compound 14	1	-H	-H	-O*n* Butyl	-H	-H	-O Methyl	-O Ethyl	-
Compound 15	1	-H	-O Methyl	-O Methyl	-H	-H	-O*n* Butyl	-H	-
Compound 16	1	-O*n* Butyl	-H	-H	-H	-H	-H	-H	-
Compound 17	1	-O*n* Butyl	-H	-H	-H	-H	-O*n* Butyl	-H	yes
Compound 18	1	-O*n* Butyl	-H	-H	-H	-H	-O Methyl	-H	yes
Compound 19	1	-O*n* Propyl	-H	-H	-H	-H	-O Methyl	-O Methyl	-
Compound 20	1	-O Ethyl	-H	-H	-H	-H	-O Methyl	-O Methyl	-
Compound 21	1	-O Methyl	-H	-H	-H	-H	-O Methyl	-O Methyl	-

D

Compound	n	R1	R2	R3	R4	R5	R6	R7	active at 10µM
Compound 24	1	-O Methyl	-H	-H	-H	-H	-O Methyl	-O Methyl	-
Compound 25	1	-O*iso* Butyl	-H	-H	-H	-H	-O Methyl	-O Methyl	-
Compound 26	1	-*n* Butyl	-H	-H	-H	-H	-O Methyl	-O Methyl	-
Compound 27	1	-H	-O*n* Butyl	-H	-H	-H	-O Methyl	-O Methyl	-
Compound 28	1	Butyramide	-H	-H	-H	-H	-O Methyl	-O Methyl	-
Compound 29	1	-O*n* Propyl	-H	-F	-H	-H	-O Methyl	-O Methyl	-
Compound 30	1	-O*n* Propyl	-H	-H	-F	-H	-O Methyl	-O Methyl	
Compound 31	1	-O*n* Butyl	-H	-H	-H	-H			yes
Compound 32	1	-H	-O Methyl	-H	-H	-H	-O Methyl	-O Methyl	-
Compound 33	1	-O*n* Propyl	-F	-H	-H	-H	-O Methyl	-O Methyl	-
Compound 34	1	-O*n* Butyl	-H	-H	-H	-H	-O Ethyl	-O Ethyl	-
Compound 35	1	-O Benzyl	-H	-H	-H	-H	-O Methyl	-O Methyl	yes

Figure 19: Activity of different cinnamic acid amides.

(A) Chemical structure formula of Tranilast, **(B)** Markush structure of cinnamic acid amides tested in the following. **(C)** Table of commercially available cinnamic acid amides evaluated for inhibitory activity towards TGFβ1-induced ECM deposition at 10 µM. **(D)** Table of cinnamic acid amides synthesized by

the laboratory of Prof. Oliver Plettenburg specifically for these experiments and tested for inhibitory activity towards TGFβ1-induced ECM deposition at 10 µM.

Surprisingly, a substitution of the carboxy-group at R1 by a butoxy-group along with the elimination of the methoxy-group at the meta position at the “B”-ring lead to an outstanding increase in potency of up to >100 fold. Here, compound 4, 12, 17, 18 sharing the butoxy substitution at R1 and similar substitution patterns at R6 and R7 showed activity for the inhibition of TGFβ1-induced ECM deposition at 10 µM and below (**Figure 19 C**). Tests with additional compounds specifically designed and newly synthesized for this SAR study by medicinal chemistry revealed two additional active compounds, namely compound 31 and 35 (**Figure 19 D**). Additionally, to the butoxyl-group R1-substitution,, the substitution with a o-benzyl-group (compound 35) led to an antifibrotic activity at 10 µM concentration and below. Furthermore, a substitution at R6/7 leading to the formation of a benzodioxol at ring “B” (compound 31) showed a similar activity. Detailed potency estimations for all of these compounds are summarized in **Figure 20 A-G**.

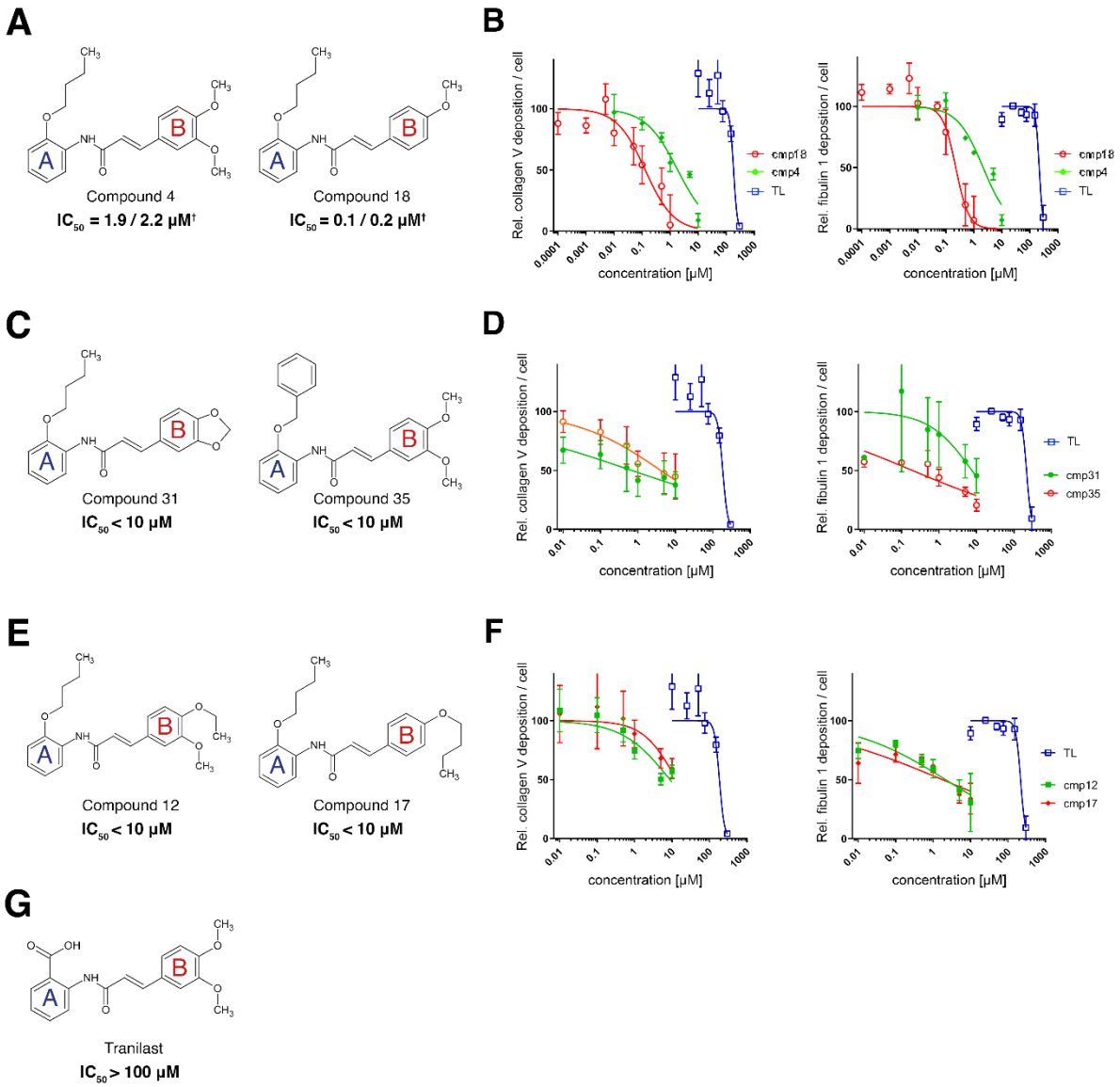

Figure 20: Potency of Tranilast and selected N-2-phenyl-3-(phenyl)-acrylamides.
Dose-response-curve of the inhibition of TGFβ1-induced Collagen V and Fibulin-1 deposition of **(A-B)** compound 4 and 18, **(C-D)** compound 31 and 35 as well as **(E-F)** compound 12 and 17 compared to **(G)** Tranilast. Statistics in (A): Estimated IC_{50} values for †Fibulin-1 deposition and Collagen V deposition, respectively using approximated sigmoid dose response curves are shown. Alternatively, in (C), (E) and (G), IC_{50} ranges are given, as IC50 value determination was not possible due to large standard deviations.

To confirm the inhibitory activity of N23Ps on TGFβ1-induced ECM deposition in phLFs, I investigated the effects of TGFβ1 and compound 4 on phLF ECM deposition by means of timelapse live-cell imaging experiments (**Figure 21 A**). Within 48 h post treatment with TGFβ1

and compound 4, a dynamic compound 4-mediated inhibition of TGFβ1-induced ECM deposition could be confirmed qualitatively and quantitatively (**Figure 21 B**).

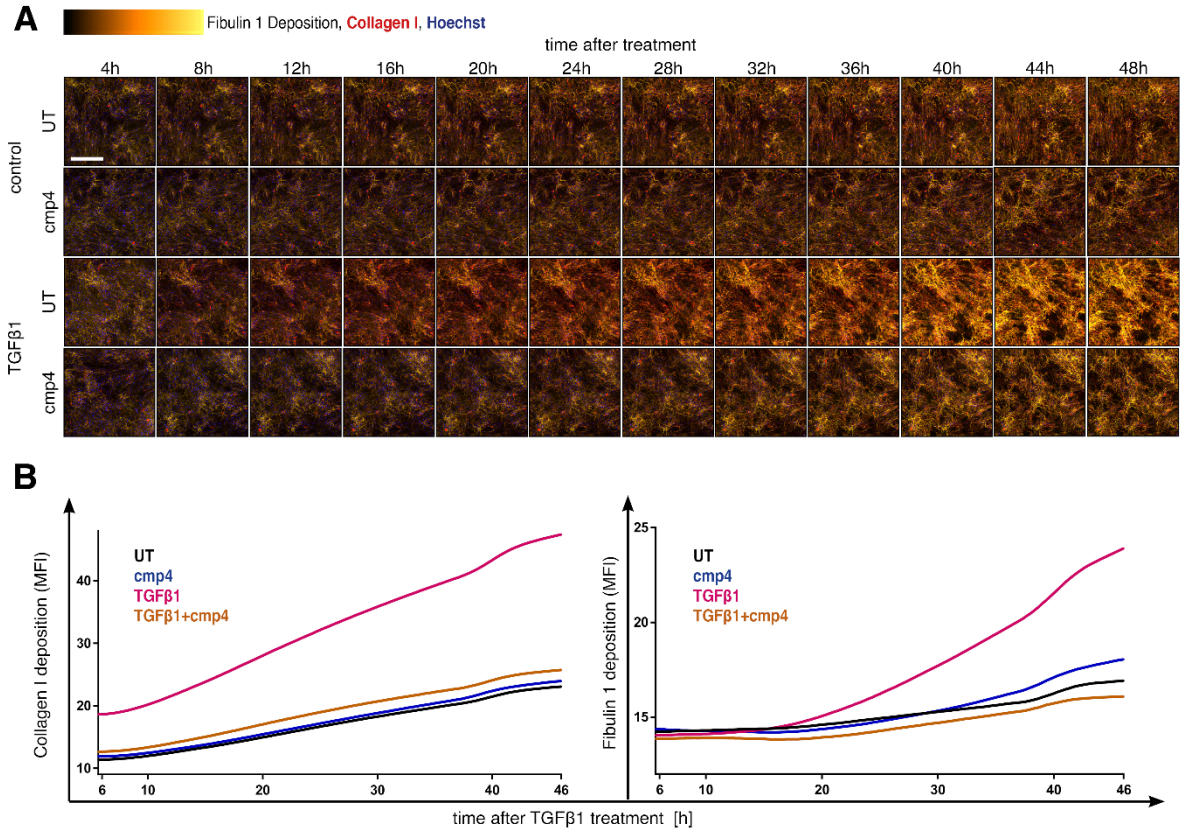

Figure 21: Live imaging of ECM deposition by phLFs upon TGFβ1 and compound 4 treatment. **(A)** Maximum intensity projection of confocally imaged deposited extracellular matrix in a 48 h live-cell experiment showing dynamic ECM deposition by phLFs with and without TGFβ1 and compound 4 (cmp4) treatment. Immunolabeled Collagen I is shown in red and Fibulin-1 is shown as a gold look-up table color with Hoechst nuclei counterstaining. Scale bar 500 µm. **(B)** Quantification by mean fluorescence intensity of dynamic deposition of Collagen I and Fibulin 1 of phLFs with and without TGFβ1 and cmp4 treatment.

Next, I hypothesized that N23Ps could inhibit TGFβ1-induced fibroblast-myofibroblast-transdifferentiation. By immunofluorescence staining of αSMA, a significant TGFβ1-induced upregulation of cytoskeletal αSMA expression and an inhibition thereof by all N23Ps was observed (**Figure 22 A-B**). Interestingly, N23P-treated phLFs displayed obvious cytoskeleton rearrangements according to αSMA stainings, suggestive of cell morphology changes.

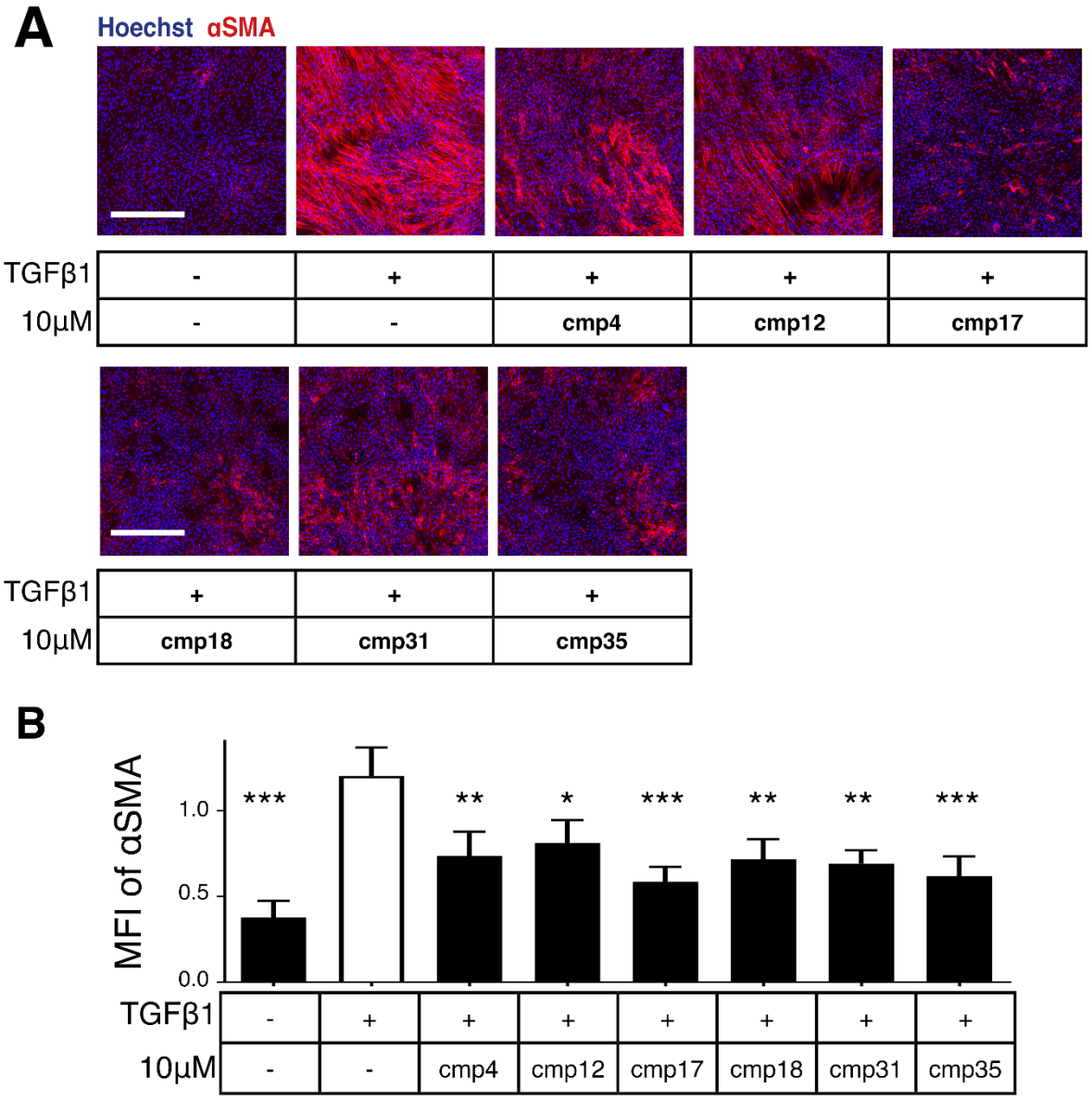

Figure 22: N23Ps inhibit TGFβ1-induced αSMA expression.

(A) αSMA expression of phLFs$^{\pm TGF\beta1\pm N23P}$ treatment by αSMA immunostaining and Hoechst nuclei counterstaining. Scale bar 500 μm. **(B)** Quantification of these stainings in three different patient cell lines. Statistics in (B): One-way ANOVA with Bonferroni-correction. * p<0.0.5, ** p<0.01, *** p<0.001. n = 3 (phLFs from three different patients). Data are presented as means ± SEM.

Indeed, follow-up experiments by using calcein and phalloidin staining of cytoplasm and F-actin, respectively, showed dramatic changes in cell morphology towards a round or polygonal cell shape (**Figure 23 A**). Rounding of phLFs^{+cmp4} was quantified using the CellProfiler software (**Figure 23 B-D**).

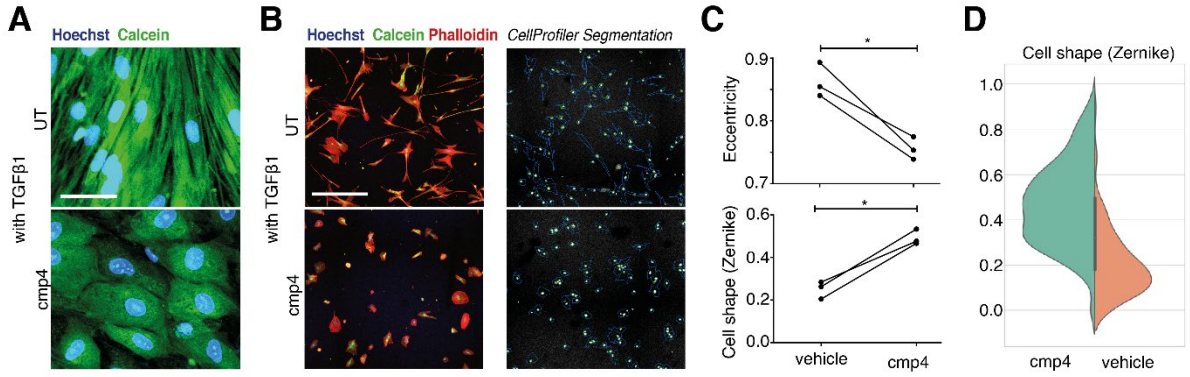

Figure 23: N23Ps affect cell shape changes.
(A) Calcein cytoplasm staining and Hoechst nuclei counterstaining of TGFβ1-stimulated phLF ± 10 µM compound 4 treatment. Scale bar 500 µm. **(B)** Calcein cell cytoplasm staining, phalloidin actin-cytoskeleton staining, and Hoechst nuclei counterstaining of TGFβ1-stimulated phLF ± 10 µM compound 4 treatment and subsequent single cell segmentation by the CellProfiler software. Scale bar 500 µm. **(C)** Quantification of cell shape (Zernike) and cell eccentricity parameter of the phalloidin / Hoechst staining. **(D)** Distribution of cell shape (Zernike) parameter in phLFs with and without cmp4 treatment as violin plot. Statistics in (C): Paired t tests. *p < 0.05. n = 3 (three different patient phLFs).

In order to proof activity of N23Ps in fibroblasts from different tissue origin, I investigated the effects of TGFβ1 and compounds on primary human dermal fibroblasts. Strikingly, TGFβ1-highly induced excessive ECM deposition and N23Ps were inhibited this process. Interestingly, dermal fibroblasts showed a higher sensitivity to N23Ps effects compared to lung fibroblasts. Full inhibition of TGFβ1-induced ECM deposition was seen at 50 nM with all tested N23Ps, compared to 10 µM in phLFs.

In summary, N23Ps were discovered as a novel class of small molecules for inhibiting TGFβ1-induced ECM deposition, displaying a massive increase in potency compared to Tranilast.

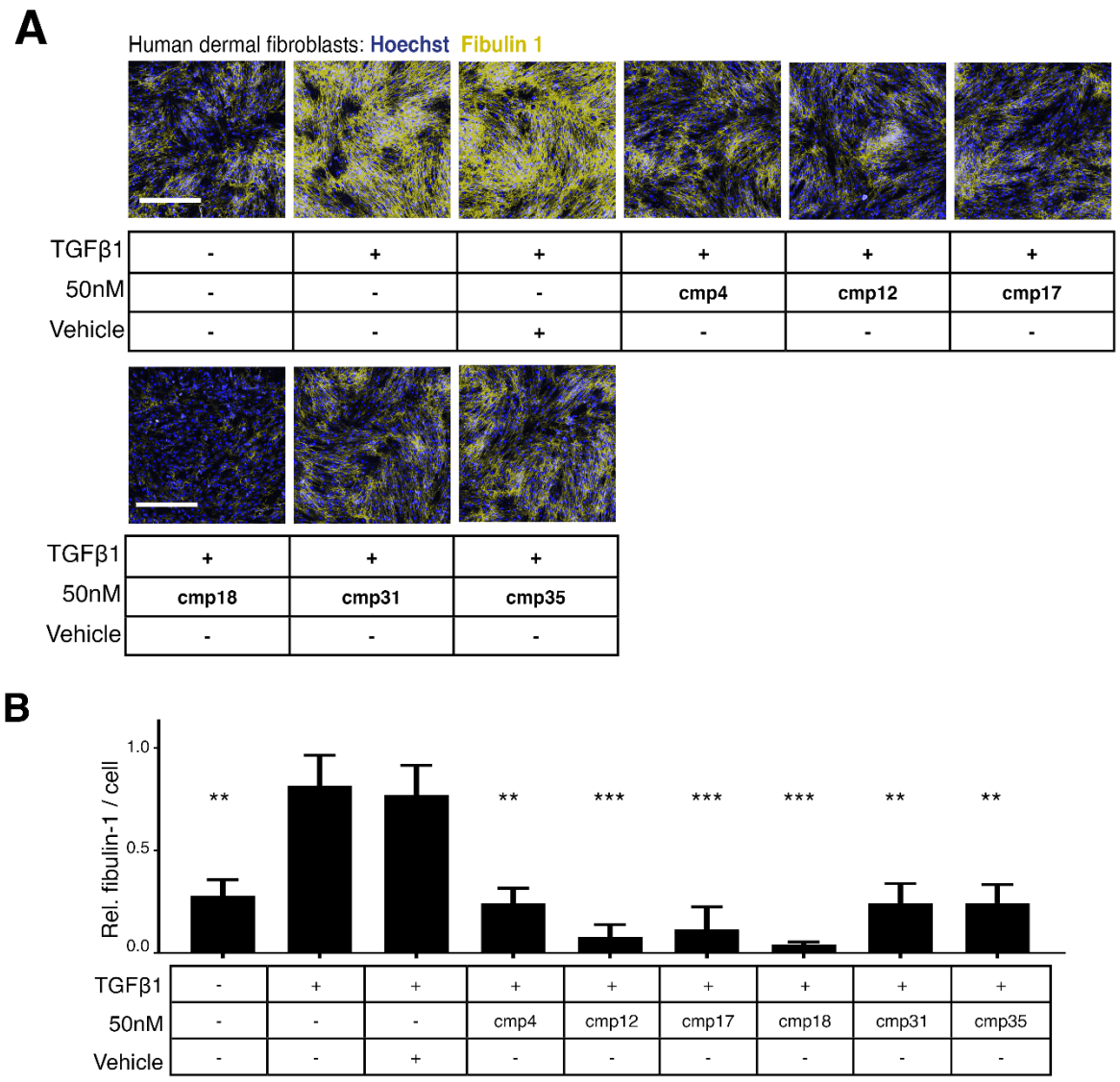

Figure 24: N23Ps inhibit ECM deposition in dermal fibroblasts.

(A) Fibulin-1 deposition of primary dermal fibroblasts$^{\pm TGF\beta1\pm N23P}$ treatment assessed by the ECM deposition assay. **(B)** Quantification of the Fibulin-1 deposition in three different dermal fibroblast cell lines. Statistics in (B): One-way ANOVA with Bonferroni-correction. * p<0.0.5, ** p<0.01, *** p<0.001. Data are presented as means ± SEM. n = 3 (human dermal fibroblasts from three different donors).

8.7. Effects of N-2-phenyl-3-(phenyl)-acrylamides on the phLF transcriptome

To investigate molecular mechanisms of N23P pharmacology, a microarray-based transcriptomics experiment on of phLFs was performed. An extensive bioinformatic data analysis was applied comparing transcriptome changes of myofibroblasts (phLF$^{+TGFβ1}$) with quiescent fibroblasts (phLF^{untreated}) and cmp4-treated fibroblasts / myofibroblasts (phLF^{+cmp4} and phLF$^{+TGFβ1+cmp4}$) (**Figure 25 A-B**). The dataset of bulk transcriptomics of three different IPF patient-derived phLFs was deposited in the Gene Expression Omnibus (GEO) repository (GSE141905).

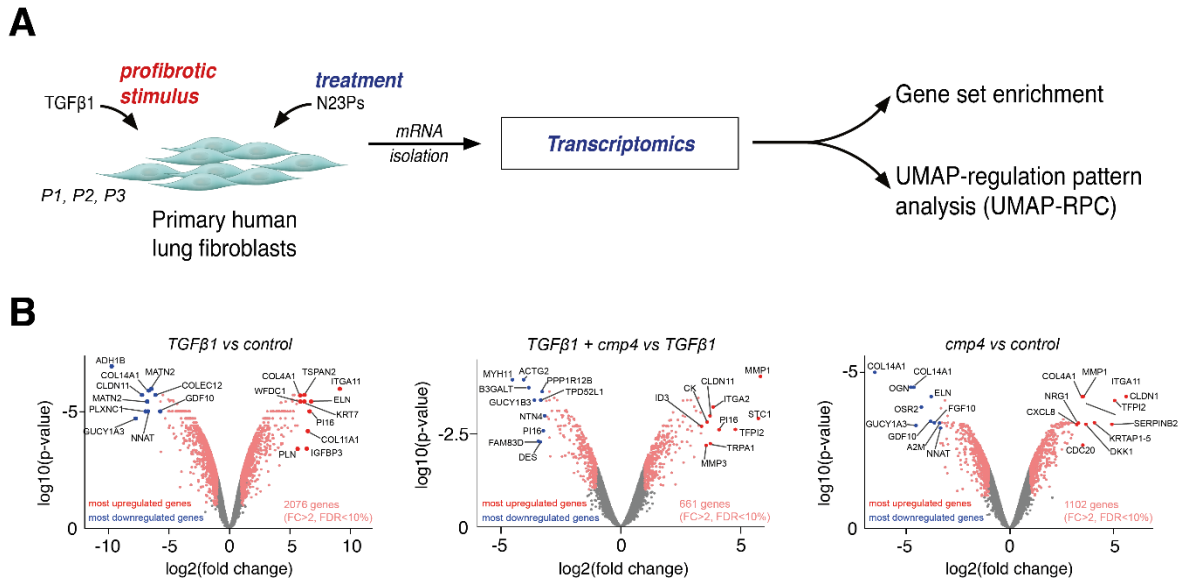

Figure 25: Transcriptomic changes of cmp4 treatment of phLFs.
(A) Experimental set-up of microarray-based analysis of phLF transcriptome ± TGFβ1 ± cmp4. **(B)** Volcano plots depicting all significantly differentially expressed genes (>2-fold change (FC), false discovery rate (FDR) < 10%) in phLFs$^{+TGFβ1}$ vs phLFs^{untreated}, phLFs$^{+TGFβ1+cmp4}$ vs phLFs$^{+TGFβ1}$, phLFs^{+cmp4} vs phLFs^{untreated} highlighting the 10 most up- (red) and downregulated (blue) abundant transcripts.

Comparing phLFs$^{+TGFβ1}$ vs phLFs^{untreated}, 2076 genes were found to be significantly deregulated. Comparing phLFs$^{+TGFβ1+cmp4}$ with phLFs$^{+TGFβ1}$ 661 genes were significantly deregulated. 1102 genes were significantly deregulated comparing phLFs^{untreated} with phLFs^{+cmp4} (all > 2-fold, FDR < 10%) (**Figure 26 A**). Interestingly, most genes deregulated comparing phLFs$^{+TGFβ1+cmp4}$ vs phLFs$^{+TGFβ1}$, were counter regulated, hinting at an antagonistic activity of cmp4 towards TGFβ1 signaling (**Figure 26 B**). An unbiased gene-set enrichment analysis (GSEA) comparing phLFs+TGFβ1+cmp4 compared to phLFs+TGFβ1 showed a negative enrichment for profibrotic functional gene signatures like collagen formation, extracellular matrix organization and smooth muscle contraction (**Figure 26 C-E**).

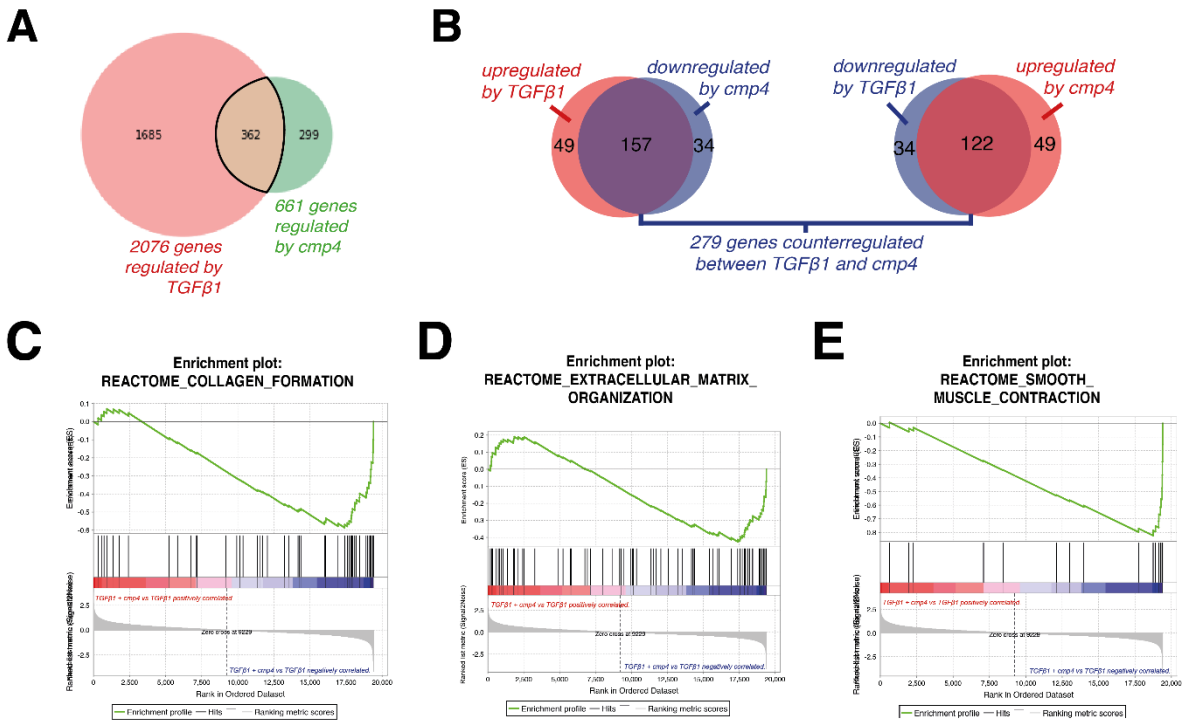

Figure 26: Gene set enrichment analysis of compound 4 effects in TGFβ1-treated phLFs.
(A) Venn diagram displaying an overlap of 362 genes between 2076 deregulated genes in phLFs$^{+TGFβ1}$ and 661 deregulated genes in phLFs$^{+TGFβ1+cmp4}$. **(B)** Venn diagram pointing out 279 out of those 362 genes are counter-regulated by TGFβ1 and compound 4. **(C)** GSEA of phLFs$^{+TGFβ1+cmp4}$ showing a negative enrichment for profibrotic gene signatures such as collagen formation, **(D)** ECM organization, and **(E)** smooth muscle contraction.

8.8. UMAP-regulation pattern recognition: a new analysis tool to investigate complex coregulations of gene expression.

Analysis of coregulated and functionally related genes is typically performed using hierarchical clustering dendrograms and heatmaps. However, these analysis methods preserve a high degree of complexity in their data visualizations. Therefore, I developed a novel data analysis tool called “uniform manifold approximation and projection for regulation pattern clustering” based on the uniform manifold approximation and projection (UMAP) method, termed “UMAP-RPC”. UMAP-RPC was designed to facilitate regulation pattern recognition on the first sight, in detail described in Gerckens et al. 2021. In the UMAP-RPC plots each dot represents a regulated gene; genes plotted in proximity show similar regulation patterns across different experimental conditions (**Figure 27 A**). For example, genes in Cluster A were upregulated in phLFs$^{+TGF\beta1}$ compared to phLFs^{untreated} (indicated by red color), downregulated in phLFs$^{+TGF\beta1+cmp4}$ compared to phLFs$^{+TGF\beta1}$ (indicated by blue color), and only weakly regulated when compared to phLF^{+cmp4} with phLFs^{untreated} (indicated by weak red, weak blue or white color-coded dots) (**Figure 27 B**). On the other side, Cluster B contains genes that were only weakly regulated in phLFs$^{+TGF\beta1}$ compared to phLFs^{untreated} but were upregulated in phLFs$^{+TGF\beta1+cmp4}$ compared to phLFs$^{+TGF\beta1}$ and phLFs^{+cmp4} compared to phLFs^{untreated}. Subsequent STRING database analysis revealed functional networks of similarly regulated genes, which provide valuable insights into interactions between TGFβ1 and compound 4 treatment (**Figure 27 C**).

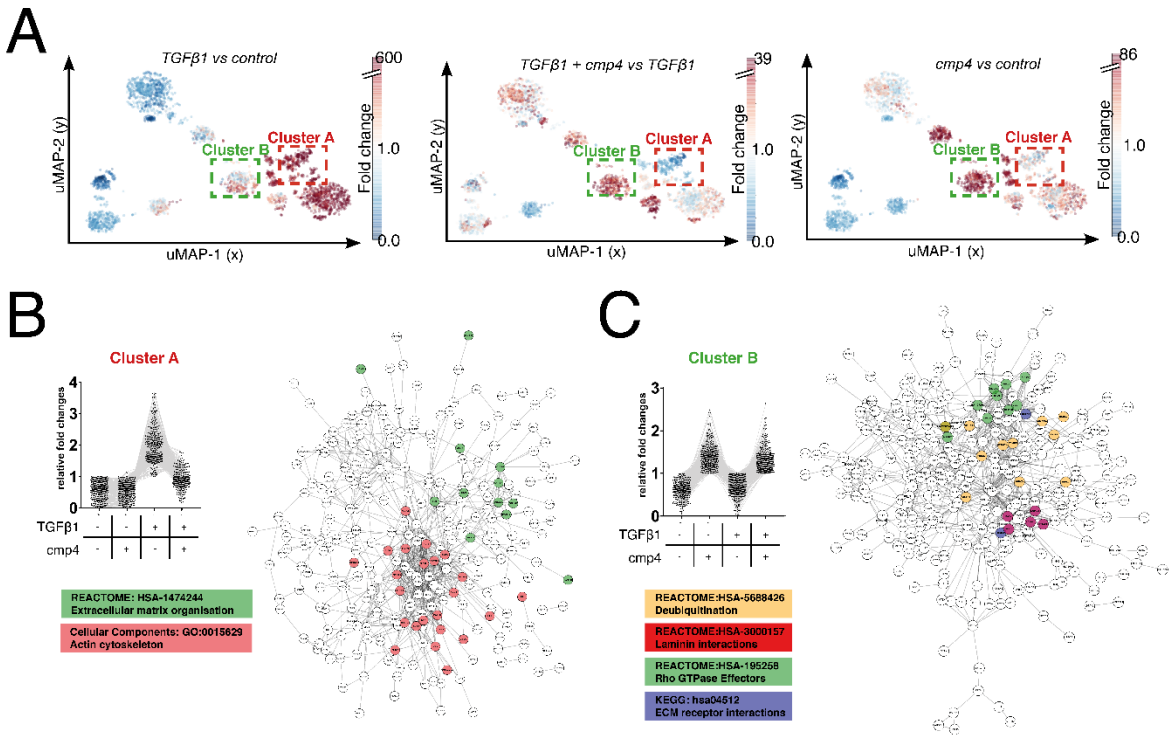

Figure 27: UMAP-RPC for the analysis of TGFβ1 and cmp4-induced transcriptomic changes.
(A) UMAP-RPC scatter plots of all differentially expressed genes (>2 fold, FDR<10%). Each point represents a single gene. Each gene's relative localization in the plot reflects to their similarities in gene-expression patterns between phLFs^{untreated}, phLFs$^{+TGFβ1}$, phLFs^{+cmp4} and phLFs$^{+TGFβ1+cmp4}$. The same plot is displayed three times with color coding overlaying each gene with the magnitude of this gene's regulation across the indicated conditions. The boxed Cluster A (red) designates genes that were mostly found up-regulated in phLFs$^{+TGFβ1}$, but not upregulated in the phLFs$^{+TGFβ1+cmp4}$, and boxed Cluster B (green) designates genes that were up-regulated in phLFs$^{+TGFβ1+cmp4}$ and phLFs^{+cmp4}. **(B)** Relative regulation of transcripts of Cluster A genes and a visualization of these genes' predicted protein-protein interaction network analysis found by the STRING database and two selected gene ontologies (HSA-1474244 and GO:0015629) highlighted. **(C)** Relative regulation of transcripts of Cluster B genes and a visualization of these genes' protein-protein interaction networks analysis found by the STRING database and four selected gene ontologies (HSA-5688426, HAS-200157, HSA195258 and HSA-04512) color-coded in yellow, red, green and blue.

Cluster A displays TGFβ1-mediated gene induction which was inhibited by compound 4. While genes in Cluster B show TGFβ1-independent effects of compound 4. Interestingly, a larger number of fibrosis-related and TGFβ1-upregulated genes which are associated with ECM organization and (myofibroblastic) actin cytoskeleton regulation were inhibited by compound 4, thus strikingly reflecting its antifibrotic activity *in-vitro* (**Figure 28 A**). Additionally, (de-) ubiquitination-associated proteins, like SMURF2, were found to be upregulated by compound4 - independent of TGFβ1 effects (**Figure 28 B**).

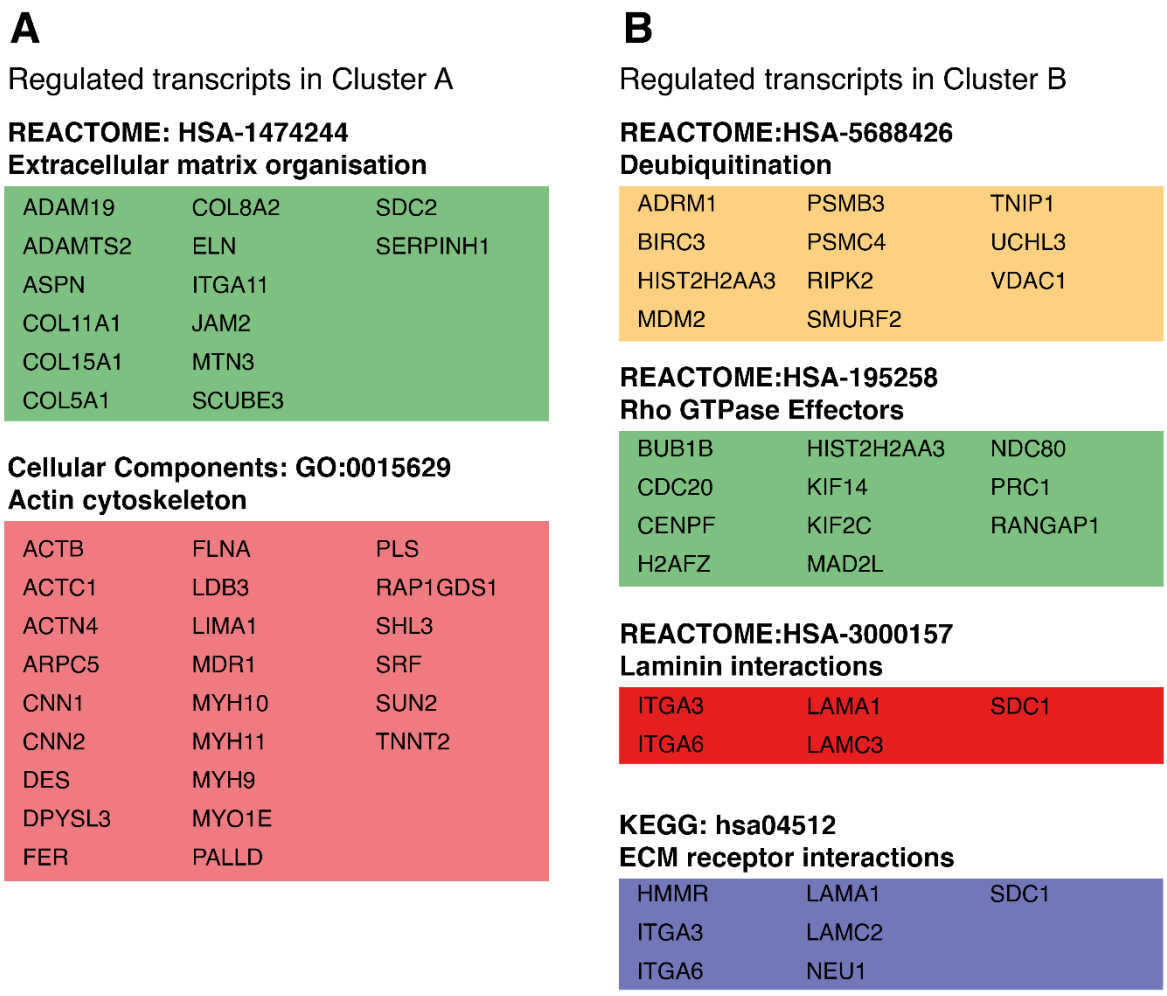

Figure 28: Transcripts in clusters A and B characterized by similar TGFβ1- and cmp4-induced transcriptomic changes.

(A) List of Cluster A genes associated with selected gene ontology terms according to functional enrichment analysis of STRING Database. **(B)** List of Cluster B genes associated with selected gene ontology terms according to functional enrichment analysis of STRING Database.

8.9. N23P inhibition of TGFβ1-induced fibroblast-myofibroblast transdifferentiation depends on SMURF2

The UMAP-RPC analysis of phLF transcriptomics suggested a role of SMURF2 in the mode of action of N23Ps, independent of TGFβ1 treatment. SMURF2 is known to negatively regulate TGFβ/Smad signaling (Zhang et al. 2001; Liu-Ya Tang et al. 2011; Xu et al. 2017). Therefore, I hypothesized that an upregulation of SMURF2 by N23Ps could lead to the negative regulation of the TGFβ1/Smad pathway. To test this hypothesis further, I performed a rescue experiment by inhibiting SMURF2 expression using RNA interference and assessed fibroblast-myofibroblasts-transdifferentiation by αSMA expression.

siRNA transfection decreased expression of SMURF2 successfully by a 3.5-fold compared to controls (**Figure 29 A**). Upon SMURF2-knockdown, I observed a rescue of compound 4-mediated inhibition of TGFβ1-induced αSMA expression in phLFs as demonstrated by immunofluorescence staining of αSMA (**Figure 29 B**). This finding was further confirmed by protein analysis using Western blotting (**Figure 29 C**). In conclusion, these experiments support the hypothesis that N23Ps led to an increased expression of SMURF2, thus inhibiting fibroblast-myofibroblasts-transdifferentation (**Figure 29 D**) - potentially by known mechanisms (Liu-Ya Tang et al. 2011).

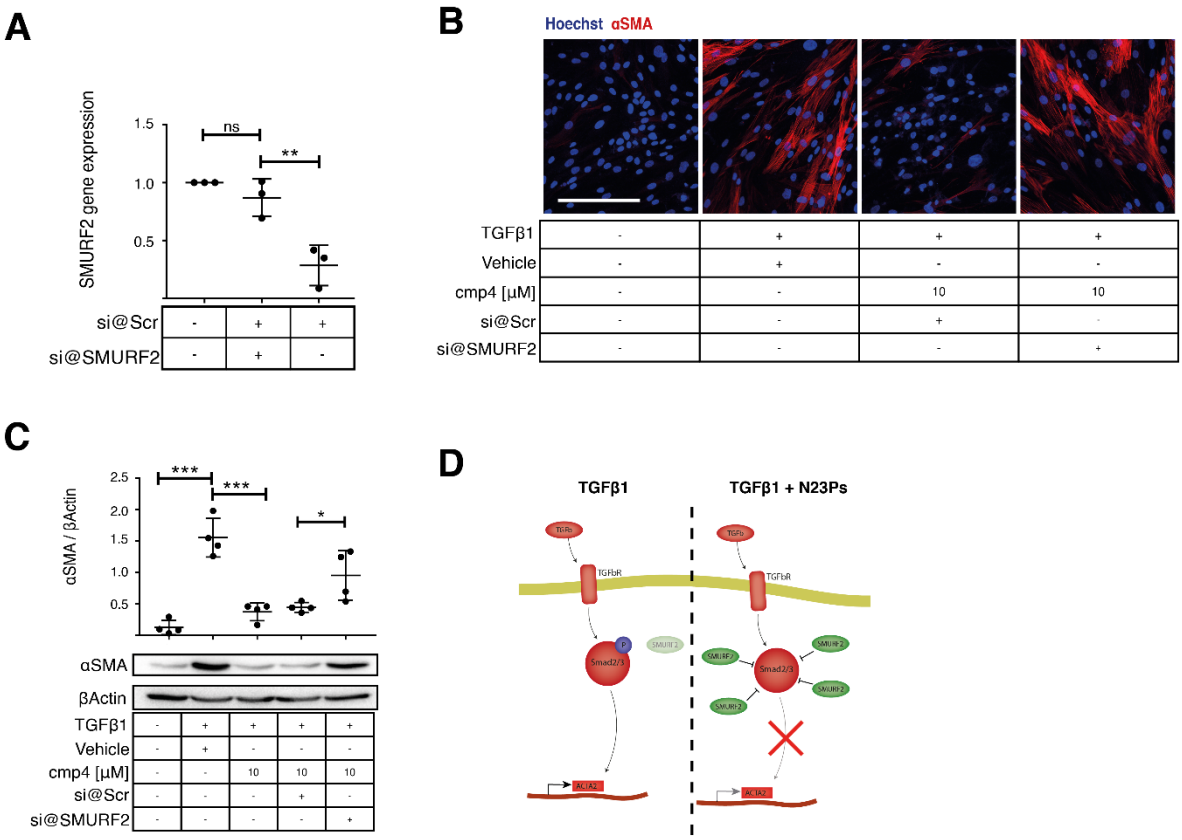

Figure 29: SMURF2-dependent inhibition of TGFβ1 signaling by cmp4.

(A) Reduction of SMURF2 expression by >70% in phLFs by RNA interference through reverse siRNA transfection. **(B)** αSMA immunofluorescence staining with Hoechst nuclei counterstaining in phLFs^{untreated}, phLFs$^{+TGFβ1}$, phLFs$^{+TGFβ1+cmp4}$ with and without SMURF2 depletion by RNA interference. Scale bar 200 µm. **(C)** Protein expression analysis of αSMA normalized to βActin by Western blot in phLFs^{untreated}, phLFs$^{+TGFβ1}$, phLFs$^{+TGFβ1+cmp4}$ with and without SMURF2 depletion by RNA interference. **(D)** Illustration depicting a possible mode of action of N23Ps by upregulation SMURF2 expression and thus inhibition of SMAD2 signaling by SMURF2 and consecutive blockage of fibroblast-myofibroblast-transdifferentiation. Statistics in (A) and (C): *p < 0.05, **p < 0.01, and ***p < 0.001. One-way ANOVA with Bonferroni correction. Data are presented as means ± SEM. n = 3-4 (phLFs from three or four different patients).

8.10. Precision cut lung slices (PCLS) as an *ex-vivo* human lung fibrosis model

After confirming the antifibrotic activity of N23Ps *in-cellulo* in IPF patient derived-primary human lung fibroblasts, N23Ps' antifibrotic activity was validated in a more complex model of human lung fibrosis using *ex-vivo* cultures of living three-dimensional human precision lung slices (hPCLS). hPCLS were previously used as a model for lung fibrosis by inducing fibrotic changes in native human peritumor lung tissue. A stimulation with a profibrotic cocktail (FC) of growth factors and other signaling molecules, namely TGFβ1, TNFα, PDGF-AB, and lysophosphatidic acid (LPA) induced tissue changes mimicking tissue injury and early fibrosis-like responses in human lung tissue (Alsafadi et al. 2017).

8.11. Validation of N23Ps' antifibrotic activity in a hPCLS fibrosis model

To assess the effects of N23Ps on FC-induced fibrotic changes in hPCLS, hPCLS were generated from resected agarose filled human lung tissue. hPCLS derived from three different patients were treated with profibrotic cocktail (FC), control cocktail (CC) containing vehicles of the profibrotic cocktail, FC + compound 4 and FC + Tranilast. Finally, protein was isolated and subjected to a LC-MS^2 proteomic analysis and validation by Western blotting and ELISA (**Figure 30**).

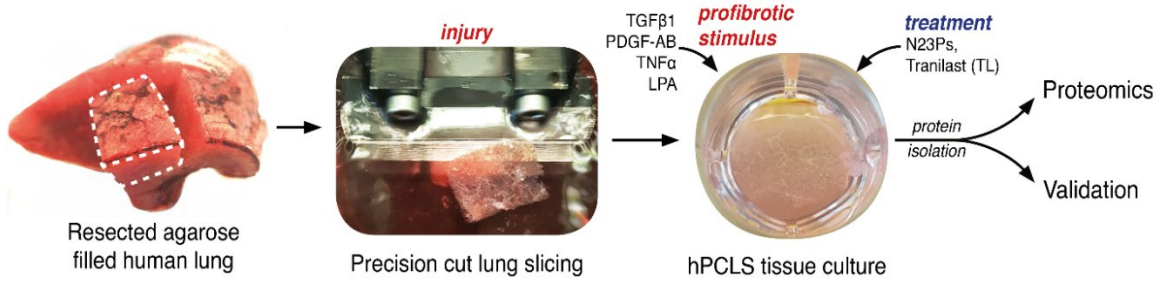

Figure 30: Experimental setup investigating the effects of N23Ps and Tranilast on hPCLS after pro-fibrotic cocktail treatment.
Agarose-filled resected human lung tissue was sliced using a vibratome into precision cut lung slices and subsequently treated with a profibrotic cocktail containing TGFβ1, TNFα, PDGF-AB and LPA as pro-fibrotic stimulus in combination with N23Ps or Tranilast. Protein from the cultured hPCLS was isolated for LC-MS^2 proteomic analysis as well as validation experiments by Western blotting and ELISA.

Proteome profiling of the conditions mentioned above identified a multitude of differentially regulated proteins (**Figure 31 A**): overall 3365 proteins were detected and 135 proteins were significantly regulated comparing hPCLS^{+FC} and hPCLS^{+CC}. The 20 most upregulated and downregulated proteins between these conditions are shown in **Figure 31 B**. Interestingly, several proteins among these 40 highly regulated proteins were associated with tissue fibrosis in the literature, with most proteins highly abundant in the hPCLS^{+FC} condition showing low abundancy in the hPCLS$^{+FC+cmp4}$ and hPCLS$^{+FC+Tranilast}$ condition (**Figure 31 C**).

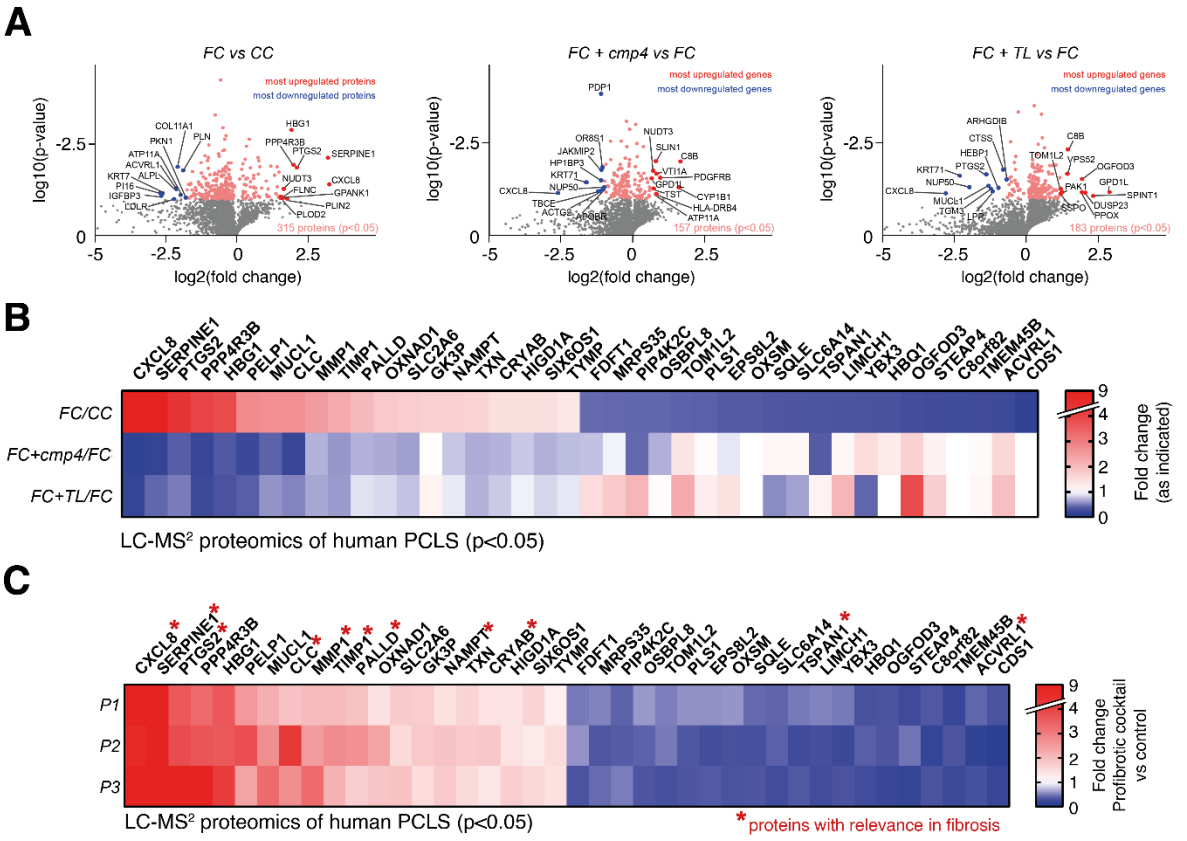

Figure 31: Proteomic changes in hPCLS by profibrotic cocktail, compound 4 and Tranilast.
(A) Volcano plots showing differential expression of proteins between hPCLS$^{+profibrotic\ cocktail\ (FC)}$ and hPCLS$^{+control\ cocktail\ (CC)}$, between hPCLS$^{+FC+compound\ 4\ (cmp4)}$ with hPCLS^{+FC} and hPCLS$^{+FC+Tranilast\ (TL)}$ with hPCLS^{+FC}. Significantly regulated (p<0.05) proteins are color-labeled (pink). The ten most up- and downregulated proteins in each volcano plot are identified by the gene name. **(B)** Heatmap of average fold changes of the 20 most up- and downregulated proteins in between the differently treated hPCLS cultures. **(C)** Heatmap of fold change of the 20 most up- and downregulated proteins for hPCLS culture of each biological replicate, demonstrating the degree of inter-patient variability.

To explore potential protein regulation patterns in this dataset of four different conditions (hPCLS^{+CC}, hPCLS^{+FC}, hPCLS$^{+FC+cmp4}$, hPCLS$^{+FC+Tranilast}$), I used the previously described UMAP-RPC analysis tool (**Figure 27**). Here, multiple clusters of proteins, which were similarly regulated between the different experimental conditions, were found (**Figure 32 A**). Cluster A contains proteins highly upregulated in hPCLS^{+FC} compared to hPCLS^{+CC} that were also downregulated when comparing hPCLS^{+FC} with hPCLS$^{+FC+cmp4}$ and hPCLS$^{+FC+Tranilast}$. Proteins with the opposite regulation pattern were found in Cluster C. Those proteins were downregulated in hPCLS^{+FC} compared to hPCLS^{+CC}, but upregulated comparing hPCLS^{+FC} with hPCLS$^{+FC+cmp4}$ and hPCLS$^{+FC+Tranilast}$. Cluster D contains proteins downregulated in hPCLS^{+FC} compared hPCLS^{+CC} that were upregulated hPCLS$^{+FC+cmp4}$ but not in hPCLS$^{+FC+Tranilast}$ compared with hPCLS^{+FC} indicating that a cluster of proteins was differentially regulated when compared to Tranilast and compound 4 treatment. Similarly, Cluster B contains proteins downregulated in hPCLS^{+FC} compared to hPCLS^{+CC}, downregulated in hPCLS$^{+FC+cmp4}$ compared to hPCLS^{+FC}, but not regulated by Tranilast. (**Figure 32 B**).

The subsequent analysis focused on Cluster A, as it seemed most interesting for investigation the Tranilast and compound 4-mediated antagonism of FC-induced changes. A STRING database analysis (Szklarczyk et al. 2021) for functional protein-protein-interactions in Cluster A found subnetworks of fibrosis-related proteins associated with gene ontology annotations "extracellular matrix organization” (HSA-1474244) and “actin cytoskeleton” (GO:0015629) (**Figure 32 C-D**). Strikingly, these match with gene ontology terms found in the UMAP-RPC analysis of phLF transcriptomics experiment described before (**Figure 27-28**).

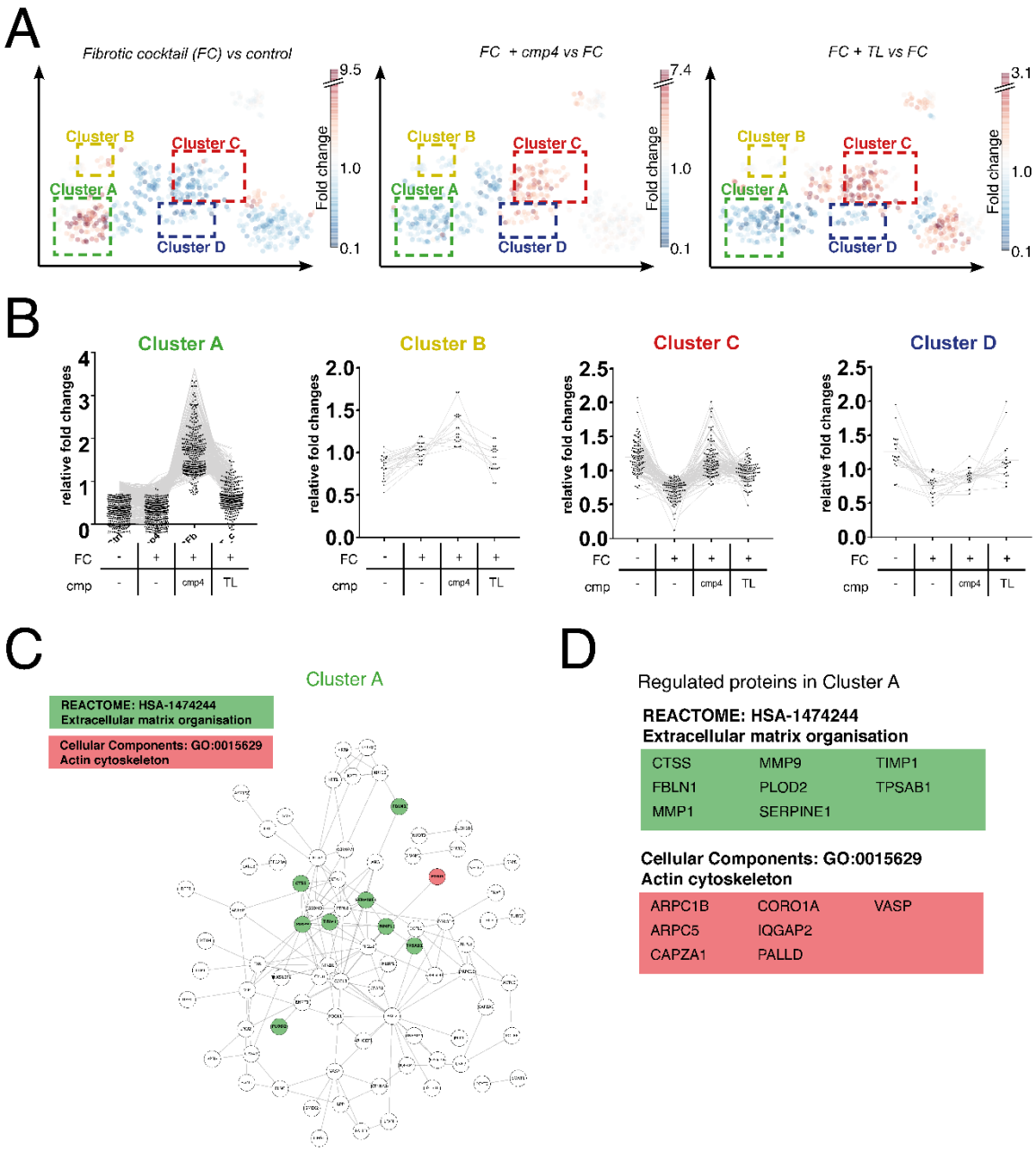

Figure 32: UMAP-RPC of proteome changes in hPCLS induced by profibrotic cocktail, compound 4 (cmp4) and Tranilast (TL) treatment.

(A) UMAP-RPC scatter plots of 580 differentially expressed proteins ($p<0.1$) plotted according to their protein regulation patterns comparing four tested conditions. The UMAP-RPC plot is displayed three times with color coding each protein with the magnitude of this protein's regulation across the indicated conditions. The boxed clusters indicate proteins with similar regulation patterns between experimental conditions. **(B)** Relative regulation of protein abundancy of proteins in Cluster A-D. **(C)** Visualization of the predicted protein-protein-interaction network analysis of Cluster A proteins found by the STRING database, with selected gene ontology annotations color-coded in red and green. **(D)** List of proteins out of Cluster A associated with these gene ontology annotations.

Finally, the regulation of two well-known fibrosis-associated proteins was validated using Western blotting and ELISA (**Figure 33 A-B**). Here, an upregulation of secreted plasminogen activator inhibitor type 1 (PAI-1) was observed in hPCLS^{+FC} compared to hPCLS^{+CC}, and vice versa a downregulation for secreted PAI-1 in hPCLS$^{+FC+cmp4}$ compared to hPCLS^{+FC}. A similar regulation pattern is seen with the cellular interleukin 8 (IL-8) content with a non-significant trend towards a downregulation (p=0.058) of IL-8 in hPCLS$^{+FC+cmp4}$ compared to hPCLS^{+FC}.

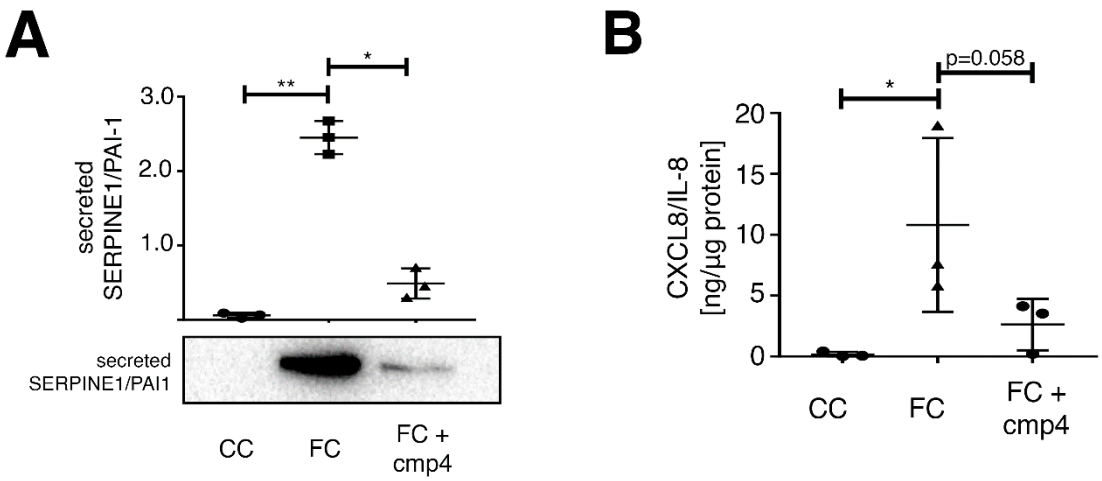

Figure 33: Secretion of PAI-1 and IL-8 in untreated, profibrotic cocktail-treated and profibrotic cocktail and cmp4-treated hPCLS.

(A) Western blot and quantification of PAI-1 secreted by hPCLS^{+CC}, hPCLS^{+FC}, hPCLS$^{+FC+cmp4}$ **(B)** Quantification of intracellular IL-8 content by ELISA showing a compound 4-mediated downregulation of FC-induced increase IL-8 expression. Statistics in (A) and (B): One-way ANOVA with Bonferroni correction. Data are presented as means ± SEM. n = 3 (three different patient hPCLS).

8.12. Summary

In summary, by utilizing, a novel ECM deposition assay was developed using patient-derived IPF phLFs and the quantification of deposited ECM proteins by immunolabeling. Next, this assay was miniaturized and transformed into a high-throughput / high-content drug screening assay and used to screen 1509 small molecules from a repurposing drug discovery library for their inhibition of TGFβ1-induced ECM deposition. By a deep learning image classification model (FANTAIL), Tranilast was identified as an inhibitor of TGFβ1-induced ECM deposition. After validation, a structure-activity relationship (SAR) of Tranilast-like small molecules brought forth N-2-phenyl-3-(phenyl)-acrylamides (N23Ps) with class-specific modifications leading to a substantial increase in potency. N23Ps effectively inhibited TGFβ1-induced fibroblast-myofibroblast-transdifferentiation and ECM deposition in phLFs and profibrotic cocktail induced changes in hPCLS. Additionally in phLFs, N23Ps affected morphology changes as well as transcriptomic changes which were not found by Tranilast treatment, hinting towards a unique antifibrotic mechanism for N23Ps. For the first time, a pharmacological activity of N23Ps was observed. In particular, the pharmacological activity of N23Ps was characterized as antagonist to profibrotic stimuli in phLFs possibly mediated by SMURF2. In lung tissue culture, N23Ps inhibited a profibrotic cocktail-induced tissue response by hPCLS.

9. Discussion

This thesis describes the establishment of a novel phenotypic and phLFs-based ECM deposition assay, its usage in a phenotypic drug discovery screening campaign for antifibrotic drugs as well as the discovery of novel cinnamic acid amides as antifibrotic small molecules.

The described ECM deposition assay allows for qualitative and quantitative assessment of ECM (fibrotic) components deposited by primary human lung fibroblasts at small scale as well as its use in high-throughput / high-content drug screening efforts. This enabled target agnostic phenotypic drug discovery in the field of lung fibrosis, where novel high-quality drug candidates are urgently needed. This and structure-activity-relationship studies of the screening hit Tranilast (3',4'-dimethoxycinnamoyl]-anthranilic acid) led to the discovery of an activity of N23Ps and other cinnamic acid amides inhibiting TGFβ1-induced ECM deposition in a SMURF2-dependent manner. This is, to my knowledge, the first time, a pharmacological activity for N23Ps and other novel cinnamic acid amides is described at all. *In-cellulo* and *ex-vivo* experiments showed antifibrotic effects of N23Ps on human cell and tissue cultures.

9.1. Drug discovery approaches for fibrotic (lung) diseases

IPF is a debilitating lethal disease associated with a devastating lung function deterioration (Lederer und Martinez 2018). While approved IPF pharmacotherapies can slow down disease progression, no drug that can halt disease progression is known. Thus, novel antifibrotic drugs that could potentially halt fibrotic disease progression are urgently needed.

Huge efforts in the antifibrotic drug and drug target discovery have been undertaken. However compounds developed in those antifibrotic drug development programs often failed in preclinical (Thannickal und Roman 2010; Yanagihara et al. 2020) and clinical stages of drug discovery (King et al. 2011; Noth et al. 2012; Raghu et al. 2017; Parker et al. 2018).

While target-based drug discovery approaches make up the largest share of drug discovery approaches, target-agnostic phenotypic drug discovery approaches have gained importance in the last decades. Interestingly, an over-proportional share of novel drugs and drug

mechanisms stemmed from phenotypic drug discovery approaches (Swinney und Anthony 2011; Swinney 2013). While the overwhelming majority of drug discovery research in lung fibrosis was a target-based approach, innovative platforms for phenotypic screenings like the ECM deposition assay might be of high value for identifying novel and highly needed drug candidates for antifibrotic drug development.

9.2. Developing a highly relevant ECM deposition assay

A review in the renowned journal “Science Translational Medicine” by Vincent et al. analyzed phenotypic drug discovery efforts retrospectively and found phenotypic drug discovery approaches most successful if the assay **a)** reflected a disease-relevant pathomechanisms as close as possible to the associated disease, **b)** used a disease-relevant stimulus inducing the disease model in the assay and **c)** had a disease-relevant assay readout recapitulating the disease manifestation as close as possible (Vincent et al. 2015). Following these guidelines, the ECM deposition assay was developed **a)** using primary IPF patient-derived fibroblasts, **b)** choosing with TGFβ1 a relevant fibrotic disease trigger, and **c)** trying to replicate TGFβ1-induced ECM deposition in its biological complexity. Here, efforts were made to model as many biomolecular fibrosis-related mechanisms as possible in the assay including TGFβ1-induced fibroblast-myofibroblast differentiation, subsequent upregulation of ECM gene and protein expression, secretion of ECM proteins into the extracellular space and the formation as well as the deposition of ECM fibers. To the best of my knowledge, no high-throughput suitable drug discovery assay recapitulating such a complex sequence of biomolecular mechanisms were described before.

Previously described drug discovery assays did only recapitulate aspects of TGFβ1-induced ECM deposition by myofibroblasts, such as fibroblast-to-myofibroblast transdifferentiation (Oh et al. 2018; Rehman et al. 2019), or transcriptomic regulation of the COL1A2 gene (Lohcharoenkal et al. 2014; Bagchi et al. 2015). Other described assays, such as the widely discussed “scar-in-a-jar” assay, did not differentiate between *deposited* insoluble extracellular matrix fibers and intracellular ECM. The experiments described in my thesis unambiguously

demonstrated that permeabilization reagents such as methanol and Triton-X100, but also crosslinking-based fixatives led to an intra-cellularization of antibodies resulting in intracellular immunostaining of pre-mature and not-yet secreted ECM components.

Here, a number of experiments demonstrated that live staining of the deposited ECM proteins enabled the exclusive immunostaining of ECM deposition. Thus, it was even possible to perform time lapse imaging to observe the interaction of phLFs assembling ECM fibers.

9.3. TGFβ1-induced ECM deposition of phLFs as an *in-cellulo* lung fibrosis model

Transforming growth factor β 1 (TGFβ1) is a well-known inductor of fibroblast-to-myofibroblast transdifferentiation (J E de Larco und G J Todaro 1978; A B Roberts et al. 1981; Harold L. Moses et al. 1981; Moses et al. 2016).It was described as master regulator of fibrogenesis (Aschner und Downey 2016) for its pivotal role in regulating fibrotic processes in a multitude of tissues.

Similar to many other in-vitro fibrosis models, I chose TGFβ1 as trigger for fibroblast-to-myofibroblast transdifferentiation. TGFβ1 reliably triggers fibroblast-to-myofibroblast transdifferentiation with consecutive functional cell changes including increased cell contractility (Desmoulière et al. 1993), as well as the increased expression and secretion of ECM components (Staab-Weijnitz et al. 2015). Previous publications reported the existence of a strong correlation between the secretome of TGFβ1-stimulated phLFs and the ECM content of IPF patient-derived lung tissue (Merl-Pham et al. 2019). Interestingly, it was indicated that ECM deposition by phLFs correlated stronger with the ECM content of IPF patient-derived lung tissue than when compared to the deposited ECM in bleomycin-induced murine lung fibrosis (Merl-Pham et al. 2019).

In the current assay and due to their known role in pulmonary fibrotic ECM organization, collagen isotypes I and V were chosen as markers indicating fibrotic ECM deposition (Onursal et al. 2021).. High-magnification imaging showed that parts of the ECM fiber network contained

either Collagen I and V only, or both. The glycoprotein Fibulin-1 served as an additional fibrotic marker as it was found to be strongly upregulated on the phLFs' surface after TGFβ1-stimulation in a previously published dataset (Heinzelmann et al. 2016). I hypothesized that the upregulation of Fibulin-1 on the cellular surface might reflect an increased deposition of Fibulin-1 in the ECM. Indeed, a strong upregulation of Fibulin-1 containing ECM was observed upon TGFβ1-stimulation. The discovery that fibulin-1 deposition is highly regulated upon TGFβ1-stimulation in phLFs was beyond what would be expected from the regulated on transcriptional and translational level. Its use in the ECM deposition assay increased the fibrotic signal in the assay and thus improved the assay's quality substantially.

9.4. Upscaling of the ECM deposition assay into a HT/HC drug screening assay

For complex cell culture-based assays, miniaturization and conversion into a high-throughput screening suitable format remains a challenge. To perform thousands of ECM deposition assays in 384-well plate wells in parallel, a robotic liquid handling system was used. was. Next, coupling automatic data acquisition by means of a confocal laser scanning microscope together with deep learning-based image analysis enabled testing and analysis of 1509 small molecules from a repurposing drug library. Here, convolutional neural network (CNN) technology strongly simplified the analysis of high-content screening data. The FANTAIL CNN provided a confident selection of ECM deposition inhibitors and effectively filtered compounds causing cytotoxicity or high-content imaging artefacts.

9.5. Tranilast as antifibrotic drug candidate

From all 31 drug screening hits, Tranilast was chosen as a follow-up. Tranilast, also known as N-[3',4'-dimethoxycinnamoyl] anthranilic acid, is a synthetic tryptophan derivative (Suwa et al. 2015).

Tranilast was initially developed by Kissei Pharmaceutical in 1973 as mast cell stabilizer for diseases with underlying type I hypersensitivity reaction. Tranilast was shown to improve asthma attack severity in children with bronchial asthma (Shioda 1979). But, unlike other mast

cell stabilizers such as Cromolyn and Azelastin, it was approved for clinical treatment of allergic disorders such as asthma, allergic rhinitis and atopic dermatitis in South Korea and Japan only (Prud'homme 2007). With the discovery of Tranilast affecting fibroblasts (Isaji et al. 1987; Suzawa et al. 1992b), it gained approval for treatment of hypertrophic scars and keloids in South Korea and Japan (Occleston et al. 2008).

Based on these findings, a multitude of fibrosis-associated *in-cellulo* disease models was described for Tranilast. These included models of myocardial infarction and myocardial scarring (Martin et al. 2005; Kelly et al. 2007; See et al. 2013), tubulointerstitial renal fibrosis (Mifsud et al. 2003), primary pterygium (Isaji et al. 2000), postoperative intraabdominal adhesions (Adachi et al. 1999) and bleomycin-induced lung fibrosis (Mori et al. 1995; Aoki et al. 2012). Additionally, antiproliferative effects of Tranilast in gliomas, gastric, lung, prostate and pancreatic cancer models were described (Darakhshan und Pour 2015).

A multitude of proposed mechanisms described in *in-vitro* and *in-cellulo* assays pointed towards a pharmacological pleiotropy of Tranilast: a non-exhaustive list of reported activities includes cytotoxicity on human corneal fibroblasts, inhibition of TGFβ signaling in human corneal (Ochiai et al. 2001; Kim et al. 2015), gingival (Maita et al. 2004), rat cardiac fibroblasts (See et al. 2013) and rat stellate cells (Ikeda et al. 1996), inhibition of proliferation in human skin (Suzawa et al. 1992a) and pterygium-derived fibroblasts (Isaji et al. 2000), inhibition of cell migration in gingival (Maita et al. 2004) and pterygium-derived fibroblasts (Isaji et al. 2000), malignant glioma cells (Platten et al. 2001), and neutrophils (Shimizu et al. 2006), and inhibition of ECM synthesis in human skin fibroblasts (Yamada et al. 1994), human pterygium-derived fibroblasts (Isaji et al. 2000), rat cardiac fibroblasts (See et al. 2013), rat stellate cells (Ikeda et al. 1996) and primary myometrial cells (Nishijima et al. 2013) as well as the inhibition of lipopolysaccharide (LPS), polyinosinic:polycytidylic acid (Poly:IC) and interleukin stimulated inflammatory cell responses (Ikeda et al. 1996; Inoue et al. 1997; Capper et al. 2000; Ochiai et al. 2001; Pae et al. 2008; Liu et al. 2014; Baba et al. 2016). While Tranilast was recently reported to regulate multiple biomolecular signaling pathways and act anti-inflammatory

through NLRP3 inhibition (Huang et al. 2018), the antifibrotic mechanism of action of Tranilast still remains unknown. The pleiotropy of mechanisms described might be caused by the very high drug concentration needed to observe effects in cell culture experiments, which were often tested at very high concentrations compared to blood serum concentration measured in pharmacokinetic studies in human (Tadano et al. 1985).

In this thesis, Tranilast was found to inhibit TGFβ1-induced fibroblast-myofibroblast-transdifferentiation, suppress the upregulation of ECM gene expression and ECM deposition in phLFs, as well as prevent fibrotic changes upon FC treatment in PCLS at concentrations of > 100 µM. In fact, this is a rather low potency for Tranilast's antifibrotic activity. Taking into account the reported adverse effects of Tranilast in drug-induced hyperbilirubinemia (Danoff et al. 2004), where patients received 600 mg/d Tranilast for 3 months during the PRESTO trial (Holmes 2002). Thus, a high-dose Tranilast therapy did not seem to be very promising for a successful repurposing endeavor. However, my subsequent and comprehensive SAR studies of Tranilast derivatives revealed novel highly potent cinnamic acid compounds with much higher potency in their antifibrotic activities.

9.6. Discovery of N23Ps and other novel cinnamic acid amides as antifibrotic agents

Surprisingly, comprehensive SAR studies of Tranilast and related cinnamic acid amides revealed that a substitution of the carboxy-residue with a butoxyl-residue increased the potency of the cinnamic acid amides by orders of magnitude. The commercially available Tranilast derivatives exhibited a more than 100-fold higher potency than Tranilast itself. Additionally, newly designed cinnamic acid amides were synthesized to explore the chemical space of these novel cinnamic acid amides. Here, it was found that also a substitution of the carboxy-residue with an o-benzyl-residue showed similar potency-increasing effects. To the best of my knowledge, no pharmacological activity of N-(2-butoxy-phenyl)-3-(phenyl)-acrylamides or N-(2-benzoxy-phenyl)-3-(phenyl)-acrylamides (N23Ps) was described in the

literature before. Accordingly, a patent application was filed (Burgstaller et al. Novel anti-fibrotic drugs. EPA No. 21178481.4-1112) in June 2021.

Subsequently, the antifibrotic effects of N23Ps were further characterized by cell and tissue culture experiments. For these experiments, compound 4, the first discovered active N23P, and compound 18, the most potent among the discovered active N23Ps, were used. Like Tranilast, N23Ps were able to block TGFβ1-induced fibroblast-myofibroblast-transdifferentiation and TGFβ1-induced ECM deposition. In contrast to Tranilast, N23Ps induced a strong morphological change in phLFs. These changes correlated with ECM deposition inhibitory activity (data not shown). This finding could indicate that N23P activity might be mediated by a different MoA compared to Tranilast.

GSEA transcriptome analysis data revealed a downregulation of fibrosis-associated gene ontology terms such as “extracellular matrix organization” and the myofibroblast associated “actin cytoskeleton” after N23P treatment in phLFs. Here, my UMAP-RPC analysis tool provided valuable insights into the complex co-regulation patterns of TGFβ1 and N23P treatment, confirming a partial antagonism of TGFβ1-induced gene regulations by N23Ps, especially its SMURF2 dependency.

Finally, N23Ps antifibrotic activities were confirmed in a more complex human *ex-vivo* lung fibrosis model. Human precision cut lung slices were treated with a profibrotic cocktail to create a three-dimensional tissue culture disease model of lung fibrosis. Here, an inhibition of profibrotic cocktail-induced proteome changes in the tissue culture was observed, thus confirming the results from the *in-cellulo* experiments.

Interestingly, inhibition of TGFβ1-induced ECM deposition by N23Ps was also observed in dermal fibroblasts. Surprisingly, in dermal fibroblasts N23Ps exhibited a much stronger inhibitory effect compared to lung fibroblasts. This opens a potential therapeutic application of N23Ps in hypertrophic scar and keloid treatment and makes antifibrotic applications of N23Ps in other organ systems conceivable.

9.7. A potential mode of action of N23Ps

Transcriptomic analysis of N23P-treated phLFs revealed a network of upregulated genes supporting the hypothesis that SMURF2 is involved in the N23P-mediated inhibition of TGFβ1-induced fibroblast-to-myofibroblast transdifferentiation and ECM deposition. SMURF2 is a E3 ubiquitin-protein ligase that is known for catalyzing the ubiquitination and proteasome-mediated degradation of SMAD2. Thus, SMURF2 interferes with TGFβ receptor-mediated SMAD2/3 signaling (Xu et al. 2017). Therefore, an upregulation of SMURF2 expression by N23Ps might intervene with canonical TGFβ-signaling. Indeed, a 'rescue experiment' revealed that the siRNA-mediated knockdown of SMURF2 attenuated N23P effects on TGFβ-induced fibroblast-to-myofibroblasts transdifferentiation.

9.8. Limitations of the study

Despite a successful proof-of-concept for novel antifibrotic drug discovery, the established antifibrotic drug discovery strategy utilizing patient-derived phLF-based *in-cellulo* drug screening and ex-vivo human PCLS-based validation methods have several limitations. Firstly, the ECM deposition assay remains a single-cell type *in-cellulo* disease model, more simplified than cell type co-culture or organoid systems. Thus, small molecules discovered in this drug discovery campaign can only target fibroblast/myofibroblast biology targets. Furthermore, the stimulation of phLFs with TGFβ1 favors the discovery of inhibitors of fibroblast-to-myofibroblast transdifferentation, whereas direct inhibitors of ECM synthesis, processing and deposition might be overseen.

The use of primary cells limits the amounts of compounds being screened with the same phLF strain. While we were able to perform drug screenings with up to 30,000 compounds (data not shown) from a single patient's phLFs, proper upscaling strategies could lead to screening of more than 100,000 compounds, however might render unattainable due to the biological limit expansion capacity of phLFs undergoing senescence after a higher number of passages (Hayflick 1965; Heinzelmann et al. 2016).

The screening was carried out at concentrations of 100 µM. The relative high concentration compared to other drug screening campaigns could have yielded in a higher sensitivity of the assay but might have also resulted in the discovery of low potent inhibitors of ECM deposition. Still, Tranilast, despite having a relatively low potency in inhibiting ECM deposition, provided a useful starting point for the discovery of N23Ps. In my case, a common problem in drug screening resulting in many false positive hits due to cytotoxicity because of high concentrated drugs did not occur, as these compounds were efficiently filtered by the FANTAIL CNN.

N23Ps' antifibrotic activity was characterized in the phLF *in-cellulo* and hPCLS *ex-vivo* model. Both models showed corresponding data of N23P antagonism of profibrotic cell and tissue stimulation. Unfortunately, transcriptomic data from hPCLS could not be obtained due to complications during RNA isolation which was caused by the agarose contained in the hPCLS, as the lung tissue has to be filled with agarose for proper slicing. Thus, transcriptomic data from the phLF experiment had to be compared with hPCLS proteomic data showing few overlapping genes and proteins. Gene ontology analysis helped to overcome this challenge by comparing these datasets. Principally, the transcriptomic analysis of N23Ps affecting phLFs led to the discovery of SMURF2-dependence in inhibiting fibroblast-to-myofibroblast transdifferentation. However, a clear molecular target still remains elusive, as often seen in the initial phase of a phenotypic drug discovery campaign.

Conclusively, by focusing on human biomaterials for pharmacological studies might provide a better translatability of these results to clinical therapy development. However, additional investigations of N23Ps' activities on murine cells and tissue could be helpful for future *in-vivo* animal experiments.

9.9. Outlook

The here described ECM deposition assay provides a blueprint for antifibrotic drug discovery assays using patient-derived primary fibroblast strains. Here, the developed assay was used for the screening of various drug libraries summing up to 30,000 compounds altogether (unpublished data), which confirmed the high-throughput suitability of the assay. However, it still remains to be proofed if the current ECM deposition assay and strategy will yield compounds that translate into clinically usable therapies. By the nature of drug discovery, those conclusions can only be drawn retrospectively, years to decades after primary drug screenings were performed.

The novel compound class of N23Ps showed antifibrotic activity in human *in-cellulo* and *ex-vivo* experiments, as well as in a murine disease model of pulmonary fibrosis (preliminary data not shown and unpublished). Thus, members of N23P class qualify as serious preclinical drug candidates for the development of a novel antifibrotic drug. Until now, the tested N23Ps showed an unfavorable pharmacokinetic profile with a low oral bioavailability (data not shown). Thus, an important challenge in the development of an N23P lead compound for pre-clinical and clinical testing remains the identification of an orally bioavailable N23P derivative or the establishment of parenteral N23P administration technique, e. g. for inhalational therapy.

While a mode of action was described by demonstrating SMURF2-dependency of N23Ps, the precise mechanism of action as well as the molecular target remains elusive. Identification of the N23P drug target might provide further insight into N23P action and could predict adverse effects prior to clinical testing. For N23P target identification, e. g. photo-affinity pulldown techniques (Seo und Corson 2019) or label-free methods such as the cellular thermal shift assay (Mateus et al. 2016) might play a role.

9.10. Conclusion

In conclusion, the described ECM deposition assay enabled IPF-patient-derived phLFs-based phenotypic drug discovery screenings for antifibrotic drugs. The performed repurposing drug screening and subsequent structure-activity relationship study of Tranilast led to the discovery of novel cinnamic acid amides (N23Ps) as antifibrotic small molecules. Classical molecular biology as well as comprehensive ‘omics analysis of phLF and *ex-vivo* hPCLS treatments with N23Ps revealed an antifibrotic *in-cellulo* and *ex-vivo* activity of this novel compound class. As mode of action, a SMURF2-dependency of N23Pss on TGFβ1-induced αSMA expression was demonstrated.

10. References

A B Roberts; M A Anzano; L C Lamb; J M Smith; M B Sporn (1981): New class of transforming growth factors potentiated by epidermal growth factor: isolation from non-neoplastic tissues. In: *PNAS* 78 (9), S. 5339–5343. DOI: 10.1073/pnas.78.9.5339.

A. A. M. Al-Saffar; H. Tao; M. A. Talab (2017): Review of deep convolution neural network in image classification. In: 2017 International Conference on Radar, Antenna, Microwave, Electronics, and Telecommunications (ICRAMET). 2017 International Conference on Radar, Antenna, Microwave, Electronics, and Telecommunications (ICRAMET), S. 26–31.

Adachi, S.; Maruyama, T.; Kondo, T.; Todoroki, T.; Fukao, K. (1999): The prevention of postoperative intraperitoneal adhesions by tranilast: N-(3',4'-dimethoxycinnamoyl)anthranilic acid. In: *Surgery today* 29 (1), S. 51–54. DOI: 10.1007/BF02482970.

Adamson, Ian Y. R.; Bowden, Drummond H. (1974): The Pathogenesis of Bleomycin-Induced Pulmonary Fibrosis in Mice. In: *The American journal of pathology* 77 (2), S. 185–198.

Alsafadi, Hani N.; Staab-Weijnitz, Claudia A.; Lehmann, Mareike; Lindner, Michael; Peschel, Britta; Königshoff, Melanie; Wagner, Darcy E. (2017): An ex vivo model to induce early fibrosis-like changes in human precision-cut lung slices. In: *American journal of physiology. Lung cellular and molecular physiology* 312 (6), L896-L902. DOI: 10.1152/ajplung.00084.2017.

Alsafadi, Hani N.; Uhl, Franziska E.; Pineda, Ricardo H.; Bailey, Kolene E.; Rojas, Mauricio; Wagner, Darcy E.; Königshoff, Melanie (2020): Applications and Approaches for 3D Precision-cut Lung Slices: Disease Modeling and Drug Discovery. In: *American journal of respiratory cell and molecular biology*. DOI: 10.1165/rcmb.2019-0276TR.

American Thoracic Society (ATS), and the European Respiratory Society (ERS) (2000): American Thoracic Society. Idiopathic pulmonary fibrosis: diagnosis and treatment. International consensus statement. American Thoracic Society (ATS), and the European Respiratory Society (ERS). In: *American journal of respiratory and critical care medicine* 161 (2 Pt 1), S. 646–664. DOI: 10.1164/ajrccm.161.2.ats3-00.

American Thoracic Society, European Respiratory Society (2002): American Thoracic Society/European Respiratory Society International Multidisciplinary Consensus Classification of the Idiopathic Interstitial Pneumonias. This joint statement of the American Thoracic Society (ATS), and the European Respiratory Society (ERS) was adopted by the ATS board of directors, June 2001 and by the ERS Executive Committee, June 2001. In: *American journal of respiratory and critical care medicine* 165 (2), S. 277–304. DOI: 10.1164/ajrccm.165.2.ats01.

Andrews, Jonathan P.; Marttala, Jaana; Macarak, Edward; Rosenbloom, Joel; Uitto, Jouni (2016): Keloids: The paradigm of skin fibrosis - Pathomechanisms and treatment. In: *Matrix biology : journal of the International Society for Matrix Biology* 51, S. 37–46. DOI: 10.1016/j.matbio.2016.01.013.

Antoniou, Katerina M.; Margaritopoulos, George A.; Tomassetti, Sara; Bonella, Francesco; Costabel, Ulrich; Poletti, Venerino (2014): Interstitial lung disease. In: *European respiratory review : an official journal of the European Respiratory Society* 23 (131), S. 40–54. DOI: 10.1183/09059180.00009113.

Aoki, Yosuke; Kojo, Yoshiki; Yamada, Shizuo; Onoue, Satomi (2012): Respirable dry powder formulation of bleomycin for developing a pulmonary fibrosis animal model. In: *Journal of pharmaceutical sciences* 101 (6), S. 2074–2081. DOI: 10.1002/jps.23102.

Aschner, Yael; Downey, Gregory P. (2016): Transforming Growth Factor-beta: Master Regulator of the Respiratory System in Health and Disease. In: *American journal of respiratory cell and molecular biology* 54 (5), S. 647–655. DOI: 10.1165/rcmb.2015-0391TR.

B Moore, Bethany; Lawson, William E.; Oury, Tim D.; Sisson, Thomas H.; Raghavendran, Krishnan; Hogaboam, Cory M. (2013): Animal models of fibrotic lung disease. In: *American journal of respiratory cell and molecular biology* 49 (2), S. 167–179. DOI: 10.1165/rcmb.2013-0094TR.

Baba, Asuka; Tachi, Masahiro; Ejima, Yutaka; Endo, Yasuhiro; Toyama, Hiroaki; Matsubara, Mitsunobu et al. (2016): Anti-Allergic Drugs Tranilast and Ketotifen Dose-Dependently Exert

Mast Cell-Stabilizing Properties. In: *Cellular physiology and biochemistry : international journal of experimental cellular physiology, biochemistry, and pharmacology* 38 (1), S. 15–27. DOI: 10.1159/000438605.

Bagchi, Rushita A.; Mozolevska, Viktoriya; Abrenica, Bernard; Czubryt, Michael P. (2015): Development of a high throughput luciferase reporter gene system for screening activators and repressors of human collagen Iα2 gene expression. In: *Canadian journal of physiology and pharmacology* 93 (10), S. 887–892. DOI: 10.1139/cjpp-2014-0521.

Bai, Yangjinming; Ying, Ying (2020): The Post-translational Modifications of Smurf2 in TGF-β Signaling. In: *Frontiers in molecular biosciences* 7, S. 128. DOI: 10.3389/fmolb.2020.00128.

Banerjee, Audreesh; Trivedi, Chinmay M.; Damera, Gautam; Jiang, Meiqi; Jester, William; Hoshi, Toshinori et al. (2012): Trichostatin A Abrogates Airway Constriction, but Not Inflammation, in Murine and Human Asthma Models. In: *American journal of respiratory cell and molecular biology* 46 (2), S. 132–138. DOI: 10.1165/rcmb.2010-0276OC.

Barnes, Peter J. (2019): Small airway fibrosis in COPD. In: *The international journal of biochemistry & cell biology* 116, S. 105598. DOI: 10.1016/j.biocel.2019.105598.

Baumgartner, K. B.; Samet, J. M.; Stidley, C. A.; Colby, T. V.; Waldron, J. A. (1997): Cigarette smoking: a risk factor for idiopathic pulmonary fibrosis. In: *American journal of respiratory and critical care medicine* 155 (1), S. 242–248. DOI: 10.1164/ajrccm.155.1.9001319.

Behr, Jürgen; Prasse, Antje; Kreuter, Michael; Johow, Johannes; Rabe, Klaus F.; Bonella, Francesco et al. (2021): Pirfenidone in patients with progressive fibrotic interstitial lung diseases other than idiopathic pulmonary fibrosis (RELIEF): a double-blind, randomised, placebo-controlled, phase 2b trial. In: *The Lancet Respiratory Medicine* 9 (5), S. 476–486. DOI: 10.1016/S2213-2600(20)30554-3.

Bledsoe, Trevor J.; Nath, Sameer K.; Decker, Roy H. (2017): Radiation Pneumonitis. In: *Clinics in chest medicine* 38 (2), S. 201–208. DOI: 10.1016/j.ccm.2016.12.004.

Bleicher, Konrad H.; Böhm, Hans-Joachim; Müller, Klaus; Alanine, Alexander I. (2003): Hit and lead generation: beyond high-throughput screening. In: *Nat Rev Drug Discov* 2 (5), S. 369–378. DOI: 10.1038/nrd1086.

Boger, Dale L.; Cai, Hui (1999): Bleomycin: Synthetic and Mechanistic Studies. In: *Angew. Chem. Int. Ed.* 38 (4), S. 448–476. DOI: 10.1002/(SICI)1521-3773(19990215)38:4<448::AID-ANIE448>3.0.CO;2-W.

Bonnans, Caroline; Chou, Jonathan; Werb, Zena (2014): Remodelling the extracellular matrix in development and disease. In: *Nature reviews. Molecular cell biology* 15 (12), S. 786–801. DOI: 10.1038/nrm3904.

Booth, Adam J.; Wood, Sherri C.; Cornett, Ashley M.; Dreffs, Alyssa A.; Lu, Guanyi; Muro, Andres F. et al. (2012): Recipient-derived EDA fibronectin promotes cardiac allograft fibrosis. In: *The Journal of pathology* 226 (4), S. 609–618. DOI: 10.1002/path.3010.

Brennecke, Philip; Rasina, Dace; Aubi, Oscar; Herzog, Katja; Landskron, Johannes; Cautain, Bastien et al. (2019): EU-OPENSCREEN: A Novel Collaborative Approach to Facilitate Chemical Biology. In: *Slas Discovery* 24 (3), S. 398–413. DOI: 10.1177/2472555218816276.

Burgstaller, Gerald; Oehrle, Bettina; Gerckens, Michael; White, Eric S.; Schiller, Herbert B.; Eickelberg, Oliver (2017): The instructive extracellular matrix of the lung: basic composition and alterations in chronic lung disease. In: *The European respiratory journal* 50 (1). DOI: 10.1183/13993003.01805-2016.

Capdeville, Renaud; Buchdunger, Elisabeth; Zimmermann, Juerg; Matter, Alex (2002): Glivec (STI571, imatinib), a rationally developed, targeted anticancer drug. In: *Nature reviews. Drug discovery* 1 (7), S. 493–502. DOI: 10.1038/nrd839.

Capper, E. A.; Roshak, A. K.; Bolognese, B. J.; Podolin, P. L.; Smith, T.; Dewitt, D. L. et al. (2000): Modulation of human monocyte activities by tranilast, SB 252218, a compound demonstrating efficacy in restenosis. In: *The Journal of pharmacology and experimental therapeutics* 295 (3), S. 1061–1069.

Chaudhary, Nveed I.; Schnapp, Andreas; Park, John E. (2006): Pharmacologic differentiation of inflammation and fibrosis in the rat bleomycin model. In: *American journal of respiratory and critical care medicine* 173 (7), S. 769–776. DOI: 10.1164/rccm.200505-717OC.

Chen, C. Z. C.; Peng, Y. X.; Wang, Z. B.; Fish, P. V.; Kaar, J. L.; Koepsel, R. R. et al. (2009): The Scar-in-a-Jar: studying potential antifibrotic compounds from the epigenetic to extracellular level in a single well. In: *British journal of pharmacology* 158 (5), S. 1196–1209. DOI: 10.1111/j.1476-5381.2009.00387.x.

Cooper, P. R.; Kurten, R. C.; Zhang, J.; Nicholls, D. J.; Dainty, I. A.; Panettieri, R. A. (2011): Formoterol and salmeterol induce a similar degree of β2-adrenoceptor tolerance in human small airways but via different mechanisms. In: *British journal of pharmacology* 163 (3), S. 521–532. DOI: 10.1111/j.1476-5381.2011.01257.x.

Cox, Thomas R.; Erler, Janine T. (2011): Remodeling and homeostasis of the extracellular matrix: implications for fibrotic diseases and cancer. In: *Disease models & mechanisms* 4 (2), S. 165–178. DOI: 10.1242/dmm.004077.

Danoff, T. M.; Campbell, D. A.; McCarthy, L. C.; Lewis, K. F.; Repasch, M. H.; Saunders, A. M. et al. (2004): A Gilbert's syndrome UGT1A1 variant confers susceptibility to tranilast-induced hyperbilirubinemia. In: *The pharmacogenomics journal* 4 (1), S. 49–53. DOI: 10.1038/sj.tpj.6500221.

Darakhshan, Sara; Pour, Ali Bidmeshki (2015): Tranilast: a review of its therapeutic applications. In: *Pharmacological research* 91, S. 15–28. DOI: 10.1016/j.phrs.2014.10.009.

Degryse, Amber L.; Lawson, William E. (2011): Progress toward improving animal models for idiopathic pulmonary fibrosis. In: *The American journal of the medical sciences* 341 (6), S. 444–449. DOI: 10.1097/MAJ.0b013e31821aa000.

Delaunay, Myriam; Cadranel, Jacques; Lusque, Amélie; Meyer, Nicolas; Gounant, Valérie; Moro-Sibilot, Denis et al. (2017): Immune-checkpoint inhibitors associated with interstitial lung

disease in cancer patients. In: *The European respiratory journal* 50 (2). DOI: 10.1183/13993003.00050-2017.

Desmoulière, A.; Geinoz, A.; Gabbiani, F.; Gabbiani, G. (1993): Transforming growth factor-beta 1 induces alpha-smooth muscle actin expression in granulation tissue myofibroblasts and in quiescent and growing cultured fibroblasts. In: *The Journal of cell biology* 122 (1), S. 103–111. DOI: 10.1083/jcb.122.1.103.

Do, N. N.; Eming, S. A. (2016): Skin fibrosis: Models and mechanisms. In: *Current research in translational medicine* 64 (4), S. 185–193. DOI: 10.1016/j.retram.2016.06.003.

Donovan, Chantal; Bailey, Simon R.; Tran, Jenny; Haitsma, Gertruud; Ibrahim, Zaridatul A.; Foster, Simon R. et al. (2015): Rosiglitazone elicits in vitro relaxation in airways and precision cut lung slices from a mouse model of chronic allergic airways disease. In: *American Journal of Physiology - Lung Cellular and Molecular Physiology* 309 (10), L1219-28. DOI: 10.1152/ajplung.00156.2015.

Dunsmore, S. E.; Rannels, D. E. (1996): Extracellular matrix biology in the lung. In: *The American journal of physiology* 270 (1 Pt 1), L3-27.

D'Urso, Mirko; Kurniawan, Nicholas A. (2020): Mechanical and Physical Regulation of Fibroblast–Myofibroblast Transition: From Cellular Mechanoresponse to Tissue Pathology. In: *Front. Bioeng. Biotechnol.* 8, S. 609653. DOI: 10.3389/fbioe.2020.609653.

Ebsen, M.; Mogilevski, G.; Anhenn, O.; Maiworm, V.; Theegarten, D.; Schwarze, J.; Morgenroth, K. (2002): Infection of murine precision cut lung slices (PCLS) with respiratory syncytial virus (RSV) and chlamydophila pneumoniae using the Krumdieck technique. In: *Pathology, research and practice* 198 (11), S. 747–753. DOI: 10.1078/0344-0338-00331.

Eickelberg, Oliver; Köhler, Eleonore; Reichenberger, Frank; Bertschin, Sybille; Woodtli, Thomas; Erne, Paul et al. (1999): Extracellular matrix deposition by primary human lung fibroblasts in response to TGF-β1 and TGF-β3. In: *American Journal of Physiology - Lung*

Cellular and Molecular Physiology 276 (5), L814-L824. Online verfügbar unter http://ajplung.physiology.org/content/ajplung/276/5/L814.full.pdf.

Eickelberg, Oliver; Laurent, Geoffrey J. (2010): The quest for the initial lesion in idiopathic pulmonary fibrosis: gene expression differences in IPF fibroblasts. In: *American journal of respiratory cell and molecular biology* 42 (1), S. 1–2. DOI: 10.1165/rcmb.2009-0245ED.

European Research Infrastructure Consortium (ERIC) for chemical biology and early drug discovery (2021): EU OPENSCREEN - European high-capacity screening network: European Chemical Biology Library - Diversity Library. Online verfügbar unter https://www.eu-openscreen.eu/services/compound-collection/european-chemical-biology-library-ecbl-diversity-library.html, zuletzt aktualisiert am 23.12.2021, zuletzt geprüft am 23.12.2021.

Farver, Carol F.; Zander, Dani S. (Hg.) (2018): Pulmonary pathology. Philadelphia, PA: Elsevier (Foundations in diagnostic pathology). Online verfügbar unter http://www.sciencedirect.com/science/book/9780323393089.

Fernandez, Isis E.; Eickelberg, Oliver (2012): New cellular and molecular mechanisms of lung injury and fibrosis in idiopathic pulmonary fibrosis. In: *Lancet (London, England)* 380 (9842), S. 680–688. DOI: 10.1016/S0140-6736(12)61144-1.

Fernandez Perez, Evans R.; Daniels, Craig E.; Schroeder, Darrell R.; St Sauver, Jennifer; Hartman, Thomas E.; Bartholmai, Brian J. et al. (2010): Incidence, prevalence, and clinical course of idiopathic pulmonary fibrosis: a population-based study. In: *Chest* 137 (1), S. 129–137. DOI: 10.1378/chest.09-1002.

Flaherty, Kevin R.; Wells, Athol U.; Cottin, Vincent; Devaraj, Anand; Walsh, Simon L. F.; Inoue, Yoshikazu et al. (2019): Nintedanib in Progressive Fibrosing Interstitial Lung Diseases. In: *The New England journal of medicine* 381 (18), S. 1718–1727. DOI: 10.1056/NEJMoa1908681.

Fraietta, Ivan; Gasparri, Fabio (2016): The development of high-content screening (HCS) technology and its importance to drug discovery. In: *Expert opinion on drug discovery* 11 (5), S. 501–514. DOI: 10.1517/17460441.2016.1165203.

Frantz, Christian; Stewart, Kathleen M.; Weaver, Valerie M. (2010): The extracellular matrix at a glance. In: *Journal of cell science* 123 (Pt 24), S. 4195–4200. DOI: 10.1242/jcs.023820.

Froudarakis, Marios; Hatzimichael, Eleftheria; Kyriazopoulou, Lydia; Lagos, Konstantinos; Pappas, Periklis; Tzakos, Andreas G. et al. (2013): Revisiting bleomycin from pathophysiology to safe clinical use. In: *Critical reviews in oncology/hematology* 87 (1), S. 90–100. DOI: 10.1016/j.critrevonc.2012.12.003.

Gabbiani, G.; Le Lous, M.; Bailey, A. J.; Bazin, S.; Delaunay, A. (1976): Collagen and myofibroblasts of granulation tissue. In: *Virchows Archiv B* 21 (1), S. 133–145. DOI: 10.1007/BF02899150.

Gabbiani, G.; Ryan, G. B.; Majno, G. (1971): Presence of modified fibroblasts in granulation tissue and their possible role in wound contraction. In: *Experientia* 27 (5), S. 549–550. DOI: 10.1007/BF02147594.

Gerckens, Michael; Alsafadi, Hani N.; Wagner, Darcy E.; Lindner, Michael; Burgstaller, Gerald; Königshoff, Melanie (2019): Generation of Human 3D Lung Tissue Cultures (3D-LTCs) for Disease Modeling. In: *Journal of visualized experiments : JoVE* (144). DOI: 10.3791/58437.

Gerckens, Michael; Schorpp, Kenji; Pelizza, Francesco; Wögrath, Melanie; Reichau, Kora; Ma, Huilong et al. (2021): Phenotypic drug screening in a human fibrosis model identified a novel class of antifibrotic therapeutics. In: *Sci. Adv.* 7 (52), Artikel eabb3673. DOI: 10.1126/sciadv.abb3673.

Glanville, Allan R.; Verleden, Geert M.; Todd, Jamie L.; Benden, Christian; Calabrese, Fiorella; Gottlieb, Jens et al. (2019): Chronic lung allograft dysfunction: Definition and update of restrictive allograft syndrome-A consensus report from the Pulmonary Council of the ISHLT. In: *The Journal of heart and lung transplantation : the official publication of the International Society for Heart Transplantation* 38 (5), S. 483–492. DOI: 10.1016/j.healun.2019.03.008.

Haas, Esther C. de; Zwart, Nynke; Meijer, Coby; Nuver, Janine; Boezen, H. Marike; Suurmeijer, Albert J. H. et al. (2008): Variation in bleomycin hydrolase gene is associated with

reduced survival after chemotherapy for testicular germ cell cancer. In: *Journal of clinical oncology : official journal of the American Society of Clinical Oncology* 26 (11), S. 1817–1823. DOI: 10.1200/JCO.2007.14.1606.

Hamman, Louis; Rich, Arnold R. (1935): Fulminating Diffuse Interstitial Fibrosis of the Lungs. In: *Transactions of the American Clinical and Climatological Association* 51, S. 154–163.

Harold L. Moses; Earl L. Branum; Jacqueline A. Proper; Robert A. Robinson (1981): Transforming Growth Factor Production by Chemically Transformed Cells. In: *Cancer Res* 41 (7), S. 2842–2848. Online verfügbar unter https://cancerres.aacrjournals.org/content/41/7/2842.article-info.

Hashisako, Mikiko; Fukuoka, Junya (2015): Pathology of Idiopathic Interstitial Pneumonias. In: *Clinical medicine insights. Circulatory, respiratory and pulmonary medicine* 9 (Suppl 1), S. 123–133. DOI: 10.4137/CCRPM.S23320.

Hata, Akiko; Chen, Ye-Guang (2016): TGF-β Signaling from Receptors to Smads. In: *Cold Spring Harbor perspectives in biology* 8 (9). DOI: 10.1101/cshperspect.a022061.

Hay, Elizabeth D. (1991): Cell biology of extracellular matrix. Second edition. New York: Plenum Press.

Hayflick, L. (1965): The limited in vitro lifetime of human diploid cell strains. In: *Experimental cell research* 37 (3), S. 614–636. DOI: 10.1016/0014-4827(65)90211-9.

Hegedus, Fanni; Mathew, Laju M.; Schwartz, Robert A. (2017): Radiation dermatitis: an overview. In: *International journal of dermatology* 56 (9), S. 909–914. DOI: 10.1111/ijd.13371.

Heinzelmann, Katharina; Noskovicova, Nina; Merl-Pham, Juliane; Preissler, Gerhard; Winter, Hauke; Lindner, Michael et al. (2016): Surface proteome analysis identifies platelet derived growth factor receptor-alpha as a critical mediator of transforming growth factor-beta-induced collagen secretion. In: *The international journal of biochemistry & cell biology* 74, S. 44–59. DOI: 10.1016/j.biocel.2016.02.013.

Hetzel, M.; Bachem, M.; Anders, D.; Trischler, G.; Faehling, M. (2005): Different effects of growth factors on proliferation and matrix production of normal and fibrotic human lung fibroblasts. In: *Lung* 183 (4), S. 225–237. DOI: 10.1007/s00408-004-2534-z.

Holmes, D. R. (2002): Results of Prevention of REStenosis with Tranilast and its Outcomes (PRESTO) Trial. In: *Circulation* 106 (10), S. 1243–1250. DOI: 10.1161/01.CIR.0000028335.31300.DA.

Horman, Shane R. (2016): Complex High-Content Phenotypic Screening. In: Taosheng Chen und Sergio C. Chai (Hg.): Special Topics in Drug Discovery: InTech.

Huang, Yi; Jiang, Hua; Chen, Yun; Wang, Xiaqiong; Yang, Yanqing; Tao, Jinhui et al. (2018): Tranilast directly targets NLRP3 to treat inflammasome-driven diseases. In: *EMBO molecular medicine* 10 (4). DOI: 10.15252/emmm.201708689.

Hughes, J. P.; Rees, S.; Kalindjian, S. B.; Philpott, K. L. (2011): Principles of early drug discovery. In: *British journal of pharmacology* 162 (6), S. 1239–1249. DOI: 10.1111/j.1476-5381.2010.01127.x.

Humphreys, Benjamin D. (2018): Mechanisms of Renal Fibrosis. In: *Annual review of physiology* 80, S. 309–326. DOI: 10.1146/annurev-physiol-022516-034227.

Hynes, Richard O.; Naba, Alexandra (2012): Overview of the matrisome--an inventory of extracellular matrix constituents and functions. In: *Cold Spring Harbor perspectives in biology* 4 (1), a004903. DOI: 10.1101/cshperspect.a004903.

Ikeda, H.; Inao, M.; Fujiwara, K. (1996): Inhibitory effect of tranilast on activation and transforming growth factor beta 1 expression in cultured rat stellate cells. In: *Biochemical and biophysical research communications* 227 (2), S. 322–327. DOI: 10.1006/bbrc.1996.1508.

Inoue, H.; Ohshima, H.; Kono, H.; Yamanaka, M.; Kubota, T.; Aihara, M. et al. (1997): Suppressive effects of tranilast on the expression of inducible cyclooxygenase (COX2) in interleukin-1beta-stimulated fibroblasts. In: *Biochemical pharmacology* 53 (12), S. 1941–1944.

Isaji, M.; Kikuchi, S.; Miyata, H.; Ajisawa, Y.; Araki-Inazawa, K.; Tsukamoto, Y.; Amano, Y. (2000): Inhibitory effects of tranilast on the proliferation and functions of human pterygium-derived fibroblasts. In: *Cornea* 19 (3), S. 364–368.

Isaji, M.; Nakajoh, M.; Naito, J. (1987): Selective inhibition of collagen accumulation by N-(3,4-dimethoxycinnamoyl)anthranilic acid (N-5') in granulation tissue. In: *Biochemical pharmacology* 36 (4), S. 469–474.

Itoh, S.; Itoh, F.; Goumans, M. J.; Dijke, P. ten (2000): Signaling of transforming growth factor-beta family members through Smad proteins. In: *European journal of biochemistry* 267 (24), S. 6954–6967. DOI: 10.1046/j.1432-1327.2000.01828.x.

Izbicki, G.; Segel, M. J.; Christensen, T. G.; Conner, M. W.; Breuer, R. (2002): Time course of bleomycin-induced lung fibrosis. In: *International journal of experimental pathology* 83 (3), S. 111–119. DOI: 10.1046/j.1365-2613.2002.00220.x.

J E de Larco; G J Todaro (1978): Growth factors from murine sarcoma virus-transformed cells. In: *PNAS* 75 (8), S. 4001–4005. DOI: 10.1073/pnas.75.8.4001.

Jamur, Maria Célia; Oliver, Constance (2010): Permeabilization of Cell Membranes. In: Constance Oliver und Maria Célia Jamur (Hg.): Immunocytochemical methods and protocols. 3rd ed. / edited by Constance Oliver and Maria Célia Jamur. New York: Springer (Springer protocols, 588), S. 63–66.

Jenkins, R. Gisli; Moore, Bethany B.; Chambers, Rachel C.; Eickelberg, Oliver; Königshoff, Melanie; Kolb, Martin et al. (2017): An Official American Thoracic Society Workshop Report. Use of Animal Models for the Preclinical Assessment of Potential Therapies for Pulmonary Fibrosis. In: *American journal of respiratory cell and molecular biology* 56 (5), S. 667–679. DOI: 10.1165/rcmb.2017-0096ST.

Kapnadak, Siddhartha G.; Raghu, Ganesh (2021): Lung transplantation for interstitial lung disease. In: *European respiratory review : an official journal of the European Respiratory Society* 30 (161). DOI: 10.1183/16000617.0017-2021.

Kelly, Darren J.; Zhang, Yuan; Connelly, Kim; Cox, Alison J.; Martin, Jennifer; Krum, Henry; Gilbert, Richard E. (2007): Tranilast attenuates diastolic dysfunction and structural injury in experimental diabetic cardiomyopathy. In: *American journal of physiology. Heart and circulatory physiology* 293 (5), H2860-9. DOI: 10.1152/ajpheart.01167.2006.

Keseru, György M.; Makara, Gergely M. (2006): Hit discovery and hit-to-lead approaches. In: *Drug discovery today* 11 (15-16), S. 741–748. DOI: 10.1016/j.drudis.2006.06.016.

Keserü, György M.; Makara, Gergely M. (2009): The influence of lead discovery strategies on the properties of drug candidates. In: *Nat Rev Drug Discov* 8 (3), S. 203–212. DOI: 10.1038/nrd2796.

Kim, Jieun; Jung, Youngmi (2017): Radiation-induced liver disease: current understanding and future perspectives. In: *Experimental & molecular medicine* 49 (7), e359. DOI: 10.1038/emm.2017.85.

Kim, Tae-Im; Lee, Hun; Hong, Hye Kyoung; Kim, Kyu Seo; Choi, Seung-Il; Maeng, Yong-Sun; Kim, Eung Kweon (2015): Inhibitory Effect of Tranilast on Transforming Growth Factor-Beta-Induced Protein in Granular Corneal Dystrophy Type 2 Corneal Fibroblasts. In: *Cornea* 34 (8), S. 950–958. DOI: 10.1097/ICO.0000000000000466.

King, Talmadge E.; Bradford, Williamson Z.; Castro-Bernardini, Socorro; Fagan, Elizabeth A.; Glaspole, Ian; Glassberg, Marilyn K. et al. (2014): A phase 3 trial of pirfenidone in patients with idiopathic pulmonary fibrosis. In: *The New England journal of medicine* 370 (22), S. 2083–2092. DOI: 10.1056/NEJMoa1402582.

King, Talmadge E.; Brown, Kevin K.; Raghu, Ganesh; Du Bois, Roland M.; Lynch, David A.; Martinez, Fernando et al. (2011): BUILD-3: a randomized, controlled trial of bosentan in idiopathic pulmonary fibrosis. In: *American journal of respiratory and critical care medicine* 184 (1), S. 92–99. DOI: 10.1164/rccm.201011-1874OC.

King, Talmadge E., JR; Pardo, Annie; Selman, Moises (2011): Idiopathic pulmonary fibrosis. In: *Lancet (London, England)* 378 (9807), S. 1949–1961. DOI: 10.1016/S0140-6736(11)60052-4.

Koch, Alexandra; Saran, Shashank; Tran, Doan Duy Hai; Klebba-Färber, Sabine; Thiesler, Hauke; Sewald, Katherina et al. (2014): Murine precision-cut liver slices (PCLS): a new tool for studying tumor microenvironments and cell signaling ex vivo. In: *Cell Communication and Signaling : CCS* 12, S. 73. DOI: 10.1186/s12964-014-0073-7.

Ktistakis, N. T.; Linder, M. E.; Roth, M. G. (1992): Action of brefeldin A blocked by activation of a pertussis-toxin-sensitive G protein. In: *Nature* 356 (6367), S. 344–346. DOI: 10.1038/356344a0.

Kulkarni, Tejaswini; O'Reilly, Philip; Antony, Veena B.; Gaggar, Amit; Thannickal, Victor J. (2016): Matrix Remodeling in Pulmonary Fibrosis and Emphysema. In: *American journal of respiratory cell and molecular biology* 54 (6), S. 751–760. DOI: 10.1165/rcmb.2015-0166PS.

Lederer, David J.; Martinez, Fernando J. (2018): Idiopathic Pulmonary Fibrosis. In: *The New England journal of medicine* 378 (19), S. 1811–1823. DOI: 10.1056/NEJMra1705751.

Lehmann, Mareike; Buhl, Lara; Alsafadi, Hani N.; Klee, Stephan; Hermann, Sarah; Mutze, Kathrin et al. (2018): Differential effects of Nintedanib and Pirfenidone on lung alveolar epithelial cell function in ex vivo murine and human lung tissue cultures of pulmonary fibrosis. In: *Respiratory research* 19 (1), S. 175. DOI: 10.1186/s12931-018-0876-y.

Lehmann, Mareike; Korfei, Martina; Mutze, Kathrin; Klee, Stephan; Skronska-Wasek, Wioletta; Alsafadi, Hani N. et al. (2017): Senolytic drugs target alveolar epithelial cell function and attenuate experimental lung fibrosis ex vivo. In: *The European respiratory journal* 50 (2). DOI: 10.1183/13993003.02367-2016.

Lierova, Anna; Jelicova, Marcela; Nemcova, Marketa; Proksova, Magdalena; Pejchal, Jaroslav; Zarybnicka, Lenka; Sinkorova, Zuzana (2018): Cytokines and radiation-induced

pulmonary injuries. In: *Journal of radiation research* 59 (6), S. 709–753. DOI: 10.1093/jrr/rry067.

Liu, Tianju; Los Santos, Francina Gonzalez de; Phan, Sem H. (2017): The Bleomycin Model of Pulmonary Fibrosis. In: *Methods in molecular biology (Clifton, N.J.)* 1627, S. 27–42. DOI: 10.1007/978-1-4939-7113-8_2.

Liu, Xueping; Baarsma, Hoeke Abele; Thiam, Chung Hwee; Montrone, Corinna; Brauner, Barbara; Fobo, Gisela et al. (2016): Systematic Identification of Pharmacological Targets from Small-Molecule Phenotypic Screens. In: *Cell chemical biology* 23 (10), S. 1302–1313. DOI: 10.1016/j.chembiol.2016.08.011.

Liu, Ye; Xu, Dan; Li, Jing; Liu, Yang (2014): Inhibition of interleukin-1β-induced matrix metalloproteinase expression in human corneal fibroblasts by tranilast. In: *Current eye research* 39 (9), S. 885–893. DOI: 10.3109/02713683.2014.884598.

Liu-Ya Tang; Motozo Yamashita; Nathan P Coussens; Yi Tang; Xiangchun Wang; Cuiling Li et al. (2011): Ablation of Smurf2 reveals an inhibition in TGF-β signalling through multiple mono-ubiquitination of Smad3.

Lohcharoenkal, Warangkana; Liu, Yuxin; Wang, Liying; Yang, Yong; Rojanasakul, Yon (2014): Luciferase reporter cells as a platform to detect SMAD-dependent collagen production. In: *Journal of bioscience and bioengineering* 118 (6), S. 732–735. DOI: 10.1016/j.jbiosc.2014.05.021.

Lu, Pengfei; Takai, Ken; Weaver, Valerie M.; Werb, Zena (2011): Extracellular matrix degradation and remodeling in development and disease. In: *Cold Spring Harbor perspectives in biology* 3 (12). DOI: 10.1101/cshperspect.a005058.

Lynch, David A.; Sverzellati, Nicola; Travis, William D.; Brown, Kevin K.; Colby, Thomas V.; Galvin, Jeffrey R. et al. (2018): Diagnostic criteria for idiopathic pulmonary fibrosis: a Fleischner Society White Paper. In: *The Lancet Respiratory Medicine* 6 (2), S. 138–153. DOI: 10.1016/S2213-2600(17)30433-2.

MacDonald, Elizabeth M.; Cohn, Ronald D. (2012): TGFβ signaling: its role in fibrosis formation and myopathies. In: *Current opinion in rheumatology* 24 (6), S. 628–634. DOI: 10.1097/BOR.0b013e328358df34.

Maita, Eikichi; Sato, Mami; Yamaki, Keiko (2004): Effect of tranilast on matrix metalloproteinase-1 secretion from human gingival fibroblasts in vitro. In: *Journal of periodontology* 75 (8), S. 1054–1060. DOI: 10.1902/jop.2004.75.8.1054.

Martin, Jennifer; Kelly, Darren J.; Mifsud, Sally A.; Zhang, Yuan; Cox, Alison J.; See, Fiona et al. (2005): Tranilast attenuates cardiac matrix deposition in experimental diabetes: role of transforming growth factor-beta. In: *Cardiovascular research* 65 (3), S. 694–701. DOI: 10.1016/j.cardiores.2004.10.041.

Mason, J. W. (1987): Amiodarone. In: *N Engl J Med* 316 (8), S. 455–466. DOI: 10.1056/NEJM198702193160807.

Mateus, André; Määttä, Tomi A.; Savitski, Mikhail M. (2016): Thermal proteome profiling: unbiased assessment of protein state through heat-induced stability changes. In: *Proteome science* 15, S. 13. DOI: 10.1186/s12953-017-0122-4.

Merl-Pham, Juliane; Basak, Trayambak; Knüppel, Larissa; Ramanujam, Deepak; Athanason, Mark; Behr, Jürgen et al. (2019): Quantitative proteomic profiling of extracellular matrix and site-specific collagen post-translational modifications in an in vitro model of lung fibrosis. In: *Matrix Biology Plus* 1. DOI: 10.1016/j.mbplus.2019.04.002.

Meyer, Keith C.; Nathan, Steven D. (2014): Idiopathic Pulmonary Fibrosis. Totowa, NJ: Humana Press.

Mifsud, Sally; Kelly, Darren J.; Qi, Weier; Zhang, Yuan; Pollock, Carol A.; Wilkinson-Berka, Jennifer L.; Gilbert, Richard E. (2003): Intervention with tranilast attenuates renal pathology and albuminuria in advanced experimental diabetic nephropathy. In: *Nephron. Physiology* 95 (4), p83-91.

Mishra, Paras Kumar; Givvimani, Srikanth; Chavali, Vishalakshi; Tyagi, Suresh C. (2013): Cardiac matrix: a clue for future therapy. In: *Biochimica et biophysica acta* 1832 (12), S. 2271–2276. DOI: 10.1016/j.bbadis.2013.09.004.

Moeller, Antje; Ask, Kjetil; Warburton, David; Gauldie, Jack; Kolb, Martin (2008): The bleomycin animal model. A useful tool to investigate treatment options for idiopathic pulmonary fibrosis? In: *The international journal of biochemistry & cell biology* 40 (3), S. 362–382. DOI: 10.1016/j.biocel.2007.08.011.

Mora, Ana L.; Rojas, Mauricio; Pardo, Annie; Selman, Moises (2017): Emerging therapies for idiopathic pulmonary fibrosis, a progressive age-related disease. In: *Nature reviews. Drug discovery* 16 (11), S. 755–772. DOI: 10.1038/nrd.2017.170.

Mori, H.; Tanaka, H.; Kawada, K.; Nagai, H.; Koda, A. (1995): Suppressive effects of tranilast on pulmonary fibrosis and activation of alveolar macrophages in mice treated with bleomycin: role of alveolar macrophages in the fibrosis. In: *Japanese journal of pharmacology* 67 (4), S. 279–289.

Moses, Harold L.; Roberts, Anita B.; Derynck, Rik (2016): The Discovery and Early Days of TGF-β: A Historical Perspective. In: *Cold Spring Harb Perspect Biol* 8 (7), a021865. DOI: 10.1101/cshperspect.a021865.

Naba, Alexandra; Clauser, Karl R.; Hoersch, Sebastian; Liu, Hui; Carr, Steven A.; Hynes, Richard O. (2012): The matrisome: in silico definition and in vivo characterization by proteomics of normal and tumor extracellular matrices. In: *Molecular & cellular proteomics : MCP* 11 (4), M111.014647. DOI: 10.1074/mcp.M111.014647.

Nakao, A.; Imamura, T.; Souchelnytskyi, S.; Kawabata, M.; Ishisaki, A.; Oeda, E. et al. (1997): TGF-beta receptor-mediated signalling through Smad2, Smad3 and Smad4. In: *The EMBO Journal* 16 (17), S. 5353–5362. DOI: 10.1093/emboj/16.17.5353.

Nalysnyk, Luba; Cid-Ruzafa, Javier; Rotella, Philip; Esser, Dirk (2012): Incidence and prevalence of idiopathic pulmonary fibrosis: review of the literature. In: *European respiratory*

review : an official journal of the European Respiratory Society 21 (126), S. 355–361. DOI: 10.1183/09059180.00002512.

Nattel, Stanley (2017): Molecular and Cellular Mechanisms of Atrial Fibrosis in Atrial Fibrillation. In: *JACC. Clinical electrophysiology* 3 (5), S. 425–435. DOI: 10.1016/j.jacep.2017.03.002.

Neuman, Robert E.; Logan, Milan A. (1950): THE DETERMINATION OF HYDROXYPROLINE. In: *Journal of Biological Chemistry* 184 (1), S. 299–306. DOI: 10.1016/S0021-9258(19)51149-8.

Ng, Benjamin; Dong, Jinrui; D'Agostino, Giuseppe; Viswanathan, Sivakumar; Widjaja, Anissa A.; Lim, Wei-Wen et al. (2019): Interleukin-11 is a therapeutic target in idiopathic pulmonary fibrosis. In: *Science translational medicine* 11 (511), Artikel eaaw1237. DOI: 10.1126/scitranslmed.aaw1237.

Nishijima, Saori; Sugaya, Kimio; Kadekawa, Katsumi; Ashitomi, Katsuhiro; Ueda, Tomoyuki; Yamamoto, Hideyuki (2013): High-dose tranilast administration to rats creates interstitial cystitis-like symptoms with increased vascular permeability. In: *Life sciences* 93 (23), S. 897–903. DOI: 10.1016/j.lfs.2013.10.010.

Nogueira, António; Pires, Maria João; Oliveira, Paula Alexandra (2017): Pathophysiological Mechanisms of Renal Fibrosis: A Review of Animal Models and Therapeutic Strategies. In: *In vivo (Athens, Greece)* 31 (1), S. 1–22. DOI: 10.21873/invivo.11019.

Noth, Imre; Anstrom, Kevin J.; Calvert, Sara Bristol; Andrade, Joao de; Flaherty, Kevin R.; Glazer, Craig et al. (2012): A placebo-controlled randomized trial of warfarin in idiopathic pulmonary fibrosis. In: *American journal of respiratory and critical care medicine* 186 (1), S. 88–95. DOI: 10.1164/rccm.201202-0314OC.

Nuver, Janine; Lutke Holzik, Martijn F.; van Zweeden, Martine; Hoekstra, Harald J.; Meijer, Coby; Suurmeijer, Albert J. H. et al. (2005): Genetic variation in the bleomycin hydrolase gene

and bleomycin-induced pulmonary toxicity in germ cell cancer patients. In: *Pharmacogenetics and genomics* 15 (6), S. 399–405. DOI: 10.1097/01213011-200506000-00005.

Occleston, Nick L.; O'Kane, Sharon; Goldspink, Nick; Ferguson, Mark W. J. (2008): New therapeutics for the prevention and reduction of scarring. In: *Drug discovery today* 13 (21-22), S. 973–981. DOI: 10.1016/j.drudis.2008.08.009.

Ochiai, H.; Ochiai, Y.; Chihara, E. (2001): Tranilast inhibits TGF- A1 secretion without affecting its mRNA levels in conjunctival cells. In: *The Kobe journal of medical sciences* 47 (5), S. 203–209.

Oh, Raymond S.; Haak, Andrew J.; Smith, Karry M. J.; Ligresti, Giovanni; Choi, Kyoung Moo; Xie, Tiao et al. (2018): RNAi screening identifies a mechanosensitive ROCK-JAK2-STAT3 network central to myofibroblast activation. In: *Journal of cell science* 131 (10). DOI: 10.1242/jcs.209932.

Pae, Hyun-Ock; Jeong, Sun-Oh; Koo, Bon Soon; Ha, Hun-Yong; Lee, Kang-Min; Chung, Hun-Taeg (2008): Tranilast, an orally active anti-allergic drug, up-regulates the anti-inflammatory heme oxygenase-1 expression but down-regulates the pro-inflammatory cyclooxygenase-2 and inducible nitric oxide synthase expression in RAW264.7 macrophages. In: *Biochemical and biophysical research communications* 371 (3), S. 361–365. DOI: 10.1016/j.bbrc.2008.04.054.

Pakshir, P.; Hinz, B. (2018): The big five in fibrosis: Macrophages, myofibroblasts, matrix, mechanics, and miscommunication. In: *Matrix biology : journal of the International Society for Matrix Biology* 68-69. DOI: 10.1016/j.matbio.2018.01.019.

Papiris, Spyros A.; Triantafillidou, Christina; Kolilekas, Likurgos; Markoulaki, Despoina; Manali, Effrosyni D. (2010): Amiodarone: review of pulmonary effects and toxicity. In: *Drug safety* 33 (7), S. 539–558. DOI: 10.2165/11532320-000000000-00000.

Parker, Joseph M.; Glaspole, Ian N.; Lancaster, Lisa H.; Haddad, Tarik J.; She, Dewei; Roseti, Stephanie L. et al. (2018): A Phase 2 Randomized Controlled Study of Tralokinumab in

Subjects with Idiopathic Pulmonary Fibrosis. In: *American journal of respiratory and critical care medicine* 197 (1), S. 94–103. DOI: 10.1164/rccm.201704-0784OC.

Parker, Matthew W.; Rossi, Daniel; Peterson, Mark; Smith, Karen; Sikstrom, Kristina; White, Eric S. et al. (2014): Fibrotic extracellular matrix activates a profibrotic positive feedback loop. In: *The Journal of clinical investigation* 124 (4), S. 1622–1635. DOI: 10.1172/JCI71386.

Patel, Anand C. (2013): Clinical relevance of target identity and biology: implications for drug discovery and development. In: *Journal of biomolecular screening* 18 (10), S. 1164–1185. DOI: 10.1177/1087057113505906.

Placke, M. E.; Fisher, G. I. (1987): Adult peripheral lung organ culture? A model for respiratory tract toxicology. In: *Toxicology and applied pharmacology* 90 (2), S. 284–298. DOI: 10.1016/0041-008X(87)90336-X.

Platten, M.; Wild-Bode, C.; Wick, W.; Leitlein, J.; Dichgans, J.; Weller, M. (2001): N-3,4-dimethoxycinnamoyl-anthranilic acid (tranilast) inhibits transforming growth factor-beta relesase and reduces migration and invasiveness of human malignant glioma cells. In: *International journal of cancer* 93 (1), S. 53–61.

Poroikov, V. V.; Filimonov, D. A. (2002): How to acquire new biological activities in old compounds by computer prediction. In: *Journal of computer-aided molecular design* 16 (11), S. 819–824. DOI: 10.1023/a:1023836829456.

Prud'homme, Gérald J. (2007): Pathobiology of transforming growth factor beta in cancer, fibrosis and immunologic disease, and therapeutic considerations. In: *Laboratory investigation; a journal of technical methods and pathology* 87 (11), S. 1077–1091. DOI: 10.1038/labinvest.3700669.

Raghu, G.; Collard, H. R.; Egan, J. J.; Martinez, F. J.; Behr, J.; Brown, K. K. et al. (2011): An official ATS/ERS/JRS/ALAT statement: idiopathic pulmonary fibrosis: evidence-based guidelines for diagnosis and management. In: *American journal of respiratory and critical care medicine* 183 (6), S. 788–824. DOI: 10.1164/rccm.2009-040GL.

Raghu, G.; Freudenberger, T. D.; Yang, S.; Curtis, J. R.; Spada, C.; Hayes, J. et al. (2006): High prevalence of abnormal acid gastro-oesophageal reflux in idiopathic pulmonary fibrosis. In: *The European respiratory journal* 27 (1), S. 136–142. DOI: 10.1183/09031936.06.00037005.

Raghu, Ganesh; Anstrom, Kevin J.; King, Talmadge E.; Lasky, Joseph A.; Martinez, Fernando J. (2012): Prednisone, azathioprine, and N-acetylcysteine for pulmonary fibrosis. In: *The New England journal of medicine* 366 (21), S. 1968–1977. DOI: 10.1056/NEJMoa1113354.

Raghu, Ganesh; Brown, Kevin K.; Collard, Harold R.; Cottin, Vincent; Gibson, Kevin F.; Kaner, Robert J. et al. (2017): Efficacy of simtuzumab versus placebo in patients with idiopathic pulmonary fibrosis: a randomised, double-blind, controlled, phase 2 trial. In: *The Lancet Respiratory Medicine* 5 (1), S. 22–32. DOI: 10.1016/S2213-2600(16)30421-0.

Raghu, Ganesh; Remy-Jardin, Martine; Myers, Jeffrey L.; Richeldi, Luca; Ryerson, Christopher J.; Lederer, David J. et al. (2018): Diagnosis of Idiopathic Pulmonary Fibrosis. An Official ATS/ERS/JRS/ALAT Clinical Practice Guideline. In: *American journal of respiratory and critical care medicine* 198 (5), e44-e68. DOI: 10.1164/rccm.201807-1255ST.

Raghu, Ganesh; Selman, Moisés (2015): Nintedanib and pirfenidone. New antifibrotic treatments indicated for idiopathic pulmonary fibrosis offer hopes and raises questions. In: *American journal of respiratory and critical care medicine* 191 (3), S. 252–254. DOI: 10.1164/rccm.201411-2044ED.

Rehman, Michael; Vodret, Simone; Braga, Luca; Guarnaccia, Corrado; Celsi, Fulvio; Rossetti, Giulia et al. (2019): High-throughput screening discovers antifibrotic properties of haloperidol by hindering myofibroblast activation. In: *JCI insight* 4 (8). DOI: 10.1172/jci.insight.123987.

Reinert, Tomás; Baldotto, Clarissa Serodio da Rocha; Nunes, Frederico Arthur Pereira; Scheliga, Adriana Alves de Souza (2013): Bleomycin-Induced Lung Injury. In: *Journal of Cancer Research* 2013 (22), S. 1–9. DOI: 10.1155/2013/480608.

Richeldi, Luca; Costabel, Ulrich; Selman, Moises; Kim, Dong Soon; Hansell, David M.; Nicholson, Andrew G. et al. (2011): Efficacy of a Tyrosine Kinase Inhibitor in Idiopathic Pulmonary Fibrosis.

Richeldi, Luca; Du Bois, Roland M.; Raghu, Ganesh; Azuma, Arata; Brown, Kevin K.; Costabel, Ulrich et al. (2014): Efficacy and safety of nintedanib in idiopathic pulmonary fibrosis. In: *The New England journal of medicine* 370 (22), S. 2071–2082. DOI: 10.1056/NEJMoa1402584.

Robyn L. Fisher; Mary S. Smith; Steven J. Hasal; Katherine S. Hasal; A. Jay Gandolfi; and Klaus Brendel (1994): The Use of Human Lung Slices in Toxicology (13), S. 466–471.

Rockey, Don C.; Bell, P. Darwin; Hill, Joseph A. (2015): Fibrosis--a common pathway to organ injury and failure. In: *The New England journal of medicine* 372 (12), S. 1138–1149. DOI: 10.1056/NEJMra1300575.

Rønnow, Sarah Rank; Dabbagh, Rand Qais; Genovese, Federica; Nanthakumar, Carmel B.; Barrett, Vikki J.; Good, Robert B. et al. (2020): Prolonged Scar-in-a-Jar: an in vitro screening tool for anti-fibrotic therapies using biomarkers of extracellular matrix synthesis. In: *Respiratory research* 21 (1), S. 108. DOI: 10.1186/s12931-020-01369-1.

Royce, Simon G.; Cheng, Victor; Samuel, Chrishan S.; Tang, Mimi L. K. (2012): The regulation of fibrosis in airway remodeling in asthma. In: *Molecular and cellular endocrinology* 351 (2), S. 167–175. DOI: 10.1016/j.mce.2012.01.007.

Ruiz-Ortega, Marta; Rayego-Mateos, Sandra; Lamas, Santiago; Ortiz, Alberto; Rodrigues-Diez, Raul R. (2020): Targeting the progression of chronic kidney disease. In: *Nature reviews. Nephrology*. DOI: 10.1038/s41581-019-0248-y.

Samokhin, Andriy O.; Stephens, Thomas; Wertheim, Bradley M.; Wang, Rui-Sheng; Vargas, Sara O.; Yung, Lai-Ming et al. (2018): NEDD9 targets COL3A1 to promote endothelial fibrosis and pulmonary arterial hypertension. In: *Science translational medicine* 10 (445). DOI: 10.1126/scitranslmed.aap7294.

Sand, Jannie Marie; Larsen, Lise; Hogaboam, Cory; Martinez, Fernando; Han, Meilan; Røssel Larsen, Martin et al. (2013): MMP mediated degradation of type IV collagen alpha 1 and alpha 3 chains reflects basement membrane remodeling in experimental and clinical fibrosis--validation of two novel biomarker assays. In: *PloS one* 8 (12), e84934. DOI: 10.1371/journal.pone.0084934.

Sanz, Gema; Martínez-Aranda, Luis Manuel; Tesch, Per A.; Fernandez-Gonzalo, Rodrigo; Lundberg, Tommy R. (2019): Muscle2View, a CellProfiler pipeline for detection of the capillary-to-muscle fiber interface and high-content quantification of fiber type-specific histology. In: *Journal of applied physiology (Bethesda, Md. : 1985)* 127 (6), S. 1698–1709. DOI: 10.1152/japplphysiol.00257.2019.

Schulz, Jan-Niklas; Plomann, Markus; Sengle, Gerhard; Gullberg, Donald; Krieg, Thomas; Eckes, Beate (2018): New developments on skin fibrosis - Essential signals emanating from the extracellular matrix for the control of myofibroblasts. In: *Matrix biology : journal of the International Society for Matrix Biology* 68-69, S. 522–532. DOI: 10.1016/j.matbio.2018.01.025.

See, Fiona; Watanabe, Masataka; Kompa, Andrew R.; Wang, Bing H.; Boyle, Andrew J.; Kelly, Darren J. et al. (2013): Early and delayed tranilast treatment reduces pathological fibrosis following myocardial infarction. In: *Heart, lung & circulation* 22 (2), S. 122–132. DOI: 10.1016/j.hlc.2012.08.054.

Seo, Seung-Yong; Corson, Timothy W. (2019): Small molecule target identification using photo-affinity chromatography. In: *Methods in enzymology* 622, S. 347–374. DOI: 10.1016/bs.mie.2019.02.028.

Sheppard, Dean (2006): Transforming growth factor beta: a central modulator of pulmonary and airway inflammation and fibrosis. In: *Proceedings of the American Thoracic Society* 3 (5), S. 413–417. DOI: 10.1513/pats.200601-008AW.

Shimizu, Toshiyuki; Kanai, Ken-Ichi; Kyo, Yoshiyuki; Asano, Kazuhito; Hisamitsu, Tadashi; Suzaki, Harumi (2006): Effect of tranilast on matrix metalloproteinase production from

neutrophils in-vitro. In: *The Journal of pharmacy and pharmacology* 58 (1), S. 91–99. DOI: 10.1211/jpp.58.1.0011.

Shioda (1979): A Double Blind Controlled Trial of N-(3', 4'-Dimethoxycinnamoyl) Anthranilic Acid on Children with Bronchial Asthma. In: *Allergy* 34 (4), S. 213–219. DOI: 10.1111/j.1398-9995.1979.tb01701.x.

Sittampalam, G. Sitta; Coussens, Nathan P.; Nelson, Henrike; Arkin, Michelle; Auld, Douglas; Austin, Chris et al. (2004): Assay Guidance Manual: Eli Lilly & Company and the National Center for Advancing Translational Sciences.

Skronska-Wasek, Wioletta; Mutze, Kathrin; Baarsma, Hoeke A.; Bracke, Ken R.; Alsafadi, Hani N.; Lehmann, Mareike et al. (2017): Reduced Frizzled Receptor 4 Expression Prevents WNT/β-Catenin-driven Alveolar Lung Repair in Chronic Obstructive Pulmonary Disease. In: *American journal of respiratory and critical care medicine* 196 (2), S. 172–185. DOI: 10.1164/rccm.201605-0904OC.

Staab-Weijnitz, Claudia A.; Fernandez, Isis E.; Knuppel, Larissa; Maul, Julia; Heinzelmann, Katharina; Juan-Guardela, Brenda M. et al. (2015): FK506-Binding Protein 10, a Potential Novel Drug Target for Idiopathic Pulmonary Fibrosis. In: *American journal of respiratory and critical care medicine* 192 (4), S. 455–467. DOI: 10.1164/rccm.201412-2233OC.

Suki, Bela; Stamenovic, Dimitrije; Hubmayr, Rolf (2011): Lung parenchymal mechanics. In: *Comprehensive Physiology* 1 (3), S. 1317–1351. DOI: 10.1002/cphy.c100033.

Suwa, Shihoko; Kasubata, Aya; Kato, Miyu; Iida, Megumi; Watanabe, Ken; Miura, Osamu; Fukuda, Tetsuya (2015): The tryptophan derivative, tranilast, and conditioned medium with indoleamine 2,3-dioxygenase-expressing cells inhibit the proliferation of lymphoid malignancies. In: *International journal of oncology* 46 (3), S. 1369–1376. DOI: 10.3892/ijo.2015.2825.

Suzawa, H.; Kikuchi, S.; Arai, N.; Koda, A. (1992a): The mechanism involved in the inhibitory action of tranilast on collagen biosynthesis of keloid fibroblasts. In: *Japanese journal of pharmacology* 60 (2), S. 91–96.

Suzawa, H.; Kikuchi, S.; Ichikawa, K.; Koda, A. (1992b): Inhibitory action of tranilast, an anti-allergic drug, on the release of cytokines and PGE2 from human monocytes-macrophages. In: *Japanese journal of pharmacology* 60 (2), S. 85–90.

Swinney, D. C. (2013): Phenotypic vs. target-based drug discovery for first-in-class medicines. In: *Clinical pharmacology and therapeutics* 93 (4), S. 299–301. DOI: 10.1038/clpt.2012.236.

Swinney, David C.; Anthony, Jason (2011): How were new medicines discovered? In: *Nature reviews. Drug discovery* 10 (7), S. 507–519. DOI: 10.1038/nrd3480.

Switalla, S.; Lauenstein, L.; Prenzler, F.; Knothe, S.; Förster, C.; Fieguth, H-G et al. (2010): Natural innate cytokine response to immunomodulators and adjuvants in human precision-cut lung slices. In: *Toxicology and applied pharmacology* 246 (3), S. 107–115. DOI: 10.1016/j.taap.2010.04.010.

Szklarczyk, Damian; Gable, Annika L.; Nastou, Katerina C.; Lyon, David; Kirsch, Rebecca; Pyysalo, Sampo et al. (2021): The STRING database in 2021: customizable protein-protein networks, and functional characterization of user-uploaded gene/measurement sets. In: *Nucleic acids research* 49 (D1), D605-D612. DOI: 10.1093/nar/gkaa1074.

Tadano, Kohji; Yuhki, Yoshimitsu; Aoki, Isamu; Miyazaki, Katsumi; Arita, Takaichi (1985): High-performance liquid chromatographic determination of tranilast in plasma. In: *Journal of Chromatography B: Biomedical Sciences and Applications* 341, S. 228–231. DOI: 10.1016/S0378-4347(00)84034-7.

Talman, Virpi; Ruskoaho, Heikki (2016): Cardiac fibrosis in myocardial infarction-from repair and remodeling to regeneration. In: *Cell and tissue research* 365 (3), S. 563–581. DOI: 10.1007/s00441-016-2431-9.

Tamai, Hideo; Katoh, Kazuzo; Yamaguchi, Tetsu; Hayakawa, Hirokazu; Kanmatsuse, Katsuo; Haze, Kazuo et al. (2002): The impact of tranilast on restenosis after coronary angioplasty: the Second Tranilast Restenosis Following Angioplasty Trial (TREAT-2). In: *American Heart Journal* 143 (3), S. 506–513.

Tashiro, Jun; Rubio, Gustavo A.; Limper, Andrew H.; Williams, Kurt; Elliot, Sharon J.; Ninou, Ioanna et al. (2017): Exploring Animal Models That Resemble Idiopathic Pulmonary Fibrosis. In: *Frontiers in medicine* 4, S. 118. DOI: 10.3389/fmed.2017.00118.

Thannickal, Victor J.; Roman, Jesse (2010): Challenges in translating preclinical studies to effective drug therapies in idiopathic pulmonary fibrosis. In: *American journal of respiratory and critical care medicine* 181 (6), S. 532–533. DOI: 10.1164/rccm.200911-1740ED.

Thenappan, Thenappan; Ormiston, Mark L.; Ryan, John J.; Archer, Stephen L. (2018): Pulmonary arterial hypertension: pathogenesis and clinical management. In: *BMJ (Clinical research ed.)* 360, j5492. DOI: 10.1136/bmj.j5492.

Todd, Derrick J.; Kay, Jonathan (2016): Gadolinium-Induced Fibrosis. In: *Annual review of medicine* 67, S. 273–291. DOI: 10.1146/annurev-med-063014-124936.

Uhl, Franziska E.; Vierkotten, Sarah; Wagner, Darcy E.; Burgstaller, Gerald; Costa, Rita; Koch, Ina et al. (2015): Preclinical validation and imaging of Wnt-induced repair in human 3D lung tissue cultures. In: *The European respiratory journal* 46 (4), S. 1150–1166. DOI: 10.1183/09031936.00183214.

Vaglio, Augusto; Maritati, Federica (2016): Idiopathic Retroperitoneal Fibrosis. In: *Journal of the American Society of Nephrology : JASN* 27 (7), S. 1880–1889. DOI: 10.1681/ASN.2015101110.

van der Worp, H. Bart; Howells, David W.; Sena, Emily S.; Porritt, Michelle J.; Rewell, Sarah; O'Collins, Victoria; Macleod, Malcolm R. (2010): Can animal models of disease reliably inform human studies? In: *PLoS Medicine* 7 (3), e1000245. DOI: 10.1371/journal.pmed.1000245.

Vanhove, Thomas; Goldschmeding, Roel; Kuypers, Dirk (2017): Kidney Fibrosis: Origins and Interventions. In: *Transplantation* 101 (4), S. 713–726. DOI: 10.1097/TP.0000000000001608.

Vincent, Fabien; Loria, Paula; Pregel, Marko; Stanton, Robert; Kitching, Linda; Nocka, Karl et al. (2015): Developing predictive assays: the phenotypic screening "rule of 3". In: *Science translational medicine* 7 (293), 293ps15. DOI: 10.1126/scitranslmed.aab1201.

Wagner, Brent; Drel, Viktor; Gorin, Yves (2016): Pathophysiology of gadolinium-associated systemic fibrosis. In: *American journal of physiology. Renal physiology* 311 (1), F1-F11. DOI: 10.1152/ajprenal.00166.2016.

Wang, Lishi; Liu, Hongchao; Jiao, Yan; Wang, Erjian; Clark, Stephen H.; Postlethwaite, Arnold E. et al. (2015): Differences between Mice and Humans in Regulation and the Molecular Network of Collagen, Type III, Alpha-1 at the Gene Expression Level: Obstacles that Translational Research Must Overcome. In: *International journal of molecular sciences* 16 (7), S. 15031–15056. DOI: 10.3390/ijms160715031.

White, Eric S. (2015): Lung extracellular matrix and fibroblast function. In: *Annals of the American Thoracic Society* 12 Suppl 1, S30-3. DOI: 10.1513/AnnalsATS.201406-240MG.

Wikimedia Commons (2020): A SLAS/ANSI standard compliant 384-well plate. Unter Mitarbeit von 'Photocyte'. Wikimedia Commons. Online verfügbar unter https://commons.wikimedia.org/wiki/File:384-well_plate.svg, zuletzt aktualisiert am 04.12.2021, zuletzt geprüft am 18.12.2021.

Woodcock, Hannah V.; Eley, Jessica D.; Guillotin, Delphine; Platé, Manuela; Nanthakumar, Carmel B.; Martufi, Matteo et al. (2019): The mTORC1/4E-BP1 axis represents a critical signaling node during fibrogenesis. In: *Nature communications* 10 (1), S. 6. DOI: 10.1038/s41467-018-07858-8.

Wynn, Thomas A. (2007): Common and unique mechanisms regulate fibrosis in various fibroproliferative diseases. In: *J. Clin. Invest.* 117 (3), S. 524–529. DOI: 10.1172/JCI31487.

Wynn, Thomas A.; Ramalingam, Thirumalai R. (2012): Mechanisms of fibrosis: therapeutic translation for fibrotic disease. In: *Nature medicine* 18 (7), S. 1028–1040. DOI: 10.1038/nm.2807.

Xu, Zhan; Greenblatt, Matthew B.; Yan, Guang; Feng, Heng; Sun, Jun; Lotinun, Sutada et al. (2017): SMURF2 regulates bone homeostasis by disrupting SMAD3 interaction with vitamin D receptor in osteoblasts. In: *Nature communications* 8, S. 14570. DOI: 10.1038/ncomms14570.

Yamada, H.; Tajima, S.; Nishikawa, T.; Murad, S.; Pinnell, S. R. (1994): Tranilast, a selective inhibitor of collagen synthesis in human skin fibroblasts. In: *Journal of biochemistry* 116 (4), S. 892–897.

Yanagihara, Toyoshi; Chong, Sy Giin; Vierhout, Megan; Hirota, Jeremy A.; Ask, Kjetil; Kolb, Martin (2020): Current models of pulmonary fibrosis for future drug discovery efforts. In: *Expert opinion on drug discovery* 15 (8), S. 931–941. DOI: 10.1080/17460441.2020.1755252.

Yue, Xinping; Shan, Bin; Lasky, Joseph A. (2010): TGF-beta: Titan of Lung Fibrogenesis. In: *Current enzyme inhibition* 6 (2). DOI: 10.2174/10067.

Zeisberg, Michael; Kalluri, Raghu (2012): Cellular Mechanisms of Tissue Fibrosis. 1. Common and organ-specific mechanisms associated with tissue fibrosis. In: *American journal of physiology. Cell physiology* 304 (3), C216-25. DOI: 10.1152/ajpcell.00328.2012.

Zhang, Y.; Chang, C.; Gehling, D. J.; Hemmati-Brivanlou, A.; Derynck, R. (2001): Regulation of Smad degradation and activity by Smurf2, an E3 ubiquitin ligase. In: *Proceedings of the National Academy of Sciences of the United States of America* 98 (3), S. 974–979. DOI: 10.1073/pnas.98.3.974.

Zhang, Ying E. (2009): Non-Smad pathways in TGF-beta signaling. In: *Cell research* 19 (1), S. 128–139. DOI: 10.1038/cr.2008.328.

Zhao, Siyuan; Liao, Huanhuan; Ao, Meiying; Wu, Li; Zhang, Xiaojun; Chen, Yong (2014): Fixation-induced cell blebbing on spread cells inversely correlates with phosphatidylinositol

4,5-bisphosphate level in the plasma membrane. In: *FEBS open bio* 4, S. 190–199. DOI: 10.1016/j.fob.2014.02.003.

Zhao, Xiao; Kwan, Jennifer Yin Yee; Yip, Kenneth; Liu, Peter P.; Liu, Fei-Fei (2020): Targeting metabolic dysregulation for fibrosis therapy. In: *Nature reviews. Drug discovery* 19 (1), S. 57–75. DOI: 10.1038/s41573-019-0040-5.

Zheng, Wei; Thorne, Natasha; McKew, John C. (2013): Phenotypic screens as a renewed approach for drug discovery. In: *Drug discovery today* 18 (21-22), S. 1067–1073. DOI: 10.1016/j.drudis.2013.07.001.

11. List of Tables

12. List of Figures

13. Publications and Presentations

13.1. Publications

„Spirometrie zeigt COPD früher an als gedacht.“ Kahnert K., Gerckens M. MMW - Fortschritte der Medizin, 2023 Mar;165(6):29. https://doi.org/10.1007/s15006-023-2500-4.

“Phenotypic drug screening in a human fibrosis model identified a novel class of antifibrotic therapeutics.” Gerckens, M., Schorpp, K., Pelizza, F., Wögrath, M., Reichau, K., Ma, H., Dworsky, A. M., Sengupta, A., Stoleriu, M. G., Heinzelmann, K., Merl-Pham, J., Irmler, M., Alsafadi, H. N., Trenkenschuh, E., Sarnova, L., Jirouskova, M., Frieß, W., Hauck, S. M., Beckers, Kneidinger, N., Behr, J., Hilgendorff, A., Hadian, K., Lindner, M., Königshoff M. Eickelberg, O., Gregor, M., Plettenburg, O., Yildirim, A. Ö., Burgstaller, G. (2021). Science advances, 7(52), eabb3673. https://doi.org/10.1126/sciadv.abb367

“Prevention of COVID-19 in Thoracic Surgery Patients: Lessons Learned during the First Pandemic Wave.” Stoleriu, M. G., Gerckens, M., Ströh, K., Kovács, J., Samm, N., Obereisenbuchner, F., Hetrodt, J., Schmidt, F. M., Reinmuth, N., Heiß-Neumann, M., Stacher-Priehse, E., Koch, I., Behr, J., Ketscher, C., Grützner, U., & Hatz, R. (2021). Pneumologie (Stuttgart, Germany), 75(12), 960–970. https://doi.org/10.1055/a-1526-9979

“Automated quantitative thin slice volumetric low dose CT analysis predicts disease severity in COVID-19 patients.” Stoleriu, M. G., Gerckens, M., Obereisenbuchner, F., Zaimova, I., Hetrodt, J., Mavi, S. C., Schmidt, F., Schoenlebe, A. A., Heinig-Menhard, K., Koch, I., Jörres, R. A., Spiro, J., Nowak, L., Hatz, R., Behr, J., Gesierich, W., Heiß-Neumann, M., & Dinkel, J. (2021). Clinical imaging, 79, 96–101. https://doi.org/10.1016/j.clinimag.2021.04.008

“Decellularized Human Lung Scaffolds as Complex Three-Dimensional Tissue Culture Models to Study Functional Behavior of Fibroblasts.” Burgstaller, G., Gerckens, M., Eickelberg, O., & Königshoff, M. (2021). Methods in molecular biology (Clifton, N.J.), 2299, 447–456. https://doi.org/10.1007/978-1-0716-1382-5_30

“Clinical Course of Three Postoperative Symptomatic COVID-19 Cases in Patients After Lung Lobectomy.” Stoleriu, M. G., Gerckens, M., Hetrodt, J., Heiß-Neumann, M., Koch, I., Stacher-Priehse, E., Dinkel, J., Behr, J., Grützner, U., & Hatz, R. (2020). The Annals of thoracic surgery, 110(6), e461–e463. https://doi.org/10.1016/j.athoracsur.2020.06.001

“Generation of Human 3D Lung Tissue Cultures (3D-LTCs) for Disease Modeling.” Gerckens, M., Alsafadi, H. N., Wagner, D. E., Lindner, M., Burgstaller, G., & Königshoff, M. (2019). Journal of visualized experiments: JoVE, (144), 10.3791/58437. https://doi.org/10.3791/58437

“Cell-surface phenotyping identifies CD36 and CD97 as novel markers of fibroblast quiescence in lung fibrosis.” Heinzelmann, K., Lehmann, M., Gerckens, M., Noskovičová, N., Frankenberger, M., Lindner, M., Hatz, R., Behr, J., Hilgendorff, A., Königshoff, M., & Eickelberg, O. (2018). American journal of physiology. Lung cellular and molecular physiology, 315(5), L682–L696. https://doi.org/10.1152/ajplung.00439.2017

“The instructive extracellular matrix of the lung: basic composition and alterations in chronic lung disease.” Burgstaller, G., Oehrle, B., Gerckens, M., White, E. S., Schiller, H. B., & Eickelberg, O. (2017). The European respiratory journal, 50(1), 1601805. https://doi.org/10.1183/13993003.01805-2016

13.2. Oral presentations

Februar 2020	**„Deep learning analysis of IPF extracellular matrix from 3D confocal images used for high-content drug screening“** Oral presentation at the annual meeting of the German Center for Lung Research 2020.
Oktober 2018	**„High-throughput drug screening of novel ECM deposition inhibitors in antifibrotic drug discovery“** Oral presentation at the autumn conference of the section “cell biology“ of the Germany Respiratory Society 2018.
Februar 2018	**„SOP: Preparation of human *ex-vivo* precision cut lung slices”** Oral presentation at the annual meeting of the German Center for Lung Research 2017
Juni 2017	**„Pharmacological Inhibition of the Deposition of Extracellular Matrix Molecules“** Oral presentation at the Munich Medical Student Science Conference 2017.

13.3. Poster presentations

September 2022 **„Phenotypic drug screening in a human fibrosis model identified a novel class of antifibrotic therapeutics”** Poster presentation at the International Congress of the European Respiratory Society 2022.

June 2022 **„Phenotypic drug screening in a human fibrosis model identified a novel class of antifibrotic therapeutics”** Poster presentation at the 1st Extracellular Matrix Pharmacology Congress 2022.

Februar 2020 **„Phenotypic high-content drug screening identifies a novel chemical entity with antifibrotic properties.”** Poster presentation at the annual meeting of the German Center for Lung Research 2020.

Februar 2019 **„High-throughput drug screening of novel ECM deposition inhibitors in antifibrotic drug discovery”** Poster presentation at the annual meeting of the German Center for Lung Research 2019.

Februar 2018 **„A phenotypic drug discovery pipeline for novel antifibrotic IPF therapies”** Poster presentation at the annual meeting of the German Center for Lung Research 2019.

September 2017 **„A phenotypic cell-based extracellular matrix deposition assay for target validation and drug discovery”** Poster presentation at the International Congress of the European Respiratory Society 2017.

Januar 2017 **„Modulated deposition of extracellular matrix proteins in a high content imaging assay”** Poster presentation at the annual meeting of the German Center for Lung Research 2017.

14. Acknowledgements

I would like to express my deep appreciation to my supervisor Prof. Dr. Eickelberg for the opportunity to perform my doctorate project in this institute. I am very grateful for the excellent guidance and constant support I received during the doctorate.

Furthermore, I would like to thank my supervisor Dr. Gerald Burgstaller for his excellent supervision, the tireless help, the continuous teaching, and motivation I received during my project. I am very thankful for the extremely helpful endless scientific discussions on every detail on the project. I highly appreciate the scientific rigor and the eye for detail that was exemplified by Dr. Burgstaller and shaped my scientific thinking. I also want to thank Dr. Burgstaller for his kindness, patience, and support in developing this research project together as well as for his constant efforts in encouraging and facilitating national and international collaborations that enabled this variety of experiments.

I am also very thankful for the help of all our collaborators who supported the project, specifically Dr. Ali Önder Yildirim, Dr. Anne Hilgendorff, Dr. Stefanie Hauck, Dr. Juliane Merl-Pham, Prof. Dr. Johannes Beckers, Dr. Martin Irmler, Dr. Melanie Königshoff, Dr. Darcy Wagner, Hani Alsafadi, Prof. Dr. Oliver Plettenburg, Dr. Kora Reichau, Huilong Ma, Dr. Martin Gregor, Dr. Marketa Jirouskova, Lenka Sarnova, Prof. Dr. Wolfgang Frieß, Eduard Trenkenschuh, Dr. Kamyar Hadian and Dr. Kenji Schorpp as well as the colleagues of the CPC-BioArchive, the clinical collaborators at the University Hospital of Munich (Prof. Dr. Nikolaus Kneidinger und Prof. Dr. Behr) and Asklepios Lung Clinics Munich-Gauting (Prof. Dr. Rudolf Hatz, Dr. Michael Lindner and Dr. Gabriel Stoleriu).

I would also like thank all former members of the former Eickelberg Laboratory and as well as the later Burgstaller Laboratory, especially Dr. Claudia Staab-Wejinitz, Dr. Isis Fernandez, Dr. Arunima Sengupta, Armando Dworsky, Melanie Wögrath, Daniela Dietl, Heike Hoffmann and Dibora Tibebu for their constant scientific and technical support and productive scientific discussions . Especially, I want to thank Dr. Katharina Heinzelmann and Dr. Nina Noskovičová for introducing me into the world of experimental research prior to and while my thesis project

and teaching me with a multitude of helpful technical and scientific skills that facilitated the work on my thesis immensely. I would also like to thank especially Marisa Neumann for her excellent organizational and technical support.

I would like to thank the fantastic CPC Research School team for their valuable scientific training and education as the CPC Research School 2015 / 2016 class for a very pleasurable learning experience. I am very thankful for providing me with two research scholarships to complete my thesis at the institute.

I want to express my deepest gratitude to my family for unconditional love, their support and patience during my thesis.

Finally, I would also like to thank all reviewers of this thesis who dedicated their time and energy to review and proofread my thesis.

15. Eidesstattliche Versicherung

Ich, Michael Gerckens, erkläre hiermit an Eides statt, dass ich die vorliegende Dissertation mit dem Thema

„Discovery of new cinnamic acid amides as novel antifibrotic drugs”

selbständig verfasst, mich außer der angegebenen keiner weiteren Hilfsmittel bedient und alle Erkenntnisse, die aus dem Schrifttum ganz oder annähernd übernommen sind, als solche kenntlich gemacht und nach ihrer Herkunft unter Bezeichnung der Fundstelle einzeln nachgewiesen habe.

Ich erkläre des Weiteren, dass die hier vorgelegte Dissertation nicht in gleicher oder in ähnlicher Form bei einer anderen Stelle zur Erlangung eines akademischen Grades eingereicht wurde.

München, den 02.11.2023 Michael Gerckens